

USING REGIONAL DATA SETS TO STUDY SOURCE TO SINK SEDIMENTARY
PROCESSES

John R. Gunnell

A dissertation submitted to the faculty at the University of North Carolina at Chapel Hill in partial fulfillment of the requirements for the degree of Doctor of Philosophy in the Department of Marine Sciences.

Chapel Hill
2016

Approved by:

Brent McKee

Jaye Cable

Mukesh Kumar

Harvey Seim

Brian White

© 2016
John R. Gunnell
ALL RIGHTS RESERVED

ABSTRACT

John R. Gunnell: Using Regional Data Sets to Study Source to Sink Sedimentary Processes
(Under the Direction of Brent McKee)

The study of sediment provenance, transport, and deposition encompasses a diverse set of geomorphological settings and processes. For a variety of reasons, “source to sink” sedimentary systems have historically been difficult to characterize due to operational limitations of the scientists studying them. Consequently, these systems are understood through the comparison of small-scale observational case studies. This lack of quantitative unity between studies has stymied attempts at building generalizable theory. The purpose of this dissertation is to reevaluate some longstanding intuitions in the field of sedimentary geomorphology by taking a broader vantage and integrating observations from expansive regional scopes into unified frames of reference. This undertaking has revealed important insights about the behavior of several source to sink systems that would not have been noticeable if they were studied in a narrower context. An overview of these insights by chapter is as follows:

Chapter 1: As would traditionally be expected, coastal emergent wetland inventories showed significant individual correlations with respect to wave energy and relief. Terrestrial sediment flux to the ocean, on the other hand, apparently only contributes to large scale wetland abundance when present above a threshold quantity. This suggests that estuarine processes in the vicinity of wetlands play a larger role in promoting marsh abundance than fluvial sediment supply does.

Chapter 2: Despite the complex cascade of expected landscape responses to urbanization, suspended sediment yields of U.S. Piedmont streams consistently were an order of magnitude higher in watersheds with spatial indices of extensive population growth and urban development.

Chapter 3: A comparison between modeled and measured sediment properties of marsh cores along the Northwest Atlantic coast showed that the contemporary modeling paradigm of marsh accretion can occasionally reproduce actual marsh soil characteristics. Nevertheless, rapidly subsiding Louisiana marshes as well as marshes with extreme values in organic matter density systematically deviated from modeled expectations. Current models fail to parameterize potentially important aspects of accretion and compressibility in a large number of wetlands across the United States, casting doubt on our current capacity to reasonably predict marsh vertical response to accelerated sea level rise in a variety of locations.

ACKNOWLEDGEMENTS

This dissertation would not have been possible without my wife, family, and closest friends. Their love sustains me. I have relied on my advisor Dr. Brent McKee for his steadfast support and guidance. As I continue in my career, I will try to follow his example of patience and broad perspective. I thank my committee members who have shown remarkable flexibility throughout this process. Since I moved to North Carolina to begin my graduate studies, I have been the recipient of innumerable kindnesses from the staff and students of the UNC Marine Sciences department. Also, I have to thank Dr. J.A. Nyman of LSU, who not only responded to my emails begging for his old data, but was actually kind enough to share it. His marsh soil profile data added significant value to my third chapter.

TABLE OF CONTENTS

LIST OF TABLES	ix
LIST OF FIGURES	x
LIST OF ABBREVIATIONS AND SYMBOLS	xiv
CHAPTER 1: A LARGE SCALE STUDY OF COASTAL WETLAND GEOMORPHOLOGICAL SETTINGS	1
1.1: Introduction.....	1
1.2: Methods	2
1.2.1: Data Sources	2
1.2.2: Data Extraction and Manipulation	5
1.2.3: Statistical and Computational Methods	7
1.3: Results.....	8
1.3.1: Descriptive Statistics.....	8
1.3.2: Suspended Sediment Flux Regression and Validation	12
1.3.3: Wetland Abundance Regression	17
1.4: Discussion	19
1.4.1: Estuarine vs. Fluvial Processes	19
1.4.2: Knowledge Gaps in a Changing World	22
1.5: Conclusions.....	24
REFERENCES	25

CHAPTER 2: AN ANALYSIS OF FLUVIAL SUSPENDED SEDIMENT RESPONSE TO URBANIZATION IN THE U.S. SOUTHERN PIEDMONT.....	30
2.1: Introduction.....	30
2.2: Methods	32
2.2.1: Regional Description	32
2.2.2: Gage Sites	32
2.2.3: Fluvial Sediment Flux Estimation	33
2.2.4: Spatial Analysis	35
2.3: Results.....	38
2.3.1: Sediment Flux Estimation Parameters	38
2.3.2: Watershed Delineation Performance	41
2.3.3: Spatial Characteristics between Sites	42
2.3.4: Sediment Yield Comparisons	45
2.4: Discussion.....	47
2.4.1: Methodological Limitations.....	47
2.4.2: Regional Differences	48
2.5: Conclusions.....	50
REFERENCES	51
CHAPTER 3: A REVIEW OF MARSH SOIL PROPERTIES COMPARED TO MODELED EXPECTATIONS.....	55
3.1: Introduction.....	55
3.2: Methods	56
3.2.1: Data Sources	56
3.2.2: A Common Frame of Reference.....	61

3.2.3: Model Organization	62
3.2.4: Modeling Primary Production	64
3.2.5: Modeling Mortality and Decay.....	63
3.2.6: Modeling Compaction and Accretion.....	65
3.2.7: Model Comparison and Fitting	68
3.3: Results.....	69
3.3.1: Compilation Data	69
3.3.2: Model Parameter Results	73
3.3.3: Across Site Performance.....	76
3.4: Discussion.....	79
3.4.1: Failed Convergence	79
3.4.2: Compression Error	80
3.4.3: Recommendations for Future Research.....	83
3.5: Conclusions.....	84
REFERENCES	85
APPENDIX A.1: STREAM GAGE SUMMARY	92
APPENDIX A.2: SEDIMENT RATING CURVES.....	94
APPENDIX B: MARSH CORE SUMMARY TABLES	146

LIST OF TABLES

Table 1.1- Spatial Data Sources	3
Table 1.2- Watershed Elevation Categories (Milliman and Syvitski 1992)	6
Table 1.3- Bivariate Correlation	9
Table 2.1- Changes in Land Cover (2001-2011) [% of Watershed Area]	42
Table 3.1- Summary Statistics of Cores from the Literature	59
Table 3.2- Tide Gage Information	60
Table 3.3- Equations	67
Table 3.4- Variables and Constants	68
Table A.1.1- Gage Summary Table 1	92
Table A.1.2- Gage Summary Table 2	93
Table B.1- Core Summary Data from Literature	146
Table B.2- Core Summary Data from Literature Continued1	147
Table B.3- Core Summary Data from Literature Continued2	148

LIST OF FIGURES

Figure 1.1- Terrain Variables.....	4
Figure 1.2- Climate Variables Table.....	5
Figure 1.3- Sediment Yield Descriptive Responses	10
Figure 1.4- Marsh Width Descriptive Responses	11
Figure 1.5- Diagnostic Charts for Regressions	14
Figure 1.6- GAM Terms for Sediment Yield Regression.....	15
Figure 1.7- Representativeness of the Suspended Sediment Estimate	16
Figure 1.8- GAM Terms for Coastal Wetland Abundance.....	18
Figure 2.1- Example of Sediment Rating Curve Analysis.....	35
Figure 2.2- Spatial Datasets of Human Behavior	37
Figure 2.3- Variation in Rating Curve Parameters	40
Figure 2.4- Delineated Watersheds.....	41
Figure 2.5- Mean within-Site Characteristics	44
Figure 3.1- Cores and Spatial Datasets	58
Figure 3.2- SWLI vs. Marsh Characteristics	61
Figure 3.3- Factors Affecting Accretion.....	71
Figure 3.4- Bivariate Soil Relationships.....	72
Figure 3.5- Model Performance and Inferred Variables.....	75
Figure 3.6- Systematic Model Errors.....	78
Figure A.2.1-01673000: PAMUNKEY RIVER NEAR HANOVER, VA.....	94
Figure A.2.2-02035000: JAMES RIVER AT CARTERSVILLE, VA	95
Figure A.2.3-02041650: APPOMATTOX RIVER AT MATOACA, VA	96
Figure A.2.4-02075500: DAN RIVER AT PACES, VA.....	97

Figure A.2.5-02085500: FLAT RIVER AT BAHAMA, NC	98
Figure A.2.6-0208524090: MOUNTAIN CREEK AT SR1617 NR BAHAMA, NC.....	99
Figure A.2.7-0208521324: LITTLE RIVER AT SR1461 NEAR ORANGE FACTORY, NC.....	100
Figure A.2.8-0208650112: FLAT RIVER TRIB NR WILLARDVILLE, NC	101
Figure A.2.9-0208524975: LITTLE R BL LITTLE R TRIB AT FAIRNTOSH, NC.....	102
Figure A.2.10-02085000: ENO RIVER AT HILLSBOROUGH, NC.....	103
Figure A.2.11-02096846: CANE CREEK NEAR ORANGE GROVE, NC	104
Figure A.2.12-0208700780: LITTLE LICK CR AB SR1814 NR OAK GROVE, NC.....	105
Figure A.2.13-02087183: NEUSE RIVER NEAR FALLS, NC	106
Figure A.2.14-02097464: MORGAN CREEK NEAR WHITE CROSS, NC.....	107
Figure A.2.15-02097517: MORGAN CREEK NEAR CHAPEL HILL, NC.....	108
Figure A.2.16-02116500: YADKIN RIVER AT YADKIN COLLEGE, NC	109
Figure A.2.17-02096960: HAW RIVER NEAR BYNUM, NC.....	110
Figure A.2.18-0209782609: WHITE OAK CR AT MOUTH NEAR GREEN LEVEL, NC	111
Figure A.2.19-02087580: SWIFT CREEK NEAR APEX, NC.....	112
Figure A.2.20-02087500: NEUSE RIVER NEAR CLAYTON, NC	113
Figure A.2.21-0214266000: MCDOWELL CREEK NR CHARLOTTE, NC (CSW10)	114
Figure A.2.22-02124692: GOOSE CR AT FAIRVIEW, NC.....	115
Figure A.2.23-02126000: ROCKY RIVER NEAR NORWOOD, NC	116
Figure A.2.24-02331600: CHATTAHOOCHEE RIVER NEAR CORNELIA, GA.....	117
Figure A.2.25-02333500: CHESTATEE RIVER NEAR DAHLONEGA, GA	118
Figure A.2.26-02334480: RICHLAND CREEK AT SUWANEE DAM ROAD, NEAR BUFORD,GA	119
Figure A.2.27-02334578: LEVEL CREEK AT SUWANEE DAM ROAD, NEAR SUWANEE, GA.....	120

Figure A.2.28-02217274: WHEELER CREEK AT BILL CHEEK ROAD, NEAR AUBURN, GA	121
Figure A.2.29-02334885: SUWANEE CREEK AT SUWANEE, GA	122
Figure A.2.30-02218565: APALACHEE RIVER AT FENCE ROAD, NEAR DACULA, GA.....	123
Figure A.2.31-02335350: CROOKED CREEK NEAR NORCROSS, GA.....	124
Figure A.2.32-02335870: SOPE CREEK NEAR MARIETTA, GA.....	125
Figure A.2.33-02208150: ALCOVY RIVER AT NEW HOPE ROAD, NEAR GRAYSON, GA.....	126
Figure A.2.34-02336030: N.F. PEACHTREE CREEK AT GRAVES RD, NR DORAVILLE,GA	127
Figure A.2.35-02336360: NANCY CREEK AT RICKENBACKER DRIVE, AT ATLANTA, GA	128
Figure A.2.36-02336410: NANCY CREEK AT WEST WESLEY ROAD, AT ATLANTA, GA	129
Figure A.2.37-02336120: N.F. PEACHTREE CREEK, BUFORD HWY, NEAR ATLANTA, GA	130
Figure A.2.38-02207400: BRUSHY FORK CREEK AT BEAVER ROAD, NR LOGANVILLE,GA	131
Figure A.2.39-02336300: PEACHTREE CREEK AT ATLANTA, GA.....	132
Figure A.2.40-02207385: BIG HAYNES CREEK AT LENORA ROAD, NR SNELLVILLE, GA.....	133
Figure A.2.41-02336240: S.F. PEACHTREE CREEK JOHNSON RD, NEAR ATLANTA, GA	134
Figure A.2.42-02336526: PROCTOR CREEK AT JACKSON PARKWAY, AT ATLANTA, GA	135
Figure A.2.43-02207185: NO BUSINESS CREEK AT LEE ROAD, BELOW SNELLVILLE,GA	136
Figure A.2.44-02207120: YELLOW RIVER AT GA 124, NEAR LITHONIA, GA	137
Figure A.2.45-02207220: YELLOW RIVER AT PLEASANT HILL ROAD, NR LITHONIA,GA.....	138

Figure A.2.46-02203655: SOUTH RIVER AT FORREST PARK ROAD, AT ATLANTA, GA.....	139
Figure A.2.47-02207335: YELLOW RIVER AT GEES MILL ROAD, NEAR MILSTEAD, GA.....	140
Figure A.2.48-02337500: SNAKE CREEK NEAR WHITESBURG, GA	141
Figure A.2.49-02338000: CHATTAHOOCHEE RIVER NEAR WHITESBURG, GA.....	142
Figure A.2.50-02338523: HILLABAHATCHEE CREEK AT THAXTON RD, NR FRANKLIN,GA.....	143
Figure A.2.51-02212600: FALLING CREEK NEAR JULIETTE, GA.....	144
Figure A.2.52-02339500: CHATTAHOOCHEE RIVER AT WEST POINT, GA.....	145

LIST OF ABBREVIATIONS AND SYMBOLS

B_{ag}	Total aboveground biomass
b_{bg}	Belowground biomass within a sediment cohort
B_{bg}	Total belowground biomass
BD	Dry bulk density
B_p	Annual peak value of total aboveground biomass
C_r	Recompression coefficient
C_c	Compression coefficient
C_s	Suspended sediment concentration
C_{SS}	Input variable for marsh sedimentation model parameterizing differences in sediment availability
DN	Digital Number
D_{ni}	Depth below mean high water at the North Inlet, SC
E	Duan's smearing coefficient
e	Void ratio of a sediment cohort
e_1	Reference void ratio at 1kPa
ETOPO1	Global 1' digital elevation model
GAM	Generalized Additive Model, a nonlinear regression method
GCV	Generalized Cross Validation statistic
G_s	Specific gravity of particulate matter
HAT	Highest astronomical tide
IQR	Interquartile range
k_r	Decay coefficient for refractory organic material
k_l	Decay coefficient for labile organic material

LAT	Lowest astronomical tide
M_{ag}	Total mortality of aboveground biomass
m	Mortality of belowground biomass within a sediment cohort
MD	Dry mineral density
MHW	Mean high water
NLCD	National Land Cover Database
NWIS	National Water Information System
OMD	Dry organic matter density
OM_0	Input variable for marsh sedimentation model parameterizing the proportion of incoming sediment comprised of refractory organic material
$Q(t)$	Fluvial discharge as a function of time
$Q_s(t)$	Suspended sediment flux as a function of time
$r(y)$	Sediment rating curve model residuals as a function of year
RMSE	Root mean square error of residuals between predicted and measured values
rSLR	The rate of relative sea level rise
SWLI	Standardized water level index
Stn-30p	30' Global delineated watershed data set
T	Temperature
T_{ni}	Temperature at the North Inlet, SC
%OM	Percent organic material of dry sediment based on loss on ignition
γ_z	Coefficient modifying the rate that belowground biomass decreases with respect to depth
η_0	Initial elevation of first sediment deposit in the marsh sedimentation model
μ	Coefficient modifying the rate that organic matter decay decreases with respect to depth
v_{Gp}	The ratio of peak annual growth rate to peak total annual aboveground biomass

ρ_{wet}	The wet particle density of soil material
σ_b	Coefficient modifying peak total annual aboveground biomass based on deviation from a reference temperature
σ_k	Coefficient modifying rates of organic matter decay based on based on deviation from a reference temperature
σ'	Effective compressive stress above a sediment cohort
σ'_y	Yield stress of a sediment cohort
τ	Kendell's nonparametric correlation coefficient
φ_A	Offset in julian days to account for date of peak standing biomass
φ_B	Offset in julian days to account for date of peak growth rate
χ_r	Fraction of dying biomass made up of refractory carbon

CHAPTER 1: A LARGE SCALE STUDY OF COASTAL WETLAND GEOMORPHOLOGICAL SETTINGS

1.1 Introduction

Long valued for their ecosystem services (Costanza et al., 1997), salt marshes are more recently noted for their importance in the global carbon cycle (Nellemann et al., 2009; Chmura et al., 2003) and carbon sequestration (Grimsditch et al., 2012; Pendleton et al., 2012). This is because these emergent coastal wetlands experience significant primary production, rapid sedimentation, and slow carbon remineralization (Duarte et al., 2005). Despite this growing interest, no global inventory of salt marsh area exists (Hopkinson et al., 2012). Global anthropogenic change also threatens wetland survival in a variety of climate conditions (Kirwan et al., 2010; Kirwan and Mudd 2012). Therefore, the abundance of coastal wetlands is uncertain for both the present and future. The goal of this exploratory analysis is to make a tentative estimate of how the coastal marsh's geomorphological setting influences its regional abundance using large scale datasets. This will function as an evaluation of current theory on marsh geomorphology and may guide future endeavors to predict a global inventory of coastal wetland abundance.

A rich literature of environmental case studies has informed us that marsh erosion and sedimentation vary due to differences in ambient wave energy (Fagherazzi et al., 2006), channel proximity (Cahoon and Reed 1995), marsh-table elevation (Allen 2000), and primary productivity (Morris et al., 2002). How large-scale wetland abundance evolves is studied by time series of national inventories (e.g. Dahl 2011), inferences from local case studies (e.g.

Gunnell et al., 2013; Day et al., 2011; Krull and Craft 2009), and extrapolations from mechanistic models (Fagherazzi et al., 2012). Due to a historical paucity of continental datasets, it is not certain how these various factors interact to influence large scale wetland predominance.

Until the continental-scale geomorphological settings of coastal wetlands are measured and compared to inventories, we can't claim that we understand the emergent consequences of the processes dictating marsh behavior. We have an educated expectation that marshes should predominate in systems with high accommodation space, low energy, and with relatively high suspended sediment concentrations. In this study, we have gathered datasets that will act as indices for those features and compared them to marsh abundance.

1.2 Methods

1.2.1 Data Sources

Spatial covariates from global data sets were compared to the abundance of “Estuarine and Marine Intertidal Wetlands” reported in the U.S. National Wetlands Inventory (Table 1). According to the wetland inventory, this category includes “both vegetated and non-vegetated brackish and saltwater marsh, shrubs, beach, bar, shoal, or flat”. It is our expectation that this will largely be comprised of marshland and sedimentary structures that behave similarly to marshes.

Terrain attributes (Fig. 1.1) include a high resolution global shoreline (Wessel and Smith 1996), the Stn-30p global delineated watersheds (Vörösmarty and Fekete 2011), estimates of sediment flux to the ocean (Milliman and Farnsworth 2012), and the ETOPO1 bedrock topographic map (Amante and Eakins 2009). ETOPO1, a one arc-minute resolution global map that includes both terrestrial and bathymetric measurements, was used to for measurements of absolute elevation within watersheds as well as relief near the shoreline. While higher resolution

maps are available and have been used in other global sediment flux measurements (Syvitski and Kettner 2011), ETOPO1’s inclusion of bathymetry means that river mouth and estuarine terrain analysis can include subaqueous topography. Relief was measured using the “roughness” index calculated using the ‘terrain’ function in the R raster package (Hijmans 2014). This value is the maximum range of elevations (meters) within the 8-cell neighborhood of the point being measured.

Table 1.1-Spatial Data Sources:

Feature	type (resolution)	reference
Global Shoreline	Line (~1 km)	(Wessel and Smith 1996)
Sediment Yield	Point	(Milliman and Farnsworth 2012)
Watersheds	Polygon (30’)	(Vörösmarty and Fekete 2011)
Topography	Raster (1’)	(Amante and Eakins 2009)
Temp/Precip	Raster (1.4°)	(NCAR-GIS-Program 2012)
Wave Energy	Raster (30’)	(Tolman 2009)
M2 Tidal Range	Raster (15’)	(Ray 1999)
Wetland Area	Polygon (~15 m)	(U.S. Fish and Wildlife Service 2016)

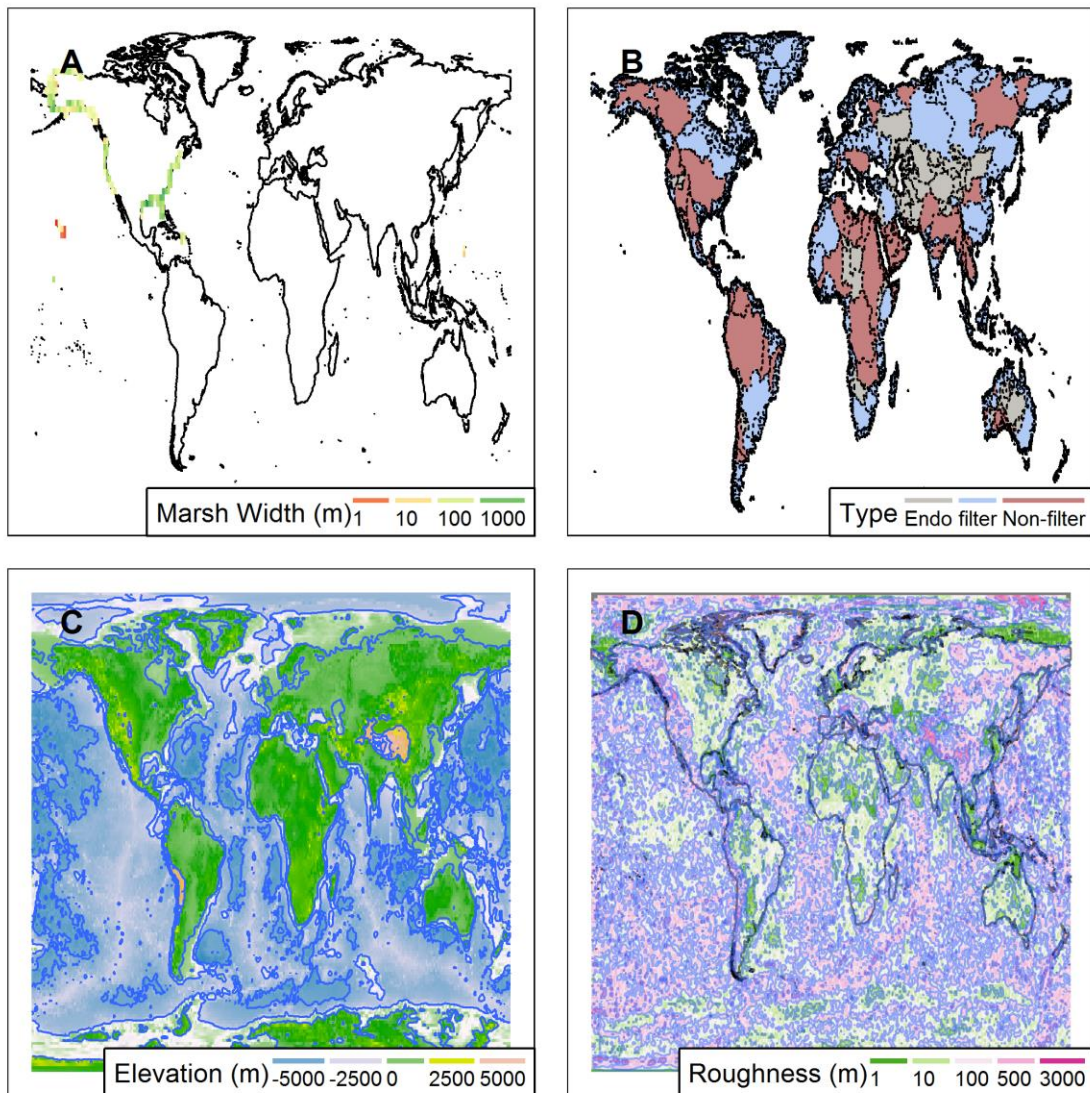
Climate variables (Fig. 1.2) include modeled surface temperature and total precipitation (NCAR-GIS-Program 2012), a modeled M2 tidal range (Ray 1990), and wave energy density derived from modeled significant wave heights (Tolman 2009). Surface Temperature and Total Precipitation datasets are monthly average projections for the historical period ranging from 1979 to 1999 (NCAR-GIS-Program 2012) on a 1.4 degree grid. These 20 year hindcasts were averaged within each cell before being projected to a final raster.

Significant wave heights and periods were from the Wave Watch III model (Tolman 2009). The dataset analyzed covers a global extent at 30 arc-minute resolution, spanning the period from February 2005 through January 2014 (NOAA 2015). Each time step was read from its grib2 file into MATLAB (R2015a) using NCTOOLBOX (Schlining et al., 2014), and wave energy density (E) was based on the deep water relationship with significant wave height (H) and

wave period (T): $E = .5H^2T$. The final value reported is the mean of all time steps at each point.

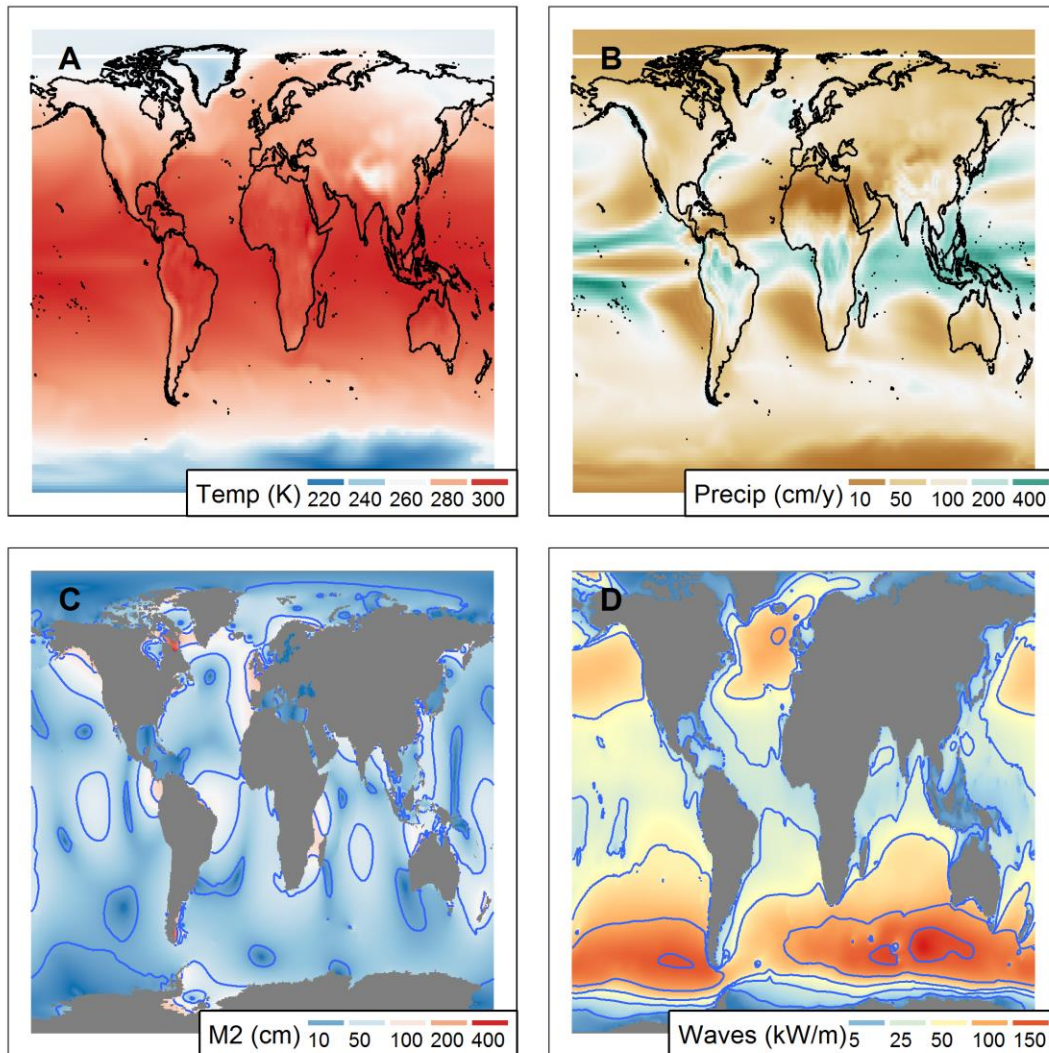
This is a qualitative measure of wave energy nearshore, because there is no accounting for bathymetric effects or wave diffraction.

Figure 1.1-Terrain Variables:



A: Coastal wetland area normalized by shoreline length. Wetlands area derived from the U.S. National Wetlands Inventory. **B:** Stn-30p global delineated watersheds colored by coastal typology of the river mouth (Dürr and Laruelle 2011). “Endo”, meaning Endorheic, river mouths were excluded from this study. **C:** Elevation based on the ETOPO1 dataset. **D:** Roughness (change in meters elevation) derived from the ETOPO1 dataset. Shorelines overlaid to draw attention to continental margins.

Figure 1.2-Climate Variables:



A: Average surface temperature from 1979-1999. Shoreline added for visualization. **B:** Average annual precipitation 1979-1999. Shoreline added for visualization. **C:** M2 (semi-diurnal contribution) tidal constituent. **D:** Offshore wave energy density.

1.2.2 Data Extraction and Manipulation

Coastal sediment flux is among the geomorphological covariates expected to affect coastal wetland abundance. Spatially explicit data and models were not immediately available, so it was necessary to develop a new estimate of continental sediment flux to the ocean. For 766 rivers, records of river mouth location, total suspended sediment flux to the ocean (MT/y), basin

area (1000s km²), and “elevation category” (an ordered factor in the table) were taken from the Milliman and Farnsworth global river database and were used in a regression analysis to project sediment flux at unmeasured locations.

Although the full Milliman and Farnsworth database is larger, this selection comprised complete cases of all attributes of interest. Where “Pre Dam” suspended sediment flux values were supplied, they were substituted for this analysis. Categorical elevations (as used in Milliman and Syvitski 1992 and others; Table 1.2) were chosen over “Maximum Elevation” measurements due to the low resolution of reported values. In many cases, reported elevations were simply the cutoff values for the categories. Additionally, “Coastal Plain” and “Lowland” categories were combined for regression due to the paucity of “Coastal Plain” samples. The data set also reports latitudes and longitudes for river mouths. These locations were used to extract underlying raster values for precipitation, temperature, and roughness from corresponding datasets described earlier.

Table 1.2 Watershed Elevation Categories (Milliman and Syvitski 1992)-

Category	Maximum Elevation	# Samples
Coastal Plain	< 100 m	19
Lowland	100 - 500 m	105
Upland	500 - 1000 m	159
Mountain	1000 - 3000 m	402
High Mountain	> 3000 m	81

For a global coverage of sediment flux to the coastal ocean, the Stn-30p delineated watersheds and associated mouths (Vörösmarty and Fekete 2011) are used as stand-ins for the actual river basins, as done by others (Syvitski and Milliman 2007). Elevation category was determined by extracting the maximum value of the ETOPO1 raster contained by the basin

polygon, then categorizing the elevation value using the previously mentioned cut off values. Basin areas were reported in the original dataset (Vörösmarty and Fekete 2011), and additional attributes (temperature, precipitation, and roughness) were extracted to the spatial points of the river mouths. These assembled predictors were then used as input data for a regression model based on the Milliman and Farnsworth data.

Wetland area and spatial covariates were extracted to 2° square spatial bins intersecting with the shoreline. The bins and all spatial fields were projected to Mollweide equal area before extraction. Values collected for the climate variables and roughness are binned averages. The value for wetland area is total intersecting area. Total transported sediment within each bin is the sum of predicted values found in exorheic Stn-30p river mouth points intersecting with each bin. The length of shoreline is the sum of the Euclidean distances between consecutive vertices of the shoreline segment intersecting with the bin. It is uncertain how this estimated length will be impacted by resolution effects (Mandelbrot 1967). Wetland area and total suspended sediment values were both divided by shoreline length within each bin to normalize for differences in coverage between bins. For this study, the normalized wetland area is referred to as “Marsh Width”.

1.2.3 Statistical and Computational Methods

Suspended sediment yield and wetland abundance were both analyzed using generalized additive models (GAMs) (Wood 2006; Hastie and Tibshirani 2009) using the “mgcv” package in R (Wood 2011; Wood 2004; Wood 2006; Wood 2003; Wood 2000). This approach was selected because both sediment yield and wetland abundance can demonstrate nonlinear response with respect to their regressors, and GAMs (unlike multiple linear regression, which has constant coefficients) vary in their response as regressor values change. Interactions between regressors are modeled in the GAM framework using tensor product smooths. A single regressor is a

spline, while a tensor smooth is a surface. These surface interaction terms (e.g. Fig. 1.6A,B; Fig. 1.8A,B,C) are not simply sums of the two terms' influence on the model. Instead, they demonstrate the unique relative impact on the model each potential pairing would have on the outcome.

Optimal model selection was selected based on minimum AIC and with the further constraint that all regressor terms be statistically significant based on Wald like tests (Wood 2006). The optimal selected model for sediment yield was used to make worldwide predictions of sediment flux to the ocean using river attributes of simulated watersheds (Stn-30p). These predicted values were used both to determine regional sediment yields adjacent to estuaries of interest, as well as to make a prediction of global cumulative sediment flux

All statistical and computational work was performed with the R statistical computing language v. 3.3.0 (R Core Team 2016). Geospatial operations were carried out using the *sp*, *maptools*, *rgdal*, and *raster* packages (Pebesma and Bivand 2005; Bivand et al., 2013; Bivand and Lewin-Koh 2014; Bivand et al., 2014; Hijmans 2014).

1.3 Results

1.3.1 Descriptive Statistics

131 bins of the U.S. coastline were characterized by extraction of spatial covariates. The total area of coastal wetlands measured from the estuarine emergent wetlands data set was less than 37000 km². Based on direct marsh inventories for the U.S., the majority of that area is salt marsh (Chmura et al., 2003). Based on the description provided by the National Wetlands Inventory, most of the remainder is probably sedimentary structures. Bins around Hawai'i had exceptionally low values for marsh width (Fig. 1.1A). This accounts for the appearance of especially flat linear regressions across all variables (Fig. 1.4) due to the effects on aspect ratio.

A measurement of bivariate correlation using the non-parametric Kendall's τ coefficient (Table 1.3) shows statistically significant relationships between marsh width and all spatial covariates except the M2 tidal constituent and shoreline-normalized annual sediment flux. Results of the sediment flux projection are in the next section.

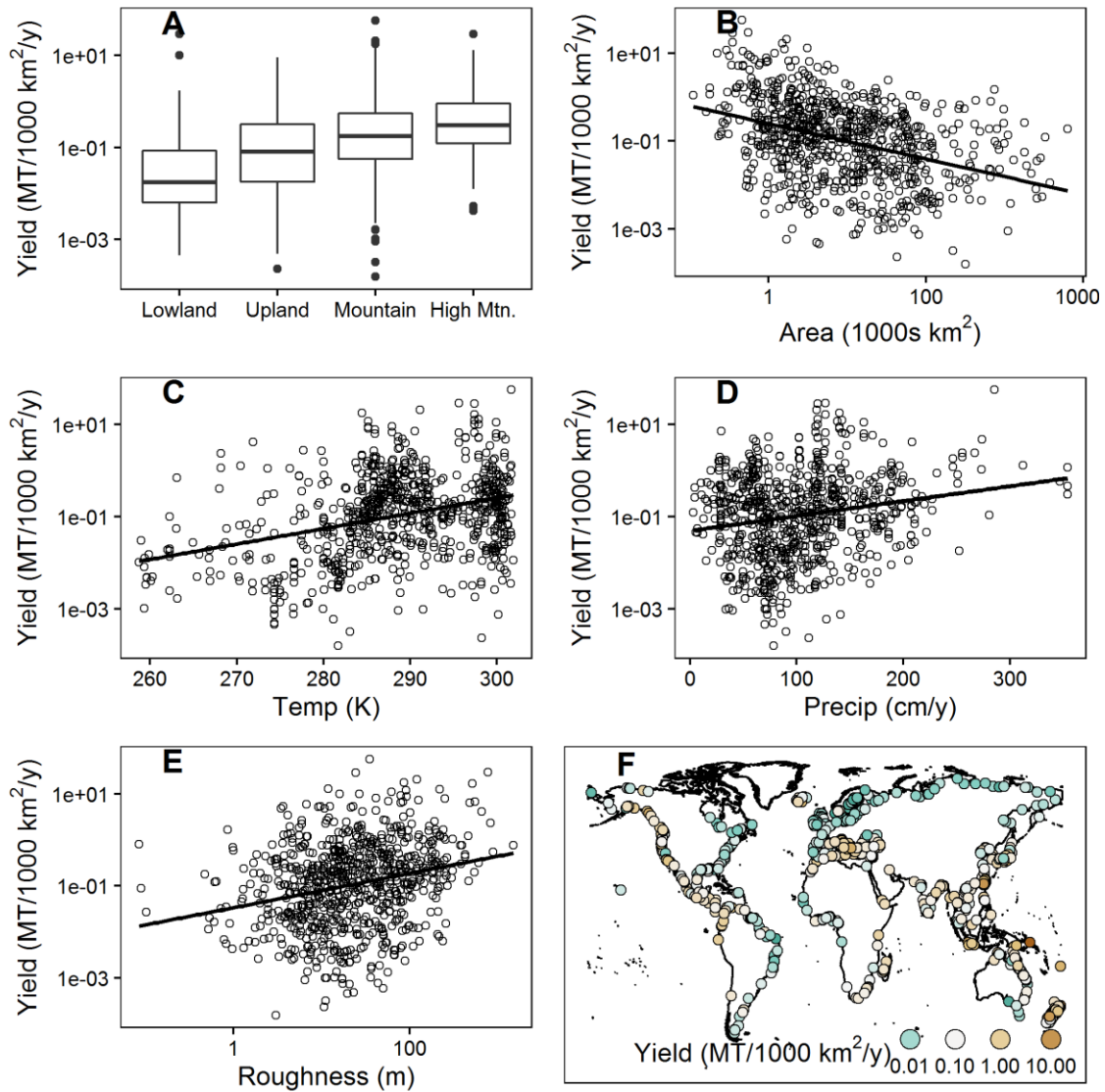
Suspended sediment yield measurements in the 766 Milliman and Farnsworth river mouths showed statistically significant correlations with all covariates. In most cases, correlation values, though statistically significant, were relatively modest in their magnitudes. Increases in river mouth roughness were correlated with higher sediment yields, but maximum elevation category also was related to increases in yield (Fig. 1.3A). Since maximum elevation can be far from the mouth, this demonstrates that fluvial sediment flux to the ocean is a product of both local and regional processes.

Table 1.3-Bivariate Correlation:

	Marsh Width		Sediment Yield	
	τ	p	τ	p
Area	-	-	-0.26	< .001
Temperature	0.15	< .05	0.2	< .001
Precipitation	0.12	< .05	0.1	< .001
Roughness	-0.34	< .001	0.17	< .001
M2	0.015	n.s.	-	-
Wave Energy	-0.2	< .001	-	-
Sediment/Shore	0.08	n.s.	-	-

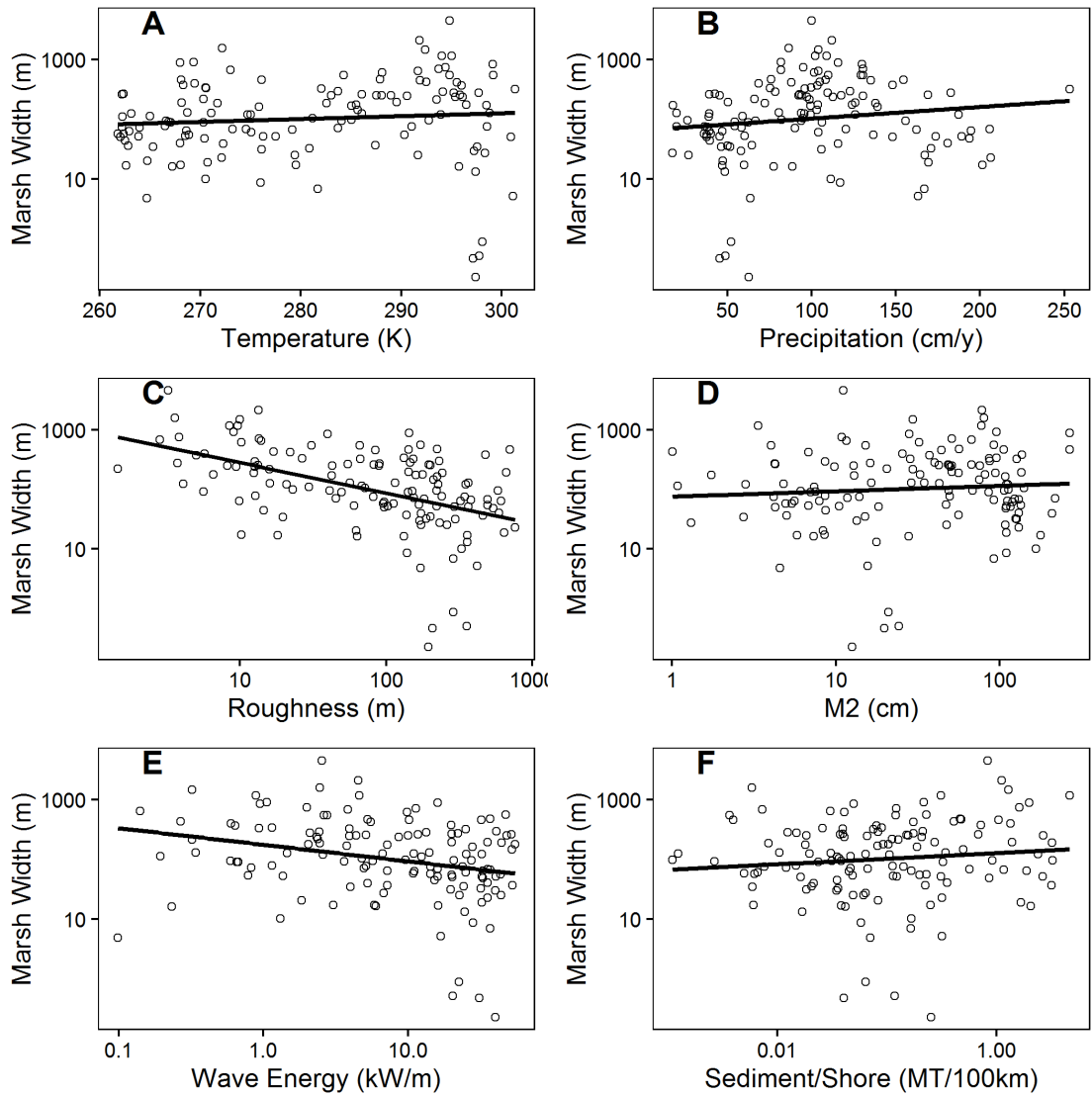
Nonparametric correlation measurements for marsh width and sediment yield vs. spatial covariates. P-values are based on the null hypothesis that $\tau = 0$.

Figure 1.3-Sediment Yield Descriptive Responses:



A: A box and whisker plot of suspended sediment yield vs. elevation category using the categories from table 1.2 with coastal plain and lowland included in the same category. **B-E:** Bivariate responses between yield and spatial features. Linear regressions are for visualization purposes to show the extent of correlation. **F:** Map of individual points from the Milliman and Farnsworth dataset colored by yield. Shoreline is added to assist visualization.

Figure 1.4-Marsh Width Descriptive Responses:



A-F: Bivariate responses between spatial covariates and marsh width. Linear regressions are added to aid visualization of correlation.

1.3.2 Suspended Sediment Flux Regression and Validation

The optimal regression model for sediment yield was the sum of three smoothed terms and one constant term:

$$E(\text{Yield})=f(\text{Area})+f(\text{Roughness})+f(\text{Precip,Temp})+ f(\text{lat, long})+\text{Elevation}$$

The regression has an adjusted r^2 of .6, shows normal residual errors (Fig. 1.5B) and a consistently proportionate relationship with known values (Fig. 1.5A). The interaction of Temperature and Precipitation was parameterized as a tensor spline with a cubic regression spline basis. Area and Roughness terms had cubic shrinkage spline bases, while Elevation classification was parameterized with an ordinal factor. To model spatial autocorrelation not captured by the other features, a thin plate regression spline depending on latitude and longitude was added.

As with other linear models, the predicted value is based on the sum of its terms. Instead of constant slopes, however, the effect of each variable on the prediction varies depending on its value. Since sediment yield was log-transformed for the regression, the value of each additive term will not be immediately intuitive. Looking at each smooth term's contribution to the predicted value of sediment yield (Fig. 1.6), consider its relative influence on the prediction and whether it adds to or subtracts from the prediction. The contributions of basin area and roughness are almost linear (Fig. 1.6C,D), and follow an intuitive pattern that parallels the actual trends in the data (Fig. 1.3B,E).

The interaction between temperature and precipitation (Fig. 1.6A) indicates that rising temperature at low precipitations leads to modest increases in sediment yield. When both temperature and precipitation are high, sediment yield is especially increased. The spatial field

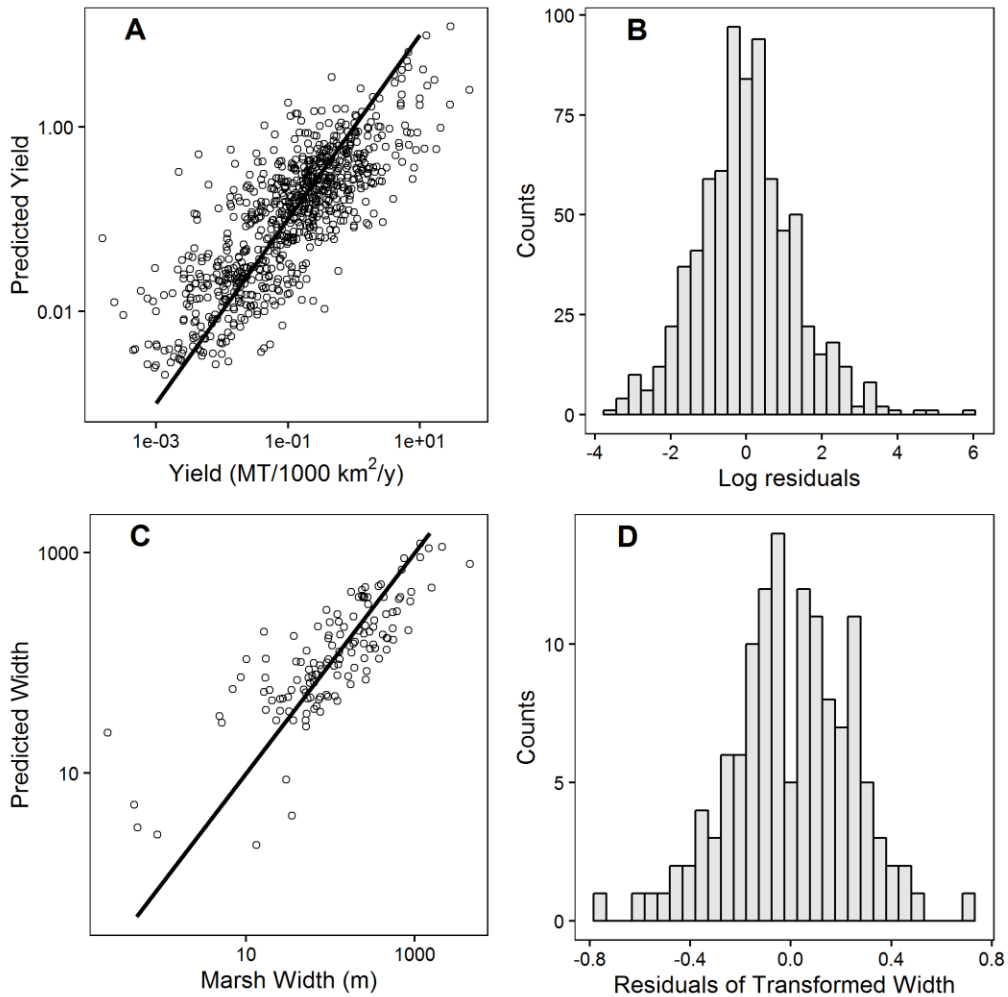
(Fig. 1.6B) shows higher term values along the Pacific Rim and lower values around the Atlantic, possibly capturing tectonic effects.

Sampling coverage is especially important when extrapolating from the model. For instance, there are very few points in regions of high precipitation but low temperature (Fig. 1.6A), possibly leading the model to predict unreasonably high values for that type of climate. Since the suspended sediment regression model is being used to generate data at unmeasured sites for this study, its representativeness needed to be evaluated. The feature space of the river mouths from Stn-30p and the Milliman and Farnsworth data set is shown in a principal components analysis (Fig. 1.7C) where the first two principal components explain the majority of the variance. The convex hull (in grey) is a region containing all the points from the Milliman and Farnsworth data set, while the cloud of points represents the nearly 6000 river mouths of Stn-30p. Two point clouds (red and blue) largely stand outside this convex hull, showing that the combination of their attributes are especially distinctive from the features represented in the training data.

Points from both clouds have the capacity to show high coefficients of variation in their estimated values for sediment yield (Fig. 1.7A), because they are in a region of the regression with broad confidence intervals. Spatially (Fig. 1.7B), the two regions largely line up with arctic watersheds (blue) and equatorial islands (red). Looking at the PC loadings (Fig. 1.7C), these equatorial river mouths have low basin area, high temperature, high precipitation, and high roughness. Since they stand at the extreme boundaries of several additive terms in the regression, the predicted yield values for these rivers are impossibly high (Fig. 1.7A). With the exception of northern Alaska, most of these problematic rivers are not in the United States, so the extrapolated river mouths used in this study should be representative. Furthermore, if the five

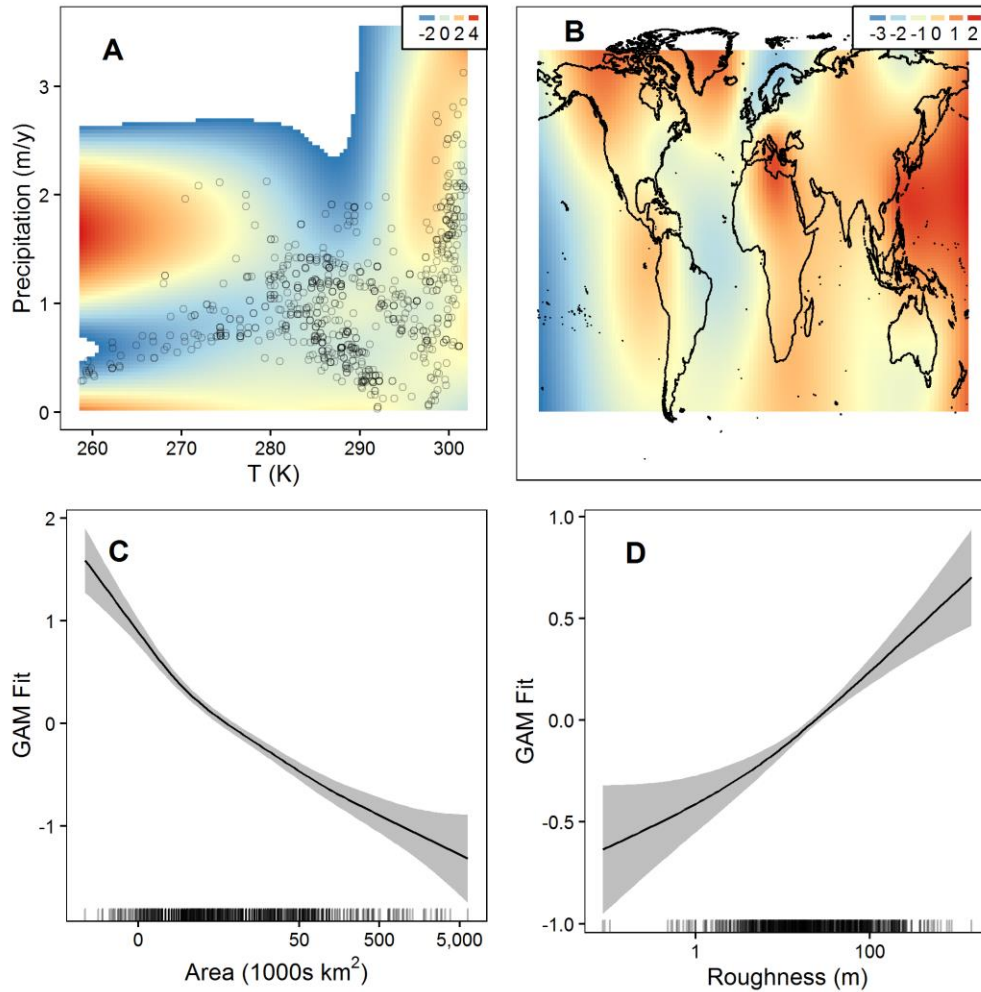
highest estimates of suspended sediment yield are removed from the prediction dataset, and our predictions are refined to exorheic basins, the sediment global flux estimate is comparable to others in the literature (Fig. 1.7D).

Figure 1.5-Diagnostic Charts for Regressions:



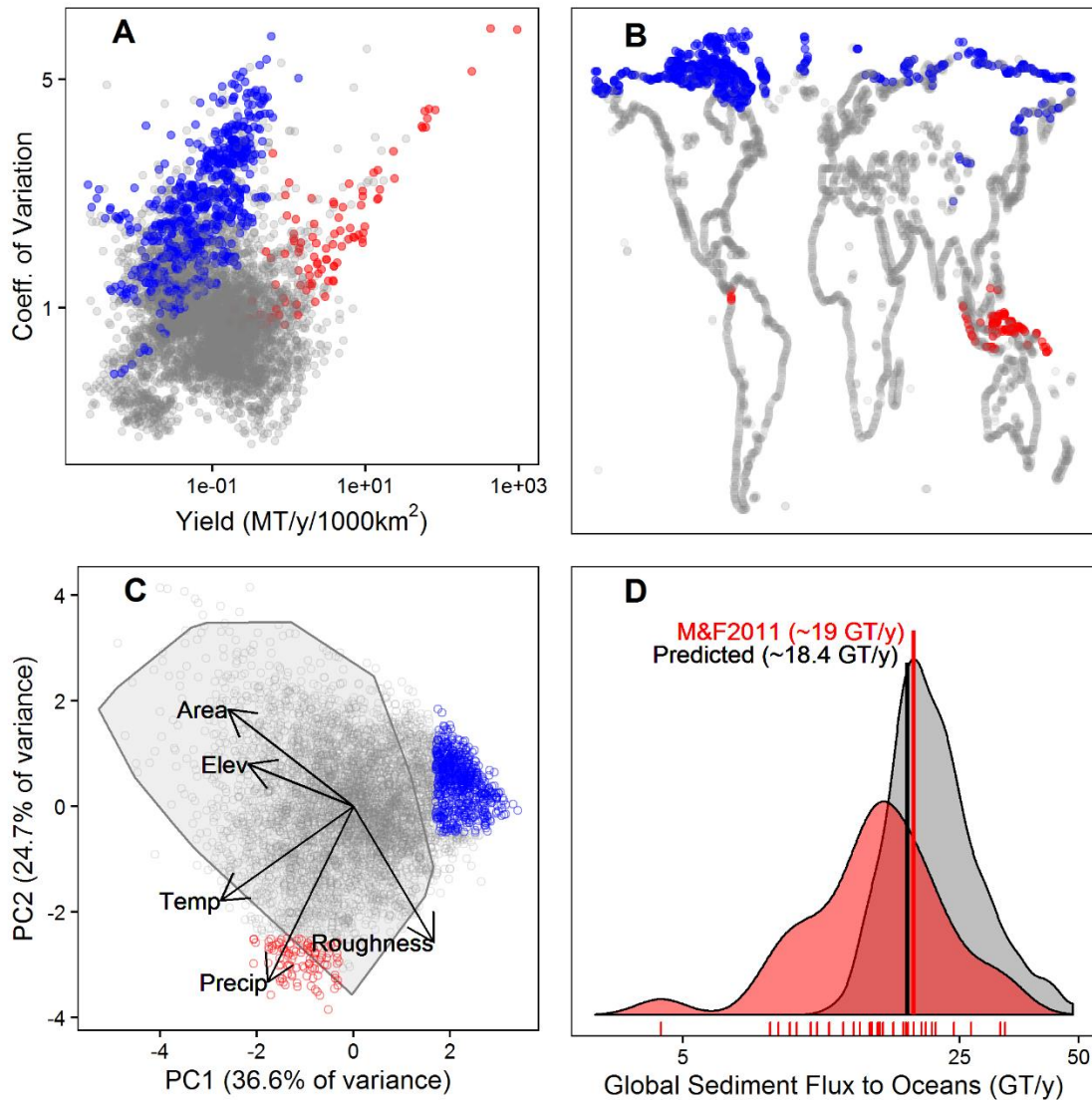
A: Actual yield measurements from Milliman and Farnsworth 2012 vs. predicted yields vs. regression. 1:1 values are along the black line. **B:** Histogram showing the distribution of predicted $\log(\text{Yield}) - \log(\text{Yield})$. The depended variable was transformed for regression. This is why the scale is different. **C:** Actual values of marsh width vs. predicted values using regression. 1:1 is represented by the black line. **D:** Histogram showing the distribution of width residuals after predicted and measured values were transformed using the same Box-Cox coefficient. Again, the dependent variable was transformed for regression.

Figure 1.6-GAM Terms for Sediment Yield Regression:



A: The Temperature & Precipitation interaction term. Legend values (like ‘GAM Fit’ for C and D) are relative addition or subtraction to the predicted value of sediment yield. Points are the Milliman and Farnsworth river mouths used as training data. **B:** Spatial interaction term. Legend values follow the same rules. Shorelines were added for visualization purposes. **C:** Basin area vs. GAM term value. The rugplot shows the distribution of values in the training data. **D:** Roughness vs. GAM term.

Figure 1.7-Representativeness of the Suspended Sediment Estimate:



A: Coefficient of variation for each estimate of suspended sediment yield vs. the estimated value of Yield. Colored points are the same as in B and C. **B:** Spatial distribution of highlighted points. **C:** Principal components analysis of both Milliman and Farnsworth 2012 points and the Stn-30p delineated river mouths based on extracted features. A convex hull contains the Milliman and Farnsworth points. Stn-30p points standing largely outside this region in the feature space were delineated using arbitrary values along the first and second principal component. Component loadings are visualized based on the direction and length of the labeled arrows. **D:** In red: A red kernel density smooth (with rugplot below) showing the distribution of estimates in the literature (gathered by Willenbring et al., 2013) of terrestrial sediment flux to the world oceans. Milliman and Farnsworth 2013 estimate is lined up with the red line segment. The cumulative estimate from this study (excluding top five highest yield sites) is in black with the 95% posterior probability interval in grey.

1.3.3 Wetland Abundance Regression

The optimal regression model for marsh width was the sum of four smoothed terms:

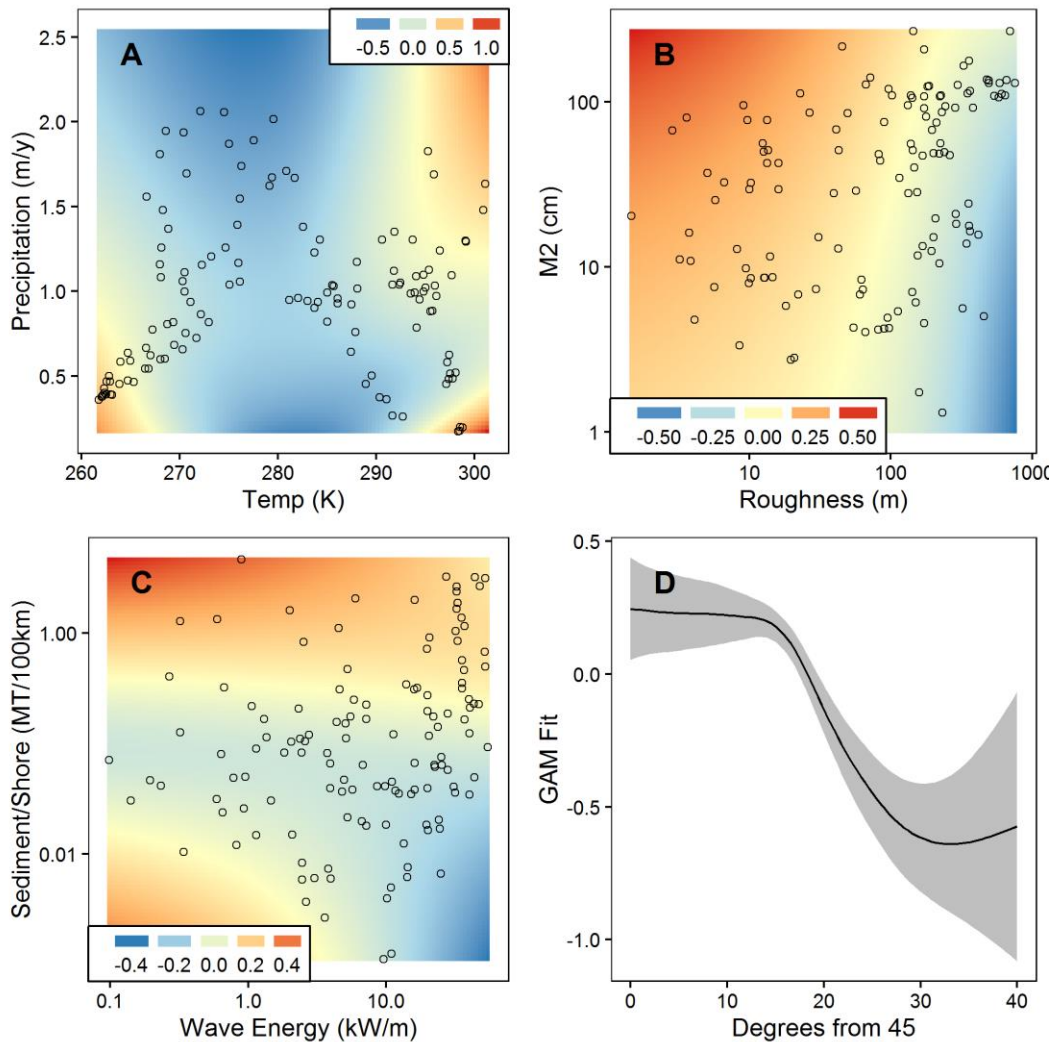
$$E(\text{Width})=f(\text{Waves}, \text{TSS})+f(\text{Roughness}, \text{M2})+f(\text{Precip}, \text{Temp})+ f(45 - \text{abs}(\text{lat}))$$

The regression has an adjusted r^2 of .58 with normal residual errors (Fig. 1.5D) and is in consistent proportion with known values (Fig. 1.5C). All three interaction terms were parameterized as a tensor spline with a cubic regression spline basis. The latitude term has a cubic shrinkage spline basis, and is meant to parameterize distance from the temperate region.

The width of coastal wetlands, as previously stated, is a shore-length normalized term for wetland abundance. This regression model of width was the most effective at explaining variation out of a set of other candidate regression models which tested the ambient features as individual smooths and as different sets of interactions. Marsh width's strong bivariate trends with respect to wave energy and roughness (Table 1.3) manifest themselves in the trend surfaces of their interaction terms (Fig. 1.8B,C), with consistently decreasing contributions to marsh width as their values increase. Shore-length normalized flux of terrestrial suspended sediment supply to the ocean, despite lacking significant bivariate correlation with marsh width (Table 1.3), apparently contributes to marsh width when present above a threshold quantity (Fig. 1.8C), but decreases in its contribution in a varying manner with respect to wave energy climate.

It is important to note that each term, while statistically significant, does not necessarily indicate substantial magnitudes of influence from each morphological parameter. M2 tidal component, for instance, does not exert a substantial change on its interaction term with Roughness except at relatively high magnitudes (Fig. 1.8B). Furthermore, interactions between features, while suggestive of interactions on the landscape-level, do not guarantee mechanistically meaningful connections between terms. Since the M2 tidal constituent is not

Figure 1.8-GAM Terms for Coastal Wetland Abundance:



Displayed is the variation in the relative contribution of each GAM term to wetland abundance if all other terms were held constant. Individual points are the values from the gridded coastlines containing National Wetlands Inventory values. **A:** GAM interaction term for Temperature & Precipitation. **B:** M2 & Roughness **C:** Wave energy density & Annual terrestrial sediment flux to the ocean normalized by shoreline length **D:** Distance from the nearest 45th parallel

strongly representative of the mixed tidal regime of the Pacific coast, it is likely that the true response of marsh width to tidal energy is not fully described here. Additionally, the latitude term, as a predictor of distance from the temperate zone, is expected to co-vary substantially with temperature and precipitation (Fig. 1.8A). This may account for the apparent lack of consistent

trends within the interaction term between temperature and precipitation (Fig. 1.8A), indicating that collinearity with latitude overwrites the effect of explicit climate variables on the regression model.

1.4 Discussion

The lack of pronounced correlations between wetland abundance and most geomorphological features indicates that wetlands exist and persist under a gradual continuum of influences. Furthermore, the apparent interactions between variables demonstrate the complexity of the system. Based on bivariate responses (Table 1.3), the strongest individual covariates are roughness and wave energy density. If we take a broader interpretation of what these covariates signify, roughness largely measures the proximity of the shoreline to the shelf break, and is an indicator of accommodation space. Wave energy density measures the potential wave energy in the absence of fetch limitation and bottom drag. These two features represent a shoreline's capacity to store sediment and its potential erosional climate respectively. In addition to latitude, these two variables have a much larger apparent influence on wetland abundance than fluvial sediment availability. Despite each spatial feature's subtle influence, it is clear that processes and features local to the estuary have the majority of apparent influence on wetland abundance.

1.4.1 Estuarine vs. Fluvial Processes

The effect of the "estuarine filter" buffering sediment transport from terrestrial systems to marine ones is a well-recognized phenomenon, and is the subject of ongoing research by groups attempting to spatially couple large scale terrestrial and marine systems (Dürr et al., 2011; Laruelle et al., 2013). Although these efforts attempt to connect interfacing systems (fluvial and marine), they have not necessarily characterized the effect of local processes acting at the

estuarine interface. The results from this large scale study imply a preeminence of local geomorphological processes in determining cumulative coastal wetland inventories.

The influence of local geomorphology on large scale sediment transport has long been apparent in continental systems. The importance of river mouth relief and climate-related erosion explains the exceptional sediment fluxes to the ocean in the small rivers of the East Indies (Milliman et al., 1999). On the other end of the size spectrum, it also explains the decline in sediment flux over the Amazon River's course. Sediment flux from the Andes outweighs sediment flux in the lower river at Obidos more than twofold (Aalto et al., 2006; Dunne et al., 1998), because the lower river has lower relief and therefore has less stream power. The fluvial sediment flux estimates derived in this study demonstrate the same significance of climate and topography at the rivers' mouths in hundreds of other locations all over the world. This study takes that intuition derived from terrestrial systems another step further downriver to demonstrate the importance of ambient coastal processes on dictating wetland abundance.

Past research in salt marshes has shown that sediment availability is certainly a factor in marsh accretion and expansion. New marshes frequently are structures resulting from recent sediment accumulation (Krull and Craft 2009; Mattheus et al., 2009; Cahoon et al., 2011), often built through sedimentary infilling of accommodation spaces such as estuaries (Kirwan et al., 2011) or crevasse splays (Cahoon et al., 2011). Accretion accelerates before the marsh forms, eventually producing an emergent sandbar or mudflat that is colonized by marsh grasses (Gunnell et al., 2013; Krull and Craft 2009). This rapid accretion continues through the marsh's incipience until it reaches a mature elevation (Pethick 1981).

Given the importance of sediment in initial marsh formation, it may be surprising that sediment flux to the ocean doesn't play a stronger role in overall wetland abundance. The

interaction between fluvial sediment flux and wave energy (Fig. 1.8C) suggests that there must be some threshold quantity of sediment available before it contributes to wetland abundance, but below that threshold and at moderate wave energies, sediment availability has no apparent effect on wetland abundance. The processes sustaining marshes are not necessarily the same ones that built the marsh in the first place, which may explain this ambivalent result across so many sites. Sediment-starved regions that previously were sediment-rich can host marshes that maintain themselves through vegetative accretion (Nyman et al., 2006). In the absence of extensive erosion, it is only due to prolonged sediment starvation and rapid sea level rise that these wetlands eventually disappear due to subsidence and vegetation die-off (Syvitski et al., 2009; Day et al., 2011). Consequently, there is an indeterminate lag period between a marsh's birth and demise regardless of sediment availability.

Higher wave energy environments demonstrate a more intuitive relationship of erosion and sedimentation offsetting each other (Fig. 1.8C). At higher sediment availabilities, increases in wave energy lead to less pronounced positive influence on wetland abundance. This may corroborate observations that over the course of marsh ontogeny, accretion rates are dependent on the effective shear stress on estuarine bottom sediments, strongly determining whether an emergent mudflat forms (Fagherazzi et al., 2006; Gunnell et al., 2013). At sites with lower incoming sediment and high wave energies, abundance is negatively affected.

The interaction between roughness and the semidiurnal tidal constituent (Fig. 1.8B) also suggest a potential role of the estuary as a sedimentary reservoir, which could forestall the effects of fluvial sediment starvation. If roughness is an index of shelf area (where low roughness indicates high accommodation space) and the M2 tidal constituent is part of a mechanism for redistribution of sediments onto emergent wetlands, then their interaction in the GAM model

makes intuitive sense. The tide's capacity to redistribute sediments retained in the estuary is rendered moot in a high roughness estuary that doesn't have the capacity to retain sediment. This interaction demonstrates the importance of long term estuarine sedimentary processes in maintaining wetland abundance. If terrestrial sediment supply were the overwhelmingly dominant means of sustaining sediment concentrations in estuarine waters, this interaction would not be a significant factor.

1.4.2 Knowledge Gaps in a Changing World

The importance of climate on coastal wetland abundance appears to be the most equivocal of the regression components (Fig. 1.8A). The collinearity of the climate variables with the distance from the temperate zone (Fig. 1.8D) means that the structure of the temperature vs. precipitation interaction is harder to interpret. The positive effect on abundance presented by high temperature and high precipitation mirrors the same interaction shown in the sediment yield regression, where wet tropical rivers have high sediment yields. Perhaps this is a remnant of the influence of sediment availability. Negative influence at high precipitation sites of intermediate temperatures suggest that stormy temperate climates are connected to decreased abundance.

Seasonal features have not been explored in this study, but there is abundant evidence that seasonal resuspension of sediments occurs in a wide variety of estuarine environments (Woodruff et al., 2001; Canuel et al., 1990; Corbett et al., 2004). Climate strongly influences terrestrial sediment fluxes, which in turn influence marsh abundance. Despite a strong relationship with respect to temperate latitudes, direct causal relationships between marsh abundance and climate can't be assessed in this study. Many spatial relationships that are a consequence of global anthropogenic change can't be appropriately measured in this manner

either because the datasets don't yet exist, or the processes of interest haven't quite happened yet.

This study appears to demonstrate that fluvial sediment flux to the ocean has a nuanced effect on coastal wetland abundance. The combination of extensive erosion and impoundment within the basins of major rivers has led to extreme historical variation in sediment flux (Syvitski and Kettner 2011; Syvitski and Milliman 2007). Smaller coastal rivers (100 and 3000 km² in basin area), despite making up ~94% of all individual rivers that drain into the ocean (Milliman and Farnsworth 2011), are not well-represented in the global data set (e.g. "Coastal Plain" rivers in Table 1.2). How these smaller rivers interact with the estuarine system and influence the available reservoir of sediment is unmeasured. Their very existence lies outside the resolution of the delineated watersheds we used in this study.

Climatological consequences such as accelerated relative sea level rise are expected to affect wetland abundance (Kirwan et al., 2010), but their consequence can't be measured using these contemporary data sets. Similarly, the ecological effect of competition between mangrove and marsh ecosystems can't be observed using U.S. inventories due to the very small contemporary overlap in geographic range (Giri et al., 2010). Changes in sediment supply in the arctic regions due to climate change can't reliably be predicted with the current global sediment data set either. This is partly because the transformation those landscapes will experience has not occurred since the last ice age ended, and naturally has not been measured. If arctic watersheds behaved similarly to other watersheds, they still would not be reliably estimated with these methods because the arctic region stands outside the feature-space of sites that have actually been sampled (Fig. 1.7C). As it stands, there is not enough data to predict the large

scale consequences of global climate change on sediment flux to the oceans or wetland inventories because the coming changes are unique and the existing datasets are sparse.

1.5 Conclusions

Perhaps the most important insights gleaned over the course of this study were with respect to terrestrial sediment flux to the global oceans. Vast regions of the world's oceans have contributing watersheds that stand outside the geomorphologically relevant feature-space of currently measured watersheds. Although these regions generally fail to intersect with the coastal United States, this lack of baseline characterization of contemporary sediment flux calls into question our capacity to predict sediment supply to the world's oceans in both the present and future.

The second important observation with respect to terrestrial sediment flux was its weak connection to wetland abundance along U.S. coastlines. The addition of terrestrial sediment only leads to increases in marsh abundance when it is present in large quantities. Vertical accretion properties particular to marsh systems as well as the role of roughness and tidal forcing to redistribute sediment within an existing reservoir may both play a larger part in sustaining marsh sedimentation over longer timescales.

Due to the nature of global change, it is impossible to predict many of the impacts on this system using this manner of study. In a consistent climate and sea level rise scenario, the processes that led to present abundance would inevitably lead to some quasi-equilibrium inventory of coastal wetlands. Nonetheless, the effects of global accelerated sea level rise and global warming lie well outside the bounds of our existing observations. This problem is exacerbated by the lack of a baseline wetland inventory or extensive sampling of sediment fluxes.

REFERENCES

- Aalto, R., T. Dunne, and J.L. Guyot. "Geomorphic controls on Andean denudation rates." *The Journal of Geology* 114.1 (2006): 85-99.
- Allen, J. Morphodynamics of Holocene Salt marshes: a review sketch from the Atlantic and Southern North Sea coasts of Europe. *Quaternary Sci. Rev.* **19**, 1839–1840 (2000).
- Amante, C., and B.W. Eakins. 2009. *ETOPO1 1 Arc-Minute Global Relief Model: Procedures, Data Sources and Analysis*. NOAA Technical Memorandum NESDIS NGDC-24. National Geophysical Data Center, NOAA. <http://dx.doi.org/10.7289/V5C8276M/>.
- Bivand, R.S., E. Pebesma, and V. Gomez-Rubio. 2013. *Applied Spatial Data Analysis with R, Second Edition*. Springer, NY. <http://www.asdar-book.org/>.
- Bivand, R., and N. Lewin-Koh. 2014. *Maptools: Tools for Reading and Handling Spatial Objects*. <http://CRAN.R-project.org/package=maptools>.
- Bivand, R., T. Keitt, and B. Rowlingson. 2014. *Rgdal: Bindings for the Geospatial Data Abstraction Library*. <http://CRAN.R-project.org/package=rgdal>.
- Brown, M. 2012. "Marine Data Literacy : Providing Instruction for Handling (Managing, Converting, Analyzing and Displaying) Oceanographic Station Data, Marine Meteorological Data, GIS-Compatible Marine and Coastal Data, and Mapped Remote Sensing Imagery." http://www.marinedataliteracy.org/grids/360_to_180.htm.
- Cahoon, D. R. and D.J. Reed. Relationships among marsh surface topography, hydroperiod, and soil accretion in a deteriorating Louisiana salt marsh. *J. Coastal Res.* **11**, 357–369 (1995).
- Cahoon, D. R., D.A. White, and J.C. Lynch. Sediment infilling and wetland formation dynamics in an active crevasse splay of the Mississippi River delta. *Geomorphology* **131**, 57–68 (2011).
- Canuel, E. A., C.S. Martens, and L.K. Benninger. "Seasonal variations in ^7Be activity in the sediments of Cape Lookout Bight, North Carolina." *Geochimica et Cosmochimica Acta* 54.1 (1990): 237-245.
- Chmura, G. and S. Anisfeld. Global carbon sequestration in tidal, saline wetland soils. *Global Biogeochem. Cy.* **17**, (2003).
- Corbett, D.R., B. McKee, and D. Duncan. "An evaluation of mobile mud dynamics in the Mississippi River deltaic region." *Marine Geology* 209.1 (2004): 91-112.
- Costanza, R. *et al.* The value of the world's ecosystem services and natural capital. *Nature* **387**, 253–260 (1997).

- Dahl, T.E. 2011. Status and trends of wetlands in the conterminous United States 2004 to 2009. U.S. Department of the Interior; Fish and Wildlife Service, Washington, D.C. 108 pp.
- Day, J. W. *et al.* Vegetation death and rapid loss of surface elevation in two contrasting Mississippi delta salt marshes: The role of sedimentation, autocompaction and sea-level rise. *Ecol. Eng.* **37**, 229–240 (2011).
- Duarte, C., J.J. Middelburg, and N. Caraco. Major role of marine vegetation on the oceanic carbon cycle. *Biogeosciences* **2**, 1–8 (2005).
- Dunne, T., et al. "Exchanges of sediment between the flood plain and channel of the Amazon River in Brazil." *Geological Society of America Bulletin* 110.4 (1998): 450-467.
- Dürr, H. H., and G.G. Laruelle. 2011. "Global Coastal Typology." Geotypes.net. <http://geotypes.net/downloads.html>.
- Dürr, H.H., G.G. Laruelle, C.M. van Kempen, C.P. Slomp, M. Meybeck, and H. Middelkoop. 2011. "Worldwide Typology of Nearshore Coastal Systems: Defining the Estuarine Filter of River Inputs to the Oceans." *Estuaries and Coasts* 34 (3). Springer Science Business Media: 441–58. doi:[10.1007/s12237-011-9381-y](https://doi.org/10.1007/s12237-011-9381-y).
- Fagherazzi, S., et al. "Critical bifurcation of shallow microtidal landforms in tidal flats and salt marshes." *Proceedings of the National Academy of Sciences* 103.22 (2006): 8337-8341.
- Fagherazzi, S. 2013. "The Ephemeral Life of a Salt Marsh." *Geology* 41 (8). Geological Society of America: 943–44. doi:[10.1130/focus082013.1](https://doi.org/10.1130/focus082013.1).
- Fagherazzi, S., M.L. Kirwan, S.M. Mudd, G.R. Guntenspergen, S. Temmerman, A. Dand, J. van de Koppel, J.M. Rybczyk, E. Reyes, C. Craft, and J. Clough. 2012. "Numerical Models of Salt Marsh Evolution: Ecological, Geomorphic, and Climatic Factors." *Rev. Geophys.* 50 (1). Wiley-Blackwell. doi:[10.1029/2011rg000359](https://doi.org/10.1029/2011rg000359).
- Giri, C., E. Ochieng, L. L. Tieszen, Z. Zhu, A. Singh, T. Loveland, J. Masek, and N. Duke. 2010. "Status and Distribution of Mangrove Forests of the World Using Earth Observation Satellite Data." *Global Ecology and Biogeography* 20 (1). Wiley-Blackwell: 154–59. doi:[10.1111/j.1466-8238.2010.00584.x](https://doi.org/10.1111/j.1466-8238.2010.00584.x).
- Grimsditch, G., J. Alder, T. Nakamura, R. Kenchington, and J. Tamelander. The blue carbon special edition – Introduction and overview. *Ocean Coast. Manage.* **1**, 1–4 (2012).
- Hastie, T., R. Tibshirani, and J. Friedman. 2009. *The Elements of Statistical Learning*. Springer New York. doi:[10.1007/978-0-387-84858-7](https://doi.org/10.1007/978-0-387-84858-7).
- Hijmans, R.J. 2014. *Raster: Raster: Geographic Data Analysis and Modeling*. <http://CRAN.R-project.org/package=raster>.

- Hopkinson, C.S., W. Cai, and X. Hu. 2012. "Carbon Sequestration in Wetland Dominated Coastal Systems a Global Sink of Rapidly Diminishing Magnitude." *Current Opinion in Environmental Sustainability* 4 (2). Elsevier BV: 186–94. doi:[10.1016/j.cosust.2012.03.005](https://doi.org/10.1016/j.cosust.2012.03.005).
- Kirwan, M.L., G.R. Guntenspergen, A. Dand, J.T. Morris, S.M. Mudd, and S. Temmerman. 2010. "Limits on the Adaptability of Coastal Marshes to Rising Sea Level." *Geophys. Res. Lett.* 37 (23). Wiley-Blackwell. doi:[10.1029/2010gl045489](https://doi.org/10.1029/2010gl045489).
- Kirwan, M. L., A. B. Murray, J. P. Donnelly, and D. R. Corbett. 2011. "Rapid Wetland Expansion During European Settlement and Its Implication for Marsh Survival Under Modern Sediment Delivery Rates." *Geology* 39 (5). Geological Society of America: 507–10. doi:[10.1130/g31789.1](https://doi.org/10.1130/g31789.1).
- Kirwan, M.L., S. Temmerman, E.E. Skeeahan, G.R. Guntenspergen, and S. Fagherazzi. 2016. "Overestimation of Marsh Vulnerability to Sea Level Rise." *Nature Climate Change* 6 (3). Nature Publishing Group: 253–60. doi:[10.1038/nclimate2909](https://doi.org/10.1038/nclimate2909).
- Krull, K. and C. Craft. Ecosystem development of a sandbar emergent tidal marsh, Altamaha River Estuary, Georgia, USA. *Wetlands* 29, 314–322 (2009).
- Laruelle, G.G., et al. "Global multi-scale segmentation of continental and coastal waters from the watersheds to the continental margins." *Hydrology and Earth System Sciences* 17.5 (2013): 2029-2051.
- Mandelbrot, B.B., 1967. How long is the coast of Britain. *Science*, 156(3775), pp.636-638.
- Mattheus, C. R., A.B. Rodriguez, and B.A. McKee. Direct connectivity between upstream and downstream promotes rapid response of lower coastal-plain rivers to land-use change. *Geophys. Res. Lett.* 36, 1–6 (2009).
- Milliman, J.D., K.L. Farnsworth, and C.S. Albertin. "Flux and fate of fluvial sediments leaving large islands in the East Indies." *Journal of Sea Research* 41.1 (1999): 97-107.
- Milliman, J.D., and K.L. Farnsworth. 2011. *River Discharge to the Coastal Ocean*. Cambridge University Press (CUP). doi:[10.1017/cbo9780511781247](https://doi.org/10.1017/cbo9780511781247).
- Milliman, J.D. and K.L. Farnsworth. 2012. "Resources for River Discharge to the Coastal Ocean: A Global Synthesis." Cambridge University Press (CUP). <http://www.cambridge.org/us/academic/subjects/earth-and-environmental-science/geomorphology-and-physical-geography/river-discharge-coastal-ocean-global-synthesis>.
- Milliman, J.D., and J. Syvitski. "Geomorphic/tectonic control of sediment discharge to the ocean: the importance of small mountainous rivers." *The Journal of Geology* (1992): 525-544.

- Mudd, S.M., S.M. Howell, and J.T. Morris. 2009. "Impact of dynamic feedbacks between sedimentation, sea-level rise, and biomass production on near-surface marsh stratigraphy and carbon accumulation." *Estuarine, Coastal and Shelf Science* 82(3). Elsevier: 377-389. doi: [10.1080/15320380802547841](https://doi.org/10.1080/15320380802547841).
- Nyman, J.A., R.J. Walters, R.D. Delaune, and W.H. Patrick. 2006. "Marsh Vertical Accretion via Vegetative Growth." *Estuarine, Coastal and Shelf Science* 69 (3-4). Elsevier BV: 370–80. doi:[10.1016/j.ecss.2006.05.041](https://doi.org/10.1016/j.ecss.2006.05.041).
- NCAR-GIS-Program. 2012. "Climate Change Scenarios, Version 2.0. Community Climate System Model, June 2004 Version 3.0. (Http://www.cesm.ucar.edu/models/ccsm3.0/) Was Used to Derive Data Products." National Center for Atmospheric Research (NCAR) / University Corporation for Atmospheric Research (UCAR).
<http://www.gisclimatechange.org>.
- Nellemann, C. et al. *Blue carbon: the role of healthy oceans in binding carbon. Environment* 1–80 (Arendal, Norway, 2009). html: www.grida.no.
- NOAA. 2015. "Wave Watch III Version 2.22 Hindcast Reanalysis." National Centers for Environmental Prediction; Environmental Modeling Center Marine Modeling; Analysis Branch, 5830 University Research Court, College Park, MD 20740: National Oceanic; Atmospheric Administration (NOAA) / National Weather Service.
<http://polar.ncep.noaa.gov/waves/download.shtml?>
- Pebesma, E.J., and R.S. Bivand. 2005. "Classes and Methods for Spatial Data in R." *R News* 5 (2): 9–13. <http://CRAN.R-project.org/doc/Rnews/>.
- Pendleton, L. et al. Estimating Global "Blue Carbon" Emissions from Conversion and Degradation of Vegetated Coastal Ecosystems. *PLoS ONE* 7, e43542 (2012).
- Pethick, J. S. Long-term Accretion Rates on Tidal Salt Marshes. *J. Sediment. Petrol.* 51, 571–577 (1981).
- Ray, R.D. 1999. *A Global Ocean Tide Model from TOPEX/Poseidon Altimetry: GOT99*. 2. Tech. Memo. 209478. NASA.
- Schlining, B., A. Crosby, and R. Signell. 2014. "NCTOOLBOX a Matlab Toolbox for Working with Common Data Model Datasets." *GitHub Repository*. GitHub.
<https://github.com/nctoolbox/nctoolbox>.
- Syvitski, J. and J.D. Milliman. "Geology, geography, and humans battle for dominance over the delivery of fluvial sediment to the coastal ocean." *The Journal of Geology* 115.1 (2007): 1-19.
- Syvitski, J., et al. "Sinking deltas due to human activities." *Nature Geoscience* 2.10 (2009): 681-686.

- Syvitski, J., and A. Kettner. 2011. "Sediment Flux and the Anthropocene." *Philosophical Transactions of the Royal Society A: Mathematical, Physical and Engineering Sciences* 369 (1938). The Royal Society: 957–75. doi:[10.1098/rsta.2010.0329](https://doi.org/10.1098/rsta.2010.0329).
- Tolman, H.L. 2009. *User Manual and System Documentation of WAVEWATCH III Version 3.14*. NOAA / NWS / NCEP / MMAB. http://polar.ncep.noaa.gov/mmab/papers/tn276/MMAB_276.pdf.
- Trimble, S.W. 1977. "The Fallacy of Stream Equilibrium in Contemporary Denudation Studies." *American Journal of Science* 277(7): 876–87. doi:[10.2475/ajs.277.7.876](https://doi.org/10.2475/ajs.277.7.876).
- UNEP. 2014. "Global Estuary Database." 219 Huntingdon Road, Cambridge, UK: United Nations Environment Programme (UNEP) - World Conservation Monitoring Center (WCMC). <http://data.unep-wcmc.org/datasets/23>.
- U. S. Fish and Wildlife Service. 2016. National Wetlands Inventory website. U.S. Department of the Interior, Fish and Wildlife Service, Washington, D.C. <http://www.fws.gov/wetlands/>
- Vörösmarty, C.J., and B. Fekete. 2011. "ISLSCP II River Routing Data (STN-30p)." Edited by Forrest G. Hall, G. Collatz, B. Meeson, S. Los, E. Brown de Colstoun, and D. Landis. ISLSCP Initiative II Collection. Oak Ridge, TN, USA: Oak Ridge National Laboratory Distributed Active Archive Center. <http://dx.doi.org/10.3334/ORNLDAAAC/1005>.
- Wessel, P., and W. H. F. Smith, A Global Self-consistent, Hierarchical, High-resolution Shoreline Database, *J. Geophys. Res.*, 101, 8741-8743, 1996
- Willenbring, J.K., A.T. Codilean, and B. McElroy. "Earth is (mostly) flat: Apportionment of the flux of continental sediment over millennial time scales." *Geology* 41.3 (2013): 343-346.
- Wood, S. N. 2000. "Modelling and Smoothing Parameter Estimation with Multiple Quadratic Penalties." *Journal of the Royal Statistical Society (B)* 62 (2): 413–28.
- Wood, S. N. 2003. "Thin-Plate Regression Splines." *Journal of the Royal Statistical Society (B)* 65 (1): 95–114.
- Wood, S. N. 2004. "Stable and Efficient Multiple Smoothing Parameter Estimation for Generalized Additive Models." *Journal of the American Statistical Association* 99 (467): 673–86.
- Wood, S. N. 2011. "Fast Stable Restricted Maximum Likelihood and Marginal Likelihood Estimation of Semiparametric Generalized Linear Models." *Journal of the Royal Statistical Society (B)* 73 (1): 3–36.
- Wood, S.N. 2006. *Generalized Additive Models: An Introduction with R*. Chapman; Hall/CRC.
- Woodruff, J.D., W.R. Geyer, C.K. Sommerfield, and N.W. Driscoll (2001), Seasonal variation of sediment deposition in the Hudson River estuary, *Mar. Geol.*, 179, 105-119.

CHAPTER 2: AN ANALYSIS OF FLUVIAL SUSPENDED SEDIMENT RESPONSE TO URBANIZATION IN THE U.S. SOUTHERN PIEDMONT

2.1 Introduction

By the year 2050, the U.S. population is expected to grow by over 120 million (Passel and Cohn 2008), and much of that new population will reside in cities. Urban areas will draw intensely on local water resources while dramatically altering their surrounding hydrology (Grimm et al., 2008). Corridors connecting metropolitan centers will continue to experience development, creating what are called “Megapolitan” regions (Lang and Dhavale 2005; Lang and Nelson 2007). Extensive land-clearing and impervious surface-creation will lead to increased erosion and consequently to increased sediment loads within watersheds (Wolman 1967; Chin 2006). Since the majority of nutrients and trace metal contaminants are carried by the fluvial sediment load (Russell et al., 1998; Meybeck and Helmer 1989), the consequences of land development have a direct bearing on water quality. There is a strong conceptual basis to assume that urban growth impairs water quality. Nevertheless, consistent measurement of historical trends in water quality responding to urbanization have proven to be elusive, and tangible consequences of this urban migration are virtually unknown.

A lack of consistency in sediment yield response to urbanization is in part due to the complexity and transient nature of anthropogenic disturbance. Erosion and sediment transport temporarily increase as recently-cleared earth is exposed and progressively converted to impervious surfaces (Wolman 1967), with streams adjacent to urban development showing

sediment yields 45-300 times the expected yield at undisturbed reference sites (Chin 2006). In some cases, watershed-scale sediment yields may remain elevated as population continues to grow (Siakeu et al. 2004). This is not simply a case of increased sediment availability as a function of land-clearing, however. The proliferation of impervious surfaces alters the hydrology of the urban landscape and leads to a series of geomorphological adjustments (Leopold 1968). Soils downslope of impervious surfaces may be more susceptible to erosion (Pappas et al. 2008), and altered peak streamflow caused by rerouting of urban runoff often leads to channel adjustment (Trimble 1997). Meanwhile, establishment and enforcement of best management practices for sediment retention in recently-cleared areas constantly changes (Kaufman 2000). The resulting landscape-scale response to urbanization is the aggregation of several complex small-scale responses. Consequently, it is difficult to measure and mechanistically predict how fluvial sediment transport should respond to urban development.

Despite this being a relatively old problem, we are no closer to estimating the potential scale or long term trajectory of increased sediment yields due to erosion from urbanization. We are taking the first practical step to resolving this problem by attempting to measure it on the regional scale (the U.S. Southern Piedmont) and search for empirical relationships. The aggregated effects of the urban stream's complex sedimentary system were assumed to be integrated within the annual sediment fluxes of watersheds. These fluxes were compared to geographic indices of urbanization to see if there is a consistent connection between the human and natural components of this coupled system.

2.2 Methods

2.2.1 Regional Description:

By restricting sampling to the Piedmont, regional variables are expected to be standardized (e.g. climate, soil characteristics, and relief). The Piedmont has relatively high relief despite not being a mountainous region, and has historically contributed substantial sediment loads to the coastal plain and ocean (Benedetti et al., 2006). The region has additional significance because its historical land use change is emblematic of the broad trends facing most post-industrial urbanizing landscapes. From the early to mid-20th century, there was a transition from agricultural land use to reforestation (Trimble 1974). However, there has been a 92% increase in population from 1970 to 2010 (Napton et al. 2009), with recent deforestation to accommodate urban expansion (Drummond and Loveland 2010). If any region is expected to have landscape response to urbanizing land use change, it is the Piedmont.

Smaller watersheds were generally preferred so that sediment deposition would not substantially influence sediment yield estimates. Serial impoundment and alluvial storage increasingly diminish sediment yield as watershed size increases (Meade and Moody 2010; Milliman and Farnsworth 2011). Notable examples of sediment retention within the Piedmont due to impoundment are the Roanoke and Cape Fear Rivers (Meade 1982; Benedetti et al., 2006).

2.2.2 Gage Sites:

To provide a standardized frame of reference, this study defines the region known as “the Piedmont” to be equivalent to the EPA’s level III ecoregion bearing the same name (Omernik 1987). Spatial queries are based on the level III shapefile provided by the EPA (USEPA 2013). National Water Information System (NWIS) gage stations (USGS 2015) falling within this

region were chosen for study if the station's data inventory had a consistent record of mean daily streamflow and a history of recording suspended sediment concentration (parameter id: 80154). Data from the NWIS was queried using the "dataRetrieval" package in the R-Programming Language (Hirsch et al., 2015). The selected gages cover nearly decadal if not multi-decadal periods of measurement and are adjacent to areas of active urban development (e.g. Richmond, VA; Research Triangle, NC; Charlotte, NC; Atlanta, GA).

2.2.3 Fluvial Sediment Flux Estimation:

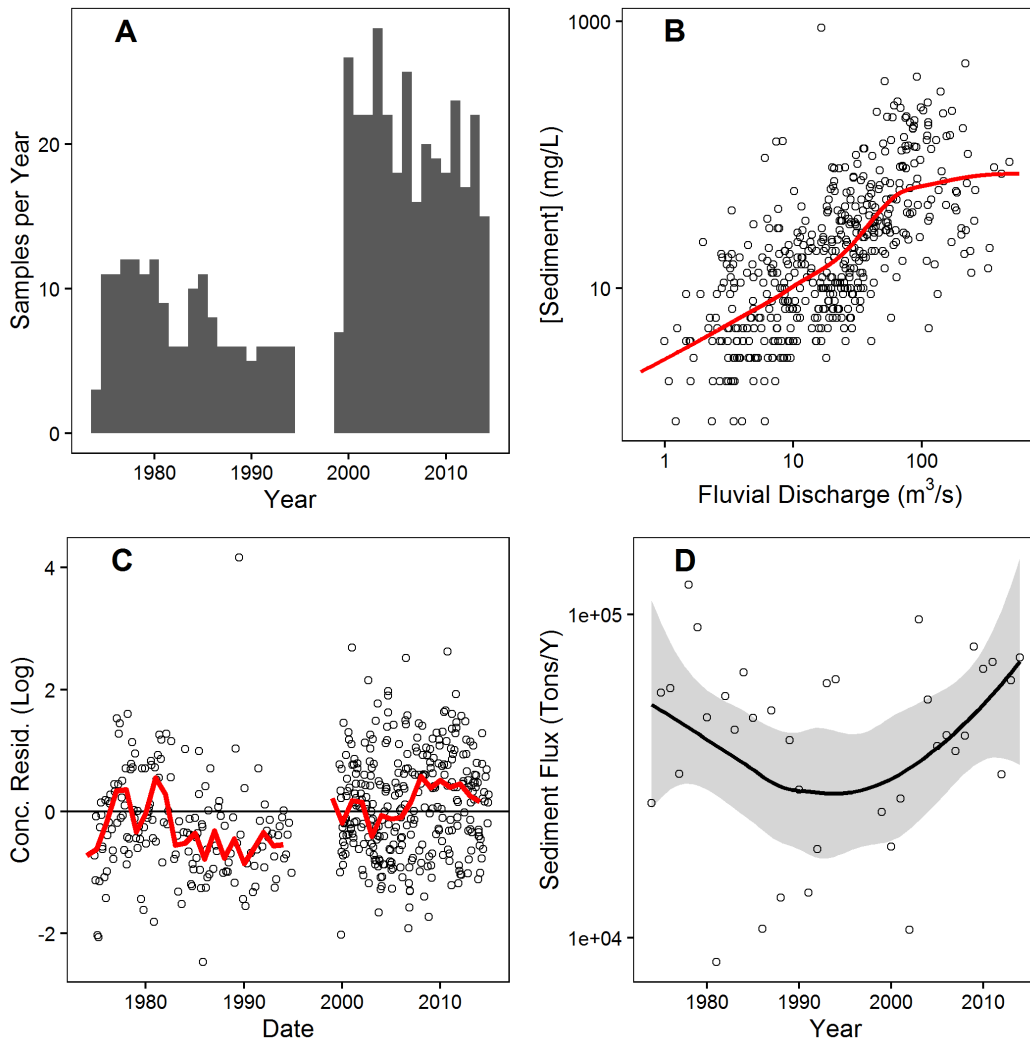
Sediment discharge is statistically modeled by taking the product of estimated sediment concentration and measured fluvial discharge. After additional corrective factors are applied, the predicted sediment flux is calculated as $Q_s(t) = E * Q(t) * C_s(Q(t)) * \exp[r(y)]$ (Cohn 1995; Warrick et al. 2013). $Q_s(t)$ is the estimated daily discharge of sediment [mass/time]. $Q(t)$ is the mean daily streamflow measured by stream gage [volume/time]. $C_s(Q(t))$ is the mean daily sediment concentration [mass/volume] predicted by fluvial discharge via regression (e.g. Fig. 2.1B). $r(y)$ is the median of the log-residuals between measured and estimated C_s within the year sediment flux is being predicted [dimensionless] (Fig. 2.1C). E is a factor for correcting against bias introduced by log-transforming the data [dimensionless]. A non-parametric smearing coefficient (Duan 1983) was used for the corrective factor in this study, as opposed to the parametric alternative (Ferguson 1986), because the parametric factor can overestimate in studies with high sample variance (Helsel and Hirsch 2002).

The relationship between suspended sediment concentration and streamflow [$C_s(Q(t))$] is traditionally modeled as a log-linear regression. Data with non-linear trends have more recently been studied using first degree loess models (Helsel and Hirsch 2002; Warrick et al. 2013), a method using locally weighted linear regression smoothing (Cleveland 1979). In addition to

being flexible with non-linear trends in the sediment rating curve, this methodology is attractive for other reasons. Smoothing with loess is readily accessible with the base statistics package for the R-programming language (R Core Team 2016). Also, since loess is still a form of linear regression, sediment rating curves based on loess inherit many of the previously described methods of rating curve correction and prediction that once were applied to simple linear fits. Loess smoothers are locally weighted regressions, and the span of the weighing window must be supplied to the model by the analyst. Smaller spans would decrease the root mean square error (RMSE) of the model, but can introduce bias by overfitting the data. In this study, it is assumed that predicted sediment concentration monotonically increases as discharge increases. Therefore, monotonicity must influence selection of span width (Helsel and Hirsch 2002). Aside from this case-specific requirement and (Cleveland 1979)'s recommendation of visualizing potential trends in residuals, there are relatively few guidelines for optimal span selection.

An automated search procedure was adopted to select an optimum span width using a consistent set of rules. A loess regression was computed for each span value from .05 to .95 by increments of .01, where span values are fractions of the domain. All models that failed to increase monotonically were rejected. For instances where monotonically increasing models did not exist at any span, suspended sediment concentration was assumed to be the geometric mean of the concentration measurements at all discharge rates. Of the remaining fitted models, the one minimizing the generalized cross validation statistic (GCV) was selected. GCV is an approximation of leave one out cross validation (Hastie et al., 2009) and is conveniently calculated in R based on summary parameters provided by the loess model object.

Figure 2.1- Example of Sediment Rating Curve Analysis:



An example site of the results from a sediment rating curve analysis to estimate suspended sediment flux at USGS gage #01673000 Pamunkey R. near Hanover, VA. **A:** Distribution of annual sediment collection. Sediment yield estimates were not made for years without samples. **B:** Sediment concentration as a function of fluvial discharge. Best-fit loess curve is in red. **C:** Residuals within each year, with median value in red. **D:** Annual cumulative sediment flux for each year sampled, with a .75 span loess smooth (95% confidence interval in grey) for visualizing any trend.

2.2.4 Spatial Analysis:

Watershed polygons were delineated using the pre-calculated NHDPlus v.2.1 (USEPA 2012) dataset, for which several of the processing-intensive steps of watershed delineation have already been carried out. Catchment polygons and the “PlusFlow” enhanced attribute table were

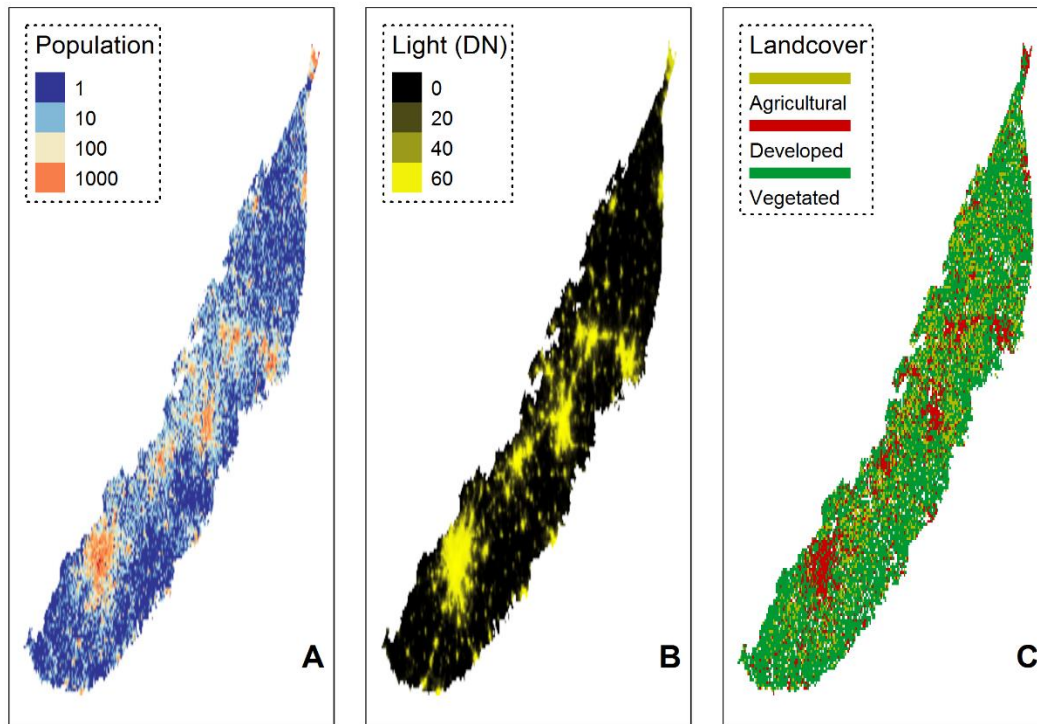
downloaded from the NHDPlus website. For each watershed, the terminal catchment was determined by spatial overlay with the USGS gage's coordinate (Latitude and Longitude supplied by NWIS query). Unique identifiers ("COMID"s) for upstream catchments were found by recursive search using the TOCOMID and FROMCOMID attributes in the "PlusFlow" table. Catchment polygons were selected based on the acquired list of COMIDs and dissolved into a single polygon.

To characterize the flux of water into the basins being studied, precipitation data were acquired from the DAYMET (Thornton et al. 2014) surface weather database, comprised of 1 km square resolution gridded daily precipitation rates spanning from 1980 to present. The netcdf files were reformatted as rasters, and area-weighted average precipitation was measured each day for each watershed by extracting the raster values to overlying basin polygons. Snowfall was not explored in the precipitation analysis. Since the Piedmont is in the Southern United States, it is uncertain how much this will impact analysis.

Three different spatial datasets describing human behavior were extracted to the watershed polygons (Fig. 2.2). Illumination data was from annual averages of the DMSP Nighttime Lights time series (NCEI 2013) for years 1992 to 2014. Nighttime lights are 30 arc-second spatial resolution (approximately 1 km on a side), and its units are average visible band digital number (DN) values multiplied by the frequency of light detection. DN is a quantification of detection that has not been calibrated to a specific unit of radiance. Annual populations within watersheds were extracted from the Landsat 30 arc-second population maps (Bhaduri et al., 2007) for the years 2000 to 2012. Changes in land cover were measured by extracting from the National Land Cover Database (NLCD) 2001 to 2011 land cover transition

map (30 meter resolution) (Fry et al., 2009; Fry et al., 2011; Homer et al., 2001; Vogelmann 2001).

Figure 2.2-Spatial Datasets of Human Behavior



The 2011 spatial datasets of human behavior extracted to the Piedmont polygon. **A:** Population **B:** Night Lights **C:** Land cover type (Open water and transitional land types (e.g. barren, scrub/shrubland, etc.) were excluded from visualization)

Computational analyses were performed using the R statistical computing language v.3.3.0 (R Core Team 2016). Geospatial analyses were carried out using several spatial packages within the R environment (i.e. the `sp`, `maptools`, and `rgdal` packages) (E. J. Pebesma and Bivand 2005; Bivand, Pebesma, and GomezRubio 2013; R. Bivand and Lewin-Koh 2014; R. Bivand, Keitt, and Rowlingson 2014). Operations using `netcdf` and raster datatypes were carried out using the “`netcdf`” (Pierce 2014) and “`raster`” (Hijmans 2014) packages.

2.3 Results

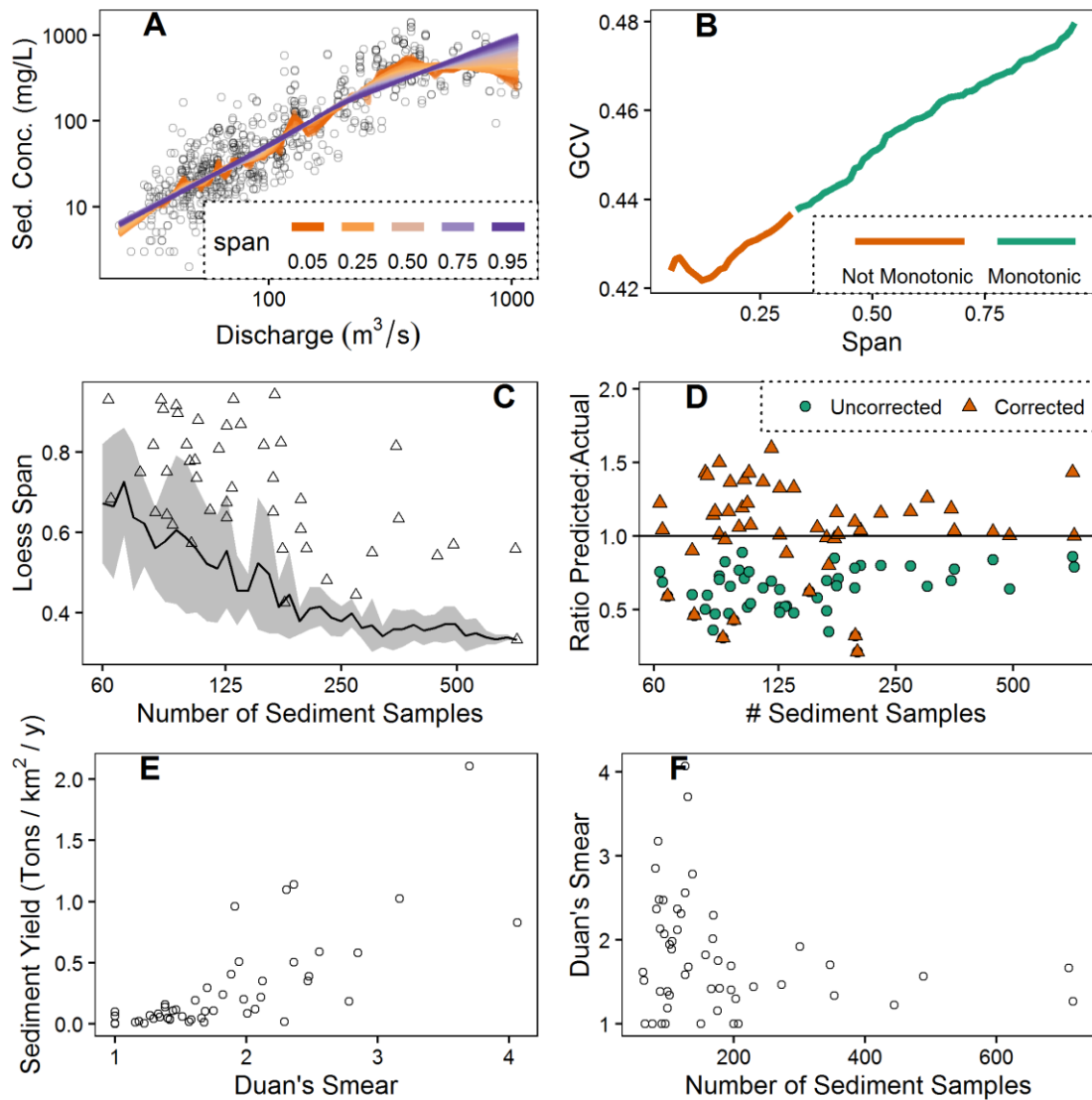
2.3.1: *Sediment Flux Estimation Parameters:*

Variations in the sediment rating curve parameters are strongly controlled by the number of sediment samples collected at the gage site. Only sites with larger sample counts have shorter spans (Fig. 2.3C). This may be due to the points within loess's weighting window having an averaging effect during the smoothing process, preventing more volatile vertical variations that are possible in sparsely populated datasets. At sufficiently narrow spans, local maxima and minima tend to form along the regression (Fig. 2.3A). This may explain why the monotonicity constraint appears to be a stronger determinant of span's lower bound than the GCV statistic. Using data from the Chattahoochee at Whitesburg as an example, the span supplying a monotonically increasing function is around two times as large as the span of minimum GCV (Fig. 2.3B).

A sampling simulation demonstrates the importance of sample size. Continuing to use data from the same gage site, random samples of the sediment measurements were drawn from the existing dataset (without replacement) and fit to an optimal loess span using the previously described framework. This was done in replicates of twelve at each of forty different sample sizes (from 60 to 717). The path (Fig 2.3C) connects the mean span at each sample size, while the grey ribbon is the standard deviation. The trend of the line is similar to the points, which are the fitted outcomes for the other individual datasets in this study. As sample size increases, span size declines, but it is not a smooth trend due to the random nature of the subsamples taken. Despite similar trends between the resampling model and the assembled summary statistics for other river gages, the Chattahoochee dataset seems to have the smallest span selection by a fairly large margin, suggesting that span is influenced by additional factors.

The correction coefficient for re-centering regression results after log-transformation (Duan 1983) does prevent the systematic underestimate of uncorrected results (Fig. 2.3D). However, it also provides additional error to the results. This smearing coefficient tends to be largest in regressions with low sample counts (Fig. 2.3F), while apparently influencing sediment yield estimates at sites with exceptional rates of sediment flux (Fig. 2.3E).

Figure 2.3- Variation in Rating Curve Parameters

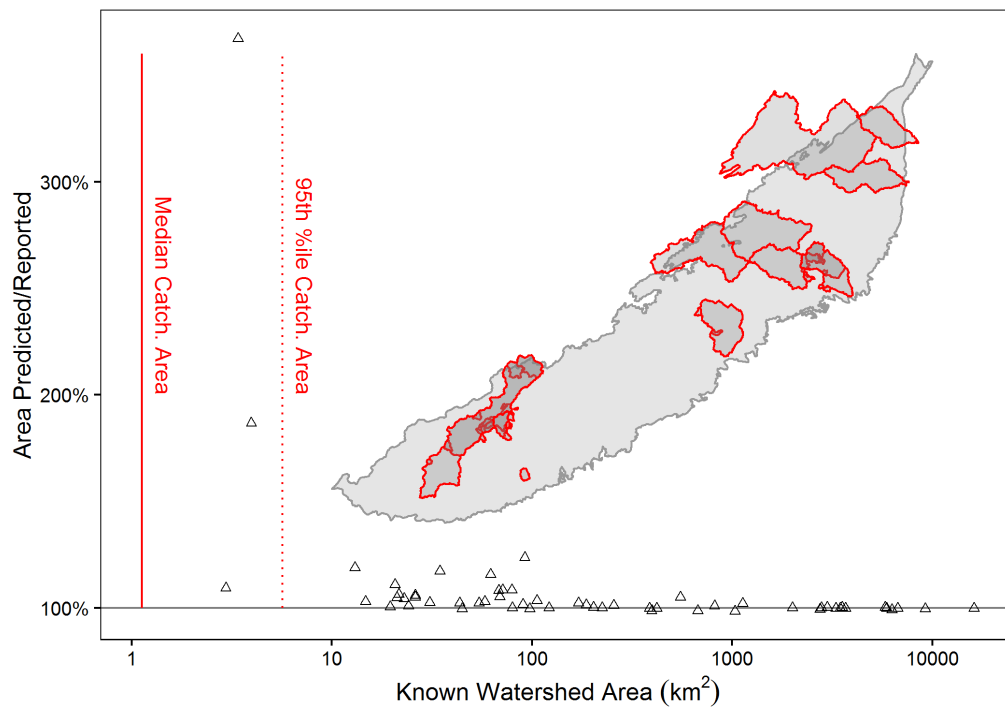


A: Sediment concentration vs. discharge at the Chattahoochee R. near Whitesburg with rating curves of variable span. **B:** GCV and monotonicity as a function of span at the Chattahoochee R. near Whitesburg. **C:** Optimal span vs. sample size. Triangular markers are the results of individual sites analyzed. The black line and ribbon are the mean and standard deviation of a resampling simulation of same Chattahoochee R. dataset. **D:** Ratio of mean predicted sediment concentrations vs. actual measurements at each site. Orange triangles have individual values that were multiplied by Duan's smearing factor, while green circles were not. **E:** Average suspended sediment yield vs. Duan's smearing factor. **F:** Duan's smearing factor vs. number of suspended sediment samples collected.

2.3.2: Watershed Delineation Performance

Known watershed areas were supplied for each gage station by the NWIS when data was queried. The area of the watersheds delineated using the NHDplus dataset was compared to these known values. Delineated watersheds are generally in good agreement with actual sizes, but appear to overestimate basin area by a small margin at most magnitudes (Fig. 2.4). The largest deviations occur as actual basin size approaches the resolution of the catchment polygons delineated by NHDplus. Catchment polygons tend to have a similar resolution to the raster datasets (Fig. 2.2). This means that the spatially extracted features of the smallest watersheds may reflect characteristics of neighboring watersheds as well as their own.

Fig. 2.4-Delineated Watersheds



Watershed polygons (outlined in red) delineated using the NHDplus precalculated data plotted over the Piedmont region. The ratio of the area of the delineated watershed to the watershed area reported by the USGS is plotted as a function of the reported value. The red vertical lines are descriptive statistics of the individual NHDplus catchments subsetted to the Piedmont region.

2.3.3 Spatial Characteristics between Sites

Average within-watershed illumination follows what appears to be a saturation pattern with respect to population density (Fig. 2.5A). This may be related to limitations of the sensors on the satellite. This sigmoidal curve apparently separates the watersheds into urban vs. rural classifications, where light is indicative of urban infrastructure resulting from increased population density. Net changes in land cover from 2001 to 2011 support this intuition (Table 2.1). The horizontal line in Fig. 2.5A separates the watersheds into “high” vs. “low” illumination classifications (this classification will be described with more detail in the next section). Highly illuminated watersheds on average showed a larger net increase in developed land cover types and greater net losses in forested cover.

Table 2.1-Changes in Land Cover (2001-2011) [% of Watershed Area]:

Region	Light	Developed	Forest	Agriculture	Transitional	#sites
Georgia	High	4.62%	-1.41%	1.47%	-4.68%	22
Georgia	Low	0.39%	-1.17%	4.50%	-3.72%	7
Northern	High	4.35%	-1.42%	3.83%	-6.76%	4
Northern	Low	0.41%	-0.41%	10.97%	-10.97%	19

Net changes in land cover types within the Piedmont watersheds analyzed in the study. Changes were based on the NLCD 2001-2011 transition layer. Values are percentages of watershed area.

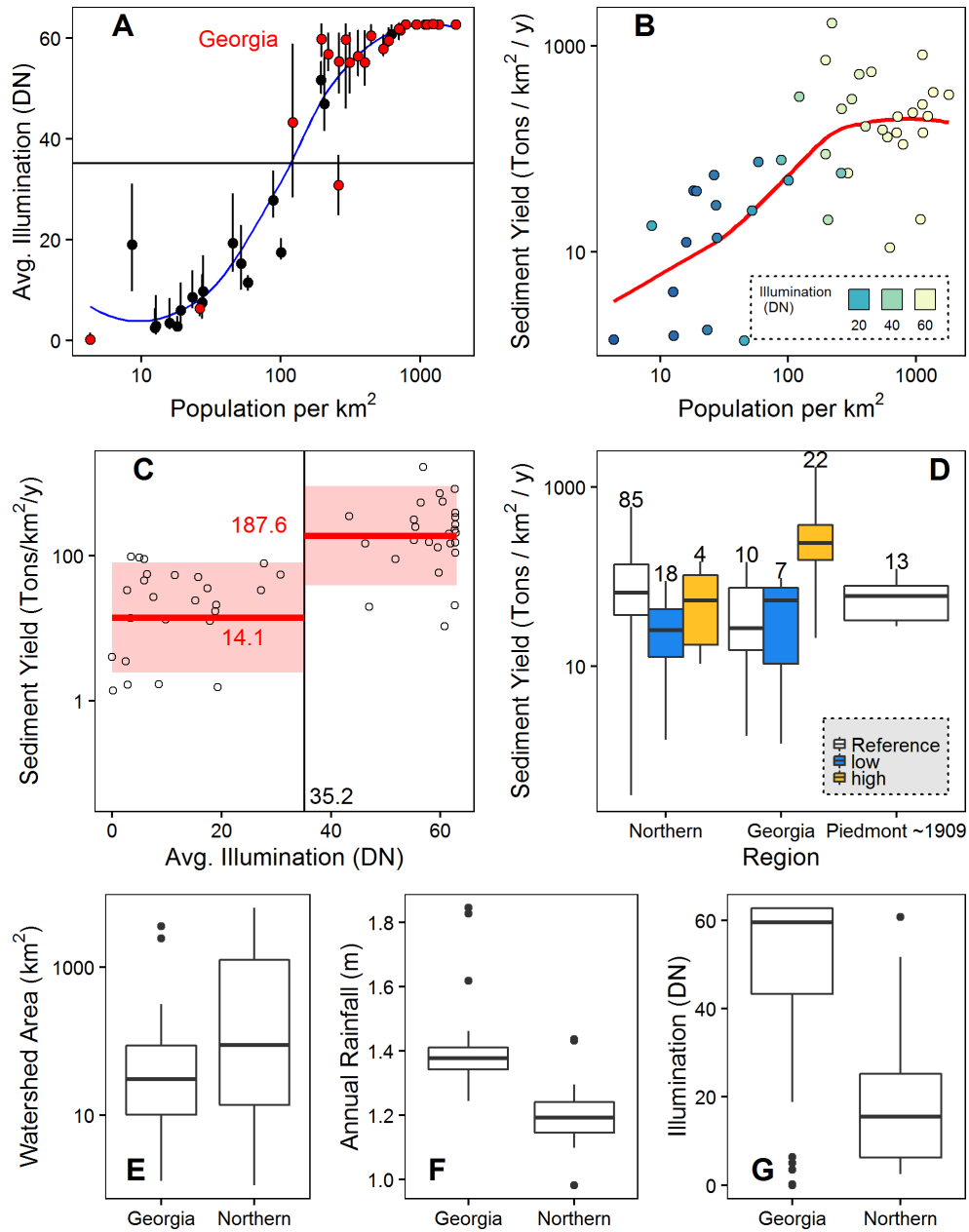
There are apparent sub-regions within this collected dataset, with roughly half of the watersheds clustered in the southwest Piedmont in Georgia, and the other half to the northeast predominantly in North Carolina and Virginia (Fig. 2.4). Despite an expected commonality in geomorphological features within the Piedmont, there are several notable points of differentiation within the dataset that break down along this regional distinction.

The majority of Georgian watersheds fall under the “high” light category (Table 2.1; Fig. 2.5A), while the inverse is true about the northern watersheds. This leads to the Georgian watersheds typically having greater illumination than northern watersheds (Fig. 2.5G). Changes

in land cover are not uniform across regions either. Rates of deforestation are higher in Georgia's "low" light watersheds, while rates of increased agricultural coverage are higher in the northern "low" light watersheds (Table 2.1). There are also greater declines in transitional land types (Shrub/scrub, grassland/herbaceous, barren) across all northern watersheds.

The two regions also experience differences in hydrologically important characteristics. The watersheds selected for study have a broader distribution in the northern region, while the majority of Georgian watersheds tend to be relatively smaller in size (2.5E). There are differences in rainfall as well, with the median annual rainfalls being roughly 15% higher than in northern watersheds.

Figure 2.5-Mean within-Site Characteristics:



A: Geometric mean of population vs. mean illumination (DN). GA sites in red. Error bars are range of values where yield was calculated. Blue .75 loess added for visualization. **B:** Geometric mean of population vs. geometric mean of sediment yield, colored by mean illumination. Red loess curve for trend. **C:** Geometric mean of sediment yield vs. mean illumination. A step function is in red, with geometric mean values and cut point annotated. The red ribbon is the geometric standard deviation. **D:** Boxplots of sediment yield vs. light group and region. Annotations are the number of sites. **E,F,G:** Boxplots of basin averages between Georgia and Northern watersheds.

2.3.4 Sediment Yield Comparisons:

Despite the potential collinearity of rainfall, illumination, and watershed area, site mean sediment yields only appear to have a strong relationship with respect to illumination. Individual linear regressions of $\log(\text{Yield})$ vs. illumination, $\log(\text{area})$, and annual rainfall only saw statistically significant relationships with respect to illumination ($r^2 = .5$; $p < .001$). This relationship was used to develop the categorical variables of “high” vs. “low” light described earlier. The step-function of illumination vs. sediment yield where mean yield [tons/km²/year] equals 14.1 at low light (< 35.2) and 187.6 at high light (>35.2) (Fig. 2.5C) was based on this relationship. The cut point in illumination (35.2) was found by choosing a cut point which minimized the sum square error of a linear regression where $\log(\text{Yield})$ is predicted by a categorical variable with values of “high” or “low”.

Greater values of suspended sediment yield were found in “high” light watersheds in Georgia than in their northern counterparts (Fig. 2.5D). “Reference” sites are drawn from the literature to establish a reasonable expectation of the range of sediment yield values. Northern reference values (Simmons 1993) are from North Carolina streams in the 1970s, Georgian reference values (Lamar 1944) are from Georgia in the first half of the 20th century, and “Piedmont ~1909” are from a collection of watersheds spanning the entire region (Dole and Stabler 1909). All yield values for the northern region fall within the range of reference yields, as do low illumination Georgian sites. High illumination Georgia sites tend to be substantially higher than any others. The net rate of conversion to developed land from forested land is not markedly different between regions (Table 2.1), and as previously mentioned, differences in illumination, rainfall, and basin area do not account for this difference. As a result, there must be some other unaccounted for regional covariate that generates this difference.

Regardless of differences in magnitude, sediment yields of “low” light watersheds are lower than those of “high” light watersheds in both regions (Fig. 2.5D). Sediment yield vs. population density parallels this stepwise relationship, because sediment yields eventually cease to increase as population density continues to increase (Fig. 2.5B). This suggests that the categorical behavior of yield vs. illumination is not simply an artifact of the saturation pattern between light and population (Fig. 2.5A). Instead, there may be some threshold of urbanizing development that leads to increased suspended sediment yields.

Although there is apparent variation across sites, there were no systematic trends within sites. Correlation between illumination and sediment yield (Kendall’s τ) was apparently random. Correlation ranged from $-.43$ to $.71$, with a median τ of $-.06$ across all sites with more than two complete cases of yield vs. light (Appendix A.1). This may be a result of inter-annual variability of the two variables within the relatively narrow time frame. Alternatively, if there is threshold between rural and urban land use that significantly alters sediment yield, perhaps none of the watersheds crossed it within the period of record.

Only two sites had a range of illumination values intersecting with the boundary between high and low illumination (Fig. 2.5A). One site is the Chattahoochee R. near Whitesburg, GA ($\tau = -.43$; $n = 21$), the site showing the strongest negative correlation between illumination and yield. Its watershed area is 6300 square kilometers, much of it intersects with Atlanta. The reason this reach of the Chattahoochee only recently crossed the threshold of illumination is due to averaging with the rural headwaters. Therefore its categorization as recently urban is erroneous. The other intersecting watershed is Wheeler Creek at Auburn, GA ($\tau = -.08$; $n = 13$). The 3.4 km² watershed northeast of Atlanta has an apparently random response of sediment yield to illumination. The watershed’s resolution is at the same scale as the NHDplus catchments as

well as the night lights grid. Extracted values may be representative of the vicinity of the gage, but not necessarily to processes confined to the watershed. The peculiarities of these two sites lead us to suspect that there aren't actually any sites that cross this potential threshold of sedimentary response to urbanization.

2.4 Discussion

Across sites, average sediment yields increased with respect to population density and night sky illumination, with highly illuminated watersheds yielding an order of magnitude more sediment per year than their less illuminated watersheds (Fig. 2.5C). Watersheds with elevated illumination were also associated with higher rates of transition into developed urban land cover (Table 2.1). Therefore, the most urban watersheds were undergoing the greatest amount of urban expansion. Given the ongoing trend of populations migrating into cities (Passel and Cohn 2008), this is not a surprising observation. The sustained land cover change within these already urban watersheds may explain why suspended sediment yields continue to be high despite the expectation that land cover disturbance leads to transient sedimentary response (Chin 2006). These results point to shared processes acting across watersheds in the Piedmont. Nevertheless, there are some differences in measured sediment yields between sites and gaps in the data that raise additional questions about the conveyance of sediment in these urbanizing streams.

2.4.1-Methodological Limitations:

The purpose of this study was to measure potential response in suspended sediment yield as a result of urbanizing land cover changes. This apparent trend across watersheds demonstrates a relationship spanning the gamut of indicators for urbanization, and may show a sedimentary response to urbanization in a space-for-time fashion. Unfortunately, no individual

watersheds appear to demonstrate the same trend over time, because none of the urban watersheds had sufficiently long records to demonstrate the phenomenon.

Scarcity of long-term datasets plague this manner of study, both in terms of geospatial data and suspended sediment records. Geospatial datasets giving insight to land development practices do not typically extend back to the mid-20th century. Furthermore, suspended sediment measurement campaigns have operational costs that make multi-decadal sediment records a rarity. Streams must be sampled regularly and stream-gauges must be maintained. Also, simply increasing the number of contemporary studies does not resolve the problem of historical data not existing.

A related problem is regarding method development of these statistical reconstructions of suspended sediment flux. Historical measurements with standardized methods of collection are precious, and they must be put the best possible use. While rating curve methodologies have become more flexible over time, the methods employed in this study have several unsatisfactory features. Model parameters demonstrate clear sensitivity to sample size (Fig. 2.3C,E,F), and there is no extant framework for model validation or quantification of uncertainty. Reliable procedures must be developed to evaluate the reliability of a suspended sediment yield estimate and to determine whether the distribution of suspended sediment concentration has been sufficiently characterized to make an estimate in the first place.

2.4.2-Regional Differences:

These observations of suspended sediment yield responding to headwater disturbances are significant, because they are contradictory of past observations in the Piedmont. In a display of “the sediment delivery problem” (Walling 1983), previously estimated yields from the Piedmont account for only 6-10% of total erosion estimates (Trimble 1977; Phillips 1991).

Despite a decline in erosion during the mid-20th century (Trimble 1974), fluvial sediment loads in the Piedmont were apparently unchanged over the century's course (Meade 1982). If the elevated suspended sediment yields truly are the consequence of urbanization, this historical context suggests that either erosion rates in urban watersheds are exceptionally higher than rates in rural watersheds, or modes of material conveyance have radically changed.

Since low illumination watersheds do not substantially differ with respect to sediment yield across regions, it seems likely that the difference is related to denudation and early transport at disturbed sites. There may be differences in soil consistency across watersheds or in sediment retention policies between states. Alternatively, there could be differences in the abundance of legacy sediments across regions, where legacy sediments are deposits from historical erosive land use (Merritts et al., 2011; James 2013). Analysis of the Piedmont's historical geography has shown that the deepest cumulative historical erosion has occurred in Georgia and South Carolina (Trimble 1974). This was primarily ascribed to differences in the thickness of the saprolite layer and due to the irresponsible soil management practices associated with early cotton agriculture (Trimble 1974). Future investigations comparing sediment yield to geographic covariates should explore explicit measurement of soil traits and historical erosive land use to see if historical observations potentially influence contemporary measurements.

Advancement of general theory regarding sediment yield response to urbanization will require that these types of regional differences be accounted for. Erosion in urban streams is a widespread phenomenon that primarily manifests itself on the local level because lower order rivers and streams are more responsive to erosional disturbances. The overarching impact of changes in land cover leads to a consistent set of potential problems (e.g. water quality impairment, reservoir infilling, etc.), but the erosion exists in a regional context with unique

geomorphological features. Until these regional factors are sufficiently characterized, predictions regarding sediment yield response to urbanization will depend on local case studies without generalizable insights.

2.5 Conclusions

Previous research of suspended sediment transport in urbanizing streams leads us to expect a subtle, time-varying response in suspended sediment yields. Instead, Piedmont watersheds demonstrate a surprisingly simple and consistent response of erosion and sediment transport due to urbanization in the region. This relationship is not supported by individual gage records, however, suggesting that the relevant transitions in land use and land cover did not occur during the period of record. Furthermore, the relationship across sites is complicated by a systematic difference with respect to region. Urban watersheds in Georgia demonstrate higher sediment yields than northern urban watersheds (Fig. 2.5D). Even though rainfall and basin area differ by region, they do not appear to significantly influence suspended sediment yield for the basins in this study. The difference must be the result of some regional covariate that has not been accounted for. In the future, when we expand this study of responses to urbanization to watersheds outside the Piedmont, this kind of problem will continue to arise.

REFERENCES

- Benedetti, M.M., M.J. Raber, M.S. Smith, and L.A. Leonard, 2006. "Mineralogical indicators of alluvial sediment sources in the Cape Fear River Basin, North Carolina." *Physical Geography* 27.3 (2006): 258-281.
- Bhaduri, B., E. Bright, P. Coleman, and M.L. Urban. 2007. "LandScan USA: A High-Resolution Geospatial and Temporal Modeling Approach for Population Distribution and Dynamics." *GeoJournal* 69 (1-2): 103–17. doi:[10.1007/s10708-007-9105-9](https://doi.org/10.1007/s10708-007-9105-9).
- Bivand, R., T. Keitt, and B. Rowlingson. 2014. "rgdal: Bindings for the Geospatial Data Abstraction Library." R package version 0.9-1 (<http://CRAN.R-project.org/package=rgdal>).
- Bivand, R., and N. Lewin-Koh. 2014. *Maptools: Tools for Reading and Handling Spatial Objects*. <http://CRAN.R-project.org/package=maptools>.
- Bivand, R.S., E.J. Pebesma, and V. Gomez-Rubio. 2013. "Applied Spatial Data Analysis with R." 2nd ed. *Springer*, NY. (<http://www.asdar-book.org>).
- Chin, A. 2006. "Urban Transformation of River Landscapes in a Global Context." *Geomorphology* 79 (3-4): 460–87. doi:[10.1016/j.geomorph.2006.06.033](https://doi.org/10.1016/j.geomorph.2006.06.033).
- Cleveland, W.S. 1979. "Robust Locally Weighted Regression and Smoothing Scatterplots." *Journal of the American Statistical Association* 74 (368). Informa UK Limited: 829–36. doi:[10.1080/01621459.1979.10481038](https://doi.org/10.1080/01621459.1979.10481038).
- Colin, T. A. 1995. "Recent Advances in Statistical Methods for the Estimation of Sediment and Nutrient Transport in Rivers." *Rev. Geophys.* 33. Wiley-Blackwell: 1117. doi:[10.1029/95rg00292](https://doi.org/10.1029/95rg00292).
- Dole, R. B., and H. Stabler. 1909. "Denudation." *US Geological Survey Water Supply Paper* 234: 78-93. U.S. Geological Survey. (<https://pubs.er.usgs.gov/publication/wsp234>).
- Drummond, M.A. and T. R. Loveland. 2010. "Land-Use Pressure and a Transition to Forest-Cover Loss in the Eastern United States." *BioScience* 60 (4). Oxford University Press (OUP): 286–98. doi:[10.1525/bio.2010.60.4.7](https://doi.org/10.1525/bio.2010.60.4.7).
- Duan, N. 1983. "Smearing Estimate: A Nonparametric Retransformation Method." *Journal of the American Statistical Association* 78 (383). Informa UK Limited: 605–10. doi:[10.1080/01621459.1983.10478017](https://doi.org/10.1080/01621459.1983.10478017).
- Fry, J.A., M. J. Coan, C. G. Homer, D. K. Meyer, and J. D. Wickham. 2009. "Completion of the National Land Cover Database (NLCD) 1992-2001 land cover change retrofit product." No. 2008-1379. US Geological Survey. (<http://pubs.usgs.gov/of/2008/1379/>).
- Fry, J.A, G. Xian, S. Jin, J. Dewitz, C. Homer, L. Yang, C. Barnes, N. Herold, and J. Wickham. 2011. "Completion of the 2006 National Land Cover Database for the conterminous United States." *Photogrammetric Engineering & Remote Sensing*, 77(9): 858-864. (<https://pubs.er.usgs.gov/publication/70034549>).

- Grimm, N.B., S.H. Faeth, N.E. Golubiewski, C.L. Redman, J. Wu, X. Bai, and J.M. Briggs. 2008. "Global change and the ecology of cities." *Science* 319(5864): 756-760. doi: [10.1126/science.1150195](https://doi.org/10.1126/science.1150195).
- Hastie, T., R. Tibshirani, and J. Friedman. 2009. *The Elements of Statistical Learning*. Springer New York. doi: [10.1007/978-0-387-84858-7](https://doi.org/10.1007/978-0-387-84858-7).
- Helsel, D.R. and R.M. Hirsch. 2002. "Statistical Methods in Water Resources: US Geological Survey Techniques of Water Resources Investigations." In *Techniques of Water-Resources Investigations Book 4*, edited by USGS, 522. U.S. Geological Survey. (<http://pubs.usgs.gov/twri/twri4a3/>).
- Hijmans, R.J. 2014. *Raster: Raster: Geographic Data Analysis and Modeling*. <http://CRAN.R-project.org/package=raster>.
- Hirsch, R., L. DeCicco, and D. Lorenz. 2015. *DataRetrieval: Retrieval Functions for USGS and EPA Hydrologic and Water Quality Data*. <http://CRAN.R-project.org/package=dataRetrieval>.
- Homer, C., C. Huang, L. Yang, B. Wylie, and M. Coan. 2004. "Development of a 2001 national land-cover database for the United States." *Photogrammetric Engineering & Remote Sensing* 70(7): 829-840. (<http://www.mrlc.gov/nlcd2001.php>).
- James, L.A. 2013. "Legacy sediment: Definitions and processes of episodically produced anthropogenic sediment." *Anthropocene* 2: 16-26.
- Kaufman, M.M. 2000. "Erosion Control at Construction Sites: The Science/Policy Gap." *Environmental Management* 26 (1): 89–97. doi: [10.1007/s002670010073](https://doi.org/10.1007/s002670010073).
- Lamar, W.L. 1944. "Chemical character of surface waters of Georgia." *US Geological Survey Water Supply Paper* 889-E: 317-380. U.S. Geological Survey. (<http://pubs.er.usgs.gov/publication/wsp889E>).
- Lang, R.E. and D. Dhavale. 2005. "America's megapolitan areas." *Land lines* 17(3): 1-4. (http://www.lincolnst.edu/pubs/1037_Land-Lines--July-2005--Volume--17--Number-3).
- Lang, R.E. and A.C. Nelson. 2007. "The rise of the megapolitans." *Planning* 73(1): 7-12.
- Leopold, L.B. 1968. *Hydrology for Urban Land Planning—A Guidebook on the Hydrologic Effects of Urban Land Use*. Circular 554. U.S. Geological Survey. (<http://pubs.er.usgs.gov/publication/cir554>).
- Meade, R.H. "Sources, sinks, and storage of river sediment in the Atlantic drainage of the United States." *The Journal of Geology* (1982): 235-252.
- Meade, R.H., and J.A. Moody. 2010. "Causes for the decline of suspended-sediment discharge in the Mississippi River system, 1940–2007." *Hydrological Processes* 24(1): 35-49. doi: [10.1002/hyp.7477](https://doi.org/10.1002/hyp.7477).

- Merritts, D., R. Walter, M. Rahnis, J. Hartranft, S. Cox, A. Gellis, A. Gellis, N. Potter, W. Hilgartner, M. Langland, M. Manion, and C. Lippincott, "Anthropocene streams and base-level controls from historic dams in the unglaciated mid-Atlantic region, USA." *Philosophical Transactions of the Royal Society A: Mathematical, Physical and Engineering Sciences* 369.1938 (2011): 976-1009.
- Meybeck, M. and R. Helmer. 1989. "The quality of rivers: from pristine stage to global pollution." *Global and Planetary Change* 1(4): 283-309. doi: [10.1016/0031-0182\(89\)90191-0](https://doi.org/10.1016/0031-0182(89)90191-0).
- Milliman, J.D. and K.L. Farnsworth. 2011. "River discharge to the coastal ocean: a global synthesis." Cambridge University Press. doi: [10.1017/cbo9780511781247](https://doi.org/10.1017/cbo9780511781247).
- Napton, D.E., R.F. Auch, R. Headley, and J.L. Taylor. 2009. "Land Changes and Their Driving Forces in the Southeastern United States." *Regional Environmental Change* 10(1): 37–53. doi:[10.1007/s10113-009-0084-x](https://doi.org/10.1007/s10113-009-0084-x).
- NCAR-GIS-Program. 2012. "Climate Change Scenarios, Version 2.0. Community Climate System Model, June 2004 Version 3.0. (Http://www.cesm.ucar.edu/models/ccsm3.0/) Was Used to Derive Data Products." National Center for Atmospheric Research (NCAR) / University Corporation for Atmospheric Research (UCAR). <http://www.gisclimatechange.org>.
- NCEI. 2013. "Version 4 DMSP-OLS Nighttime Lights Time Series" National Oceanic and Atmospheric Administration: National Centers for Environmental Information - Earth Observation Group. (<http://ngdc.noaa.gov/eog/dmsp/downloadV4composites.html>).
- Omernik, J.M. 1987. "Ecoregions of the Conterminous United States." *Annals of the Association of American Geographers* 77(1): 118–25. doi:[10.1111/j.1467-8306.1987.tb00149.x](https://doi.org/10.1111/j.1467-8306.1987.tb00149.x).
- Passel, J.S. and D.V.U.S. Cohn. 2008. "US population projections: 2005-2050." *Pew Research Center*. Doc#324199 (<http://www.popline.org/node/199218>).
- Pappas, E.A., D.R. Smith, C. Huang, W.D. Shuster, and J.V. Bonta. 2008. "Impervious Surface Impacts to Runoff and Sediment Discharge Under Laboratory Rainfall Simulation." *CATENA* 72 (1): 146–52. doi:[10.1016/j.catena.2007.05.001](https://doi.org/10.1016/j.catena.2007.05.001).
- Pebesma, E.J., 2004. "Multivariable geostatistics in S: the gstat package." *Computers & Geosciences*, 30: 683-691. doi: [10.1016/j.cageo.2004.03.012](https://doi.org/10.1016/j.cageo.2004.03.012).
- Pebesma, E.J. and R.S. Bivand. 2005. "Classes and methods for spatial data in R." *R News*, 5 (2). (<http://cran.r-project.org/doc/Rnews>).
- Phillips, J.D. 1991. "Fluvial Sediment Budgets in the North Carolina Piedmont." *Geomorphology* 4 (3-4). Elsevier BV: 231–41. doi:[10.1016/0169-555x\(91\)90006-v](https://doi.org/10.1016/0169-555x(91)90006-v).
- Pierce, D. 2014. *Ncdf: Interface to Unidata NetCDF Data Files*. <http://CRAN.R-project.org/package=ncdf>.
- R Core Team. 2015. "R: A language and environment for statistical computing". *R Foundation for Statistical Computing*. Vienna, Austria (<https://www.R-project.org/>).

- Russell, M.A., D.E. Walling, B.W. Webb, and R. Bearne. 1998. "The composition of nutrient fluxes from contrasting UK river basins." *Hydrological Processes* 12(9): 1461-1482. doi: [10.1002/\(sici\)1099-1085\(199807\)12:9<1461::aid-hyp650>3.0.co;2-6](https://doi.org/10.1002/(sici)1099-1085(199807)12:9<1461::aid-hyp650>3.0.co;2-6).
- Siakeu, J., T. Oguchi, T. Aoki, Y. Esaki, and H.P. Jarvie. 2004. "Change in Riverine Suspended Sediment Concentration in Central Japan in Response to Late 20th Century Human Activities." *CATENA* 55 (2). Elsevier BV: 231–54. doi: [10.1016/s0341-8162\(03\)00120-6](https://doi.org/10.1016/s0341-8162(03)00120-6).
- Simmons, C.E. 1993. "Sediment characteristics of North Carolina streams, 1970-79." *US Geological Survey Water Supply Paper*: 2364: 84 pp. U.S. Geological Survey. (<http://pubs.er.usgs.gov/publication/wsp2364>).
- Thornton, P.E., M.M. Thornton, B.W. Mayer, N. Wilhelm, Y. Wei, R. Devarakonda, and R.B. Cook. 2014. "Daymet: Daily Surface Weather Data on a 1-Km Grid for North America." Oak Ridge, TN, USA: Oak Ridge National Laboratory Distributed Active Archive Center. <http://dx.doi.org/10.3334/ORNLDAAC/1219>.
- Trimble, S.W. 1977. "The Fallacy of Stream Equilibrium in Contemporary Denudation Studies." *American Journal of Science* 277(7): 876–87. doi: [10.2475/ajs.277.7.876](https://doi.org/10.2475/ajs.277.7.876).
- Trimble, S.W. 1997. "Contribution of Stream Channel Erosion to Sediment Yield from an Urbanizing Watershed." *Science* 278 (5342): 1442–44. doi: [10.1126/science.278.5342.1442](https://doi.org/10.1126/science.278.5342.1442).
- Trimble, S.W. 1974. "Man-induced soil erosion on the southern Piedmont." *Soil Conserv. Soc. Am., Ankeny, Iowa*: 1700-1970.
- USEPA. 2012. "National Hydrography Dataset Plus - NHDPlus." U.S. Environmental Protection Agency (USEPA); the U.S. Geological Survey (USGS). (<http://www.horizon-systems.com/NHDPlus/>).
- USGS. 2015. "National Water Information System Data Available on the World Wide Web (Water Data for the Nation)." U.S. Geological Survey. (<http://waterdata.usgs.gov/nwis/>).
- Vogelmann, J.E., S.M. Howard, L. Yang, C.R. Larson, B.K. Wylie, and N. Van Driel. 2001. "Completion of the 1990s National Land Cover Data Set for the conterminous United States from Landsat Thematic Mapper data and ancillary data sources." *Photogrammetric Engineering and Remote Sensing* 67(6). (<http://www.mrlc.gov/nlcd1992.php>).
- Walling, D.E. "The sediment delivery problem." *Journal of Hydrology* 65.1 (1983): 209-237.
- Warrick, J.A., et al. "Trends in the suspended-sediment yields of coastal rivers of northern California, 1955–2010." *Journal of Hydrology* 489 (2013): 108-123.
- Wolman, M.G. 1967. "A Cycle of Sedimentation and Erosion in Urban River Channels." *Geografiska Annaler. Series A, Physical Geography* 49 (2/4): 385. doi: [10.2307/520904](https://doi.org/10.2307/520904).

CHAPTER 3: A REVIEW OF MARSH SOIL PROPERTIES COMPARED TO MODELED EXPECTATIONS

3.1 Introduction

Coastal wetlands are highly valued (Costanza et al. 1997), with ecosystem services including but not limited to habitat formation, wave control (Gedan et al., 2011), and carbon sequestration (Nellemann et al. 2009; Duarte et al., 2005). These prized ecosystems are decreasing in abundance, however, with recorded disappearance rates within the U.S. ranging from .03-.56% of total stocks lost per year (Frayer et al. 1983; Dahl and Johnson 1991; Dahl 2000; Dahl 2006; Dahl 2009). More extensive historical losses are reported worldwide (Hopkinson et al., 2012), with one estimate of 1-2% global marsh stocks lost per year (Duarte et al. 2008).

Coastal marsh elevation has long been understood to be dynamically responsive to relative sea level (Redfield 1972), and there is concern over the survival of marshes in response to global climate change. This has proven to be a difficult question due to the complexity of the system. Aboveground biomass influences rates of sedimentation while also being controlled by biological zonation with respect to inundation (Morris et al., 2002; Mudd et al., 2010), which has cascading effects on the marsh belowground structure by modifying production and decay of organic matter (Morris and Bowden 1986; Mudd et al., 2009). Recent efforts to systematically assess the emergent consequences of these dynamic variables have been parameterized in the form of zero-dimensional models of sedimentary processes above and belowground (Fagherazzi

et al., 2012). This codification of marsh sedimentary theory has allowed us to hypothesize about the ecosystem's response to the stresses of relative sea level rise (Kirwan et al., 2010) and temperature changes (Kirwan and Mudd 2012).

However, much of the observational data that undergirds contemporary theory is derived from the North Inlet near Charleston, SC (e.g. primary production vs elevation (Morris et al., 2002), seasonal variation in primary production (Morris and Haskin 1990), and roots to shoots ratio (Mudd et al., 2009)). These variables guiding contemporary theory are highly localized and may not account for differences across the diversity of marsh environments, which are known to exist along a gradient of temperatures, salinities, and tidal ranges (Craft 2007), producing a wide range of potential accretion rates, bulk densities, and organic matter content (Craft 2007; Chmura et al., 2003).

The goal of this study was to test the representativeness of the current modeling paradigm of marsh vertical sedimentation. We attempted to replicate by simulation the actual sediment organic profiles from a diverse set of Northwest Atlantic marshes under a common set of morphodynamic controls. Actual sediment characteristics were drawn from the literature, while controlling physical parameters were drawn from regional datasets (tidal range, rate of sea level rise, temperature). These simulation experiments revealed systematic errors in certain types of marshes, suggesting possible priorities for future work.

3.2 Methods

3.2.1 Data Sources:

99 sediment core profiles with measured bulk density (BD) and percent organic matter lost on ignition (%OM) were drawn from the published literature (Table 3.1; Fig. 3.1). In instances where values were not provided directly by the author or weren't reported in a table, values were extracted from the paper by making digitized traces of the published graphics using

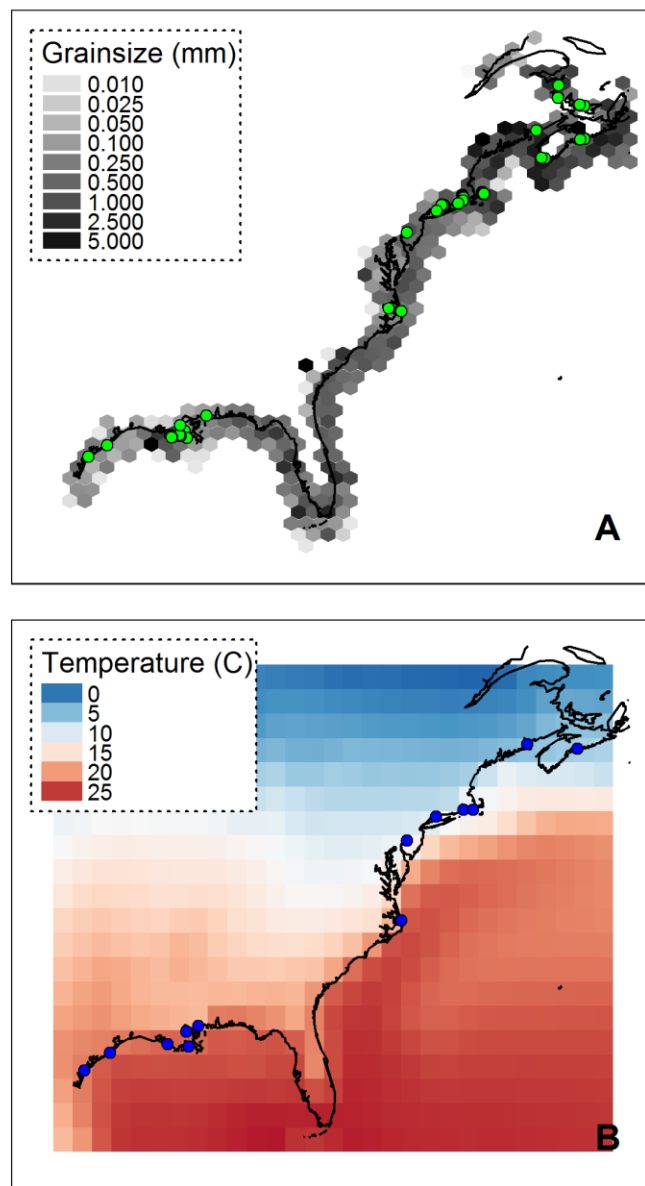
WebPlotDigitizer (Rohatgi 2016). Where percent carbon values were reported instead of %OM, a conversion was derived from an empirical relationship (Craft et al., 1991). Core locations were georeferenced in a similar manner where maps permitted. Otherwise, coring sites were georeferenced by author's reckoning based on comparison of site names, descriptions, and sketches with contemporary maps.

Average long-term temperature for each site was based on a raster extraction (1.4 degree spatial resolution) of the core location from an average of the 1970-1999 ensemble average temperature hindcast from the NCAR Community Climate System Model (NCAR-GIS-Program 2012).

Rate of relative sea level rise (rSLR) at each site was based on linear regression values provided for nearby tide gages (CO-OPS 2013b) (Table 3.2). Where a tidal range information was not provided in the research articles, values were taken from the same tide gages used for rSLR estimates (CO-OPS 2013a).

Point measurements of sediment grain size were drawn from the calculated dbSeabed database (C.J. Jenkins 1997; Chris Jenkins 2002; C.J. Jenkins 2003) of marine sediment attributes derived from the usSEABED databases for the U.S. Atlantic Coast (USGS 2005; J. Reid et al. 2005) and Gulf of Mexico (USGS 2006; Buczkowski et al. 2006) and combined with additional Canadian grain size values from a regional subset of the Canadian Expedition database (Natural Resources Canada 2016). Grain size estimates at core locations were geospatially interpolated by ordinary kriging using the compiled grain size dataset.

Figure 3.1-Cores and Spatial Datasets:



A: Green points show the locations of the cores studied here. The hexagonal bins summarize the mean grain size of underlying sediment grab samples. **B:** Blue points are the locations of tide gages whose summary data was used to supply tidal frame estimates and rates of sea level rise to the model. The underlying raster is the average of predicted temperatures from 1970-1999.

Table 3.1-Summary Statistics of Cores from the Literature:

Lat/Lon	n cores (samples per core)	Length [cm]	BD [g/cc]	%OM	Accretion [cm/y]	Temp [°C]	Grain Size [mm]
(-64.8, 45.4) ¹	15 (22)	24	0.26 (.08)	32 (10)	0.27 (.08)	6.9	0.20
(-70, 41.9) ²	3 (10)	45	0.34 (.2)	34 (17)	0.16	13.5	0.19
(-70, 41.8) ³	3 (50)	49	0.29 (.06)	27 (10)	0.36 (.09)	13.5	0.19
(-71.4, 41.6) ⁴	6 (49)	49	0.45 (.1)	25 (8)	0.36 (.15)	12.5	0.08
(-72.7, 41.3) ⁵	13 (15)	32	0.38 (.16)	24 (10.6)	0.35 (.15)	10.5	0.04
(-73.1, 41) ⁶	2 (5)	40	0.24 (.01)	22 (1)	0.55 (.11)	9.6	0.26
(-75.2, 39.9) ⁷	3 (11)	47	0.14 (.02)	16 (1)	1.25 (.14)	11.4	0.08
(-76, 35.9) ⁸	2, 2 (15)	30	0.56 (.52)	30 (32)	0.24 (.11)	17.1	0.16
(-90.3, 29.6) ⁹	1, 6 (10)	40	0.17 (.08)	49 (16)	0.92 (.35)	20.4	0.03
(-90.6, 29.3) ¹⁰	18, 7 (14)	44	0.21 (.07)	31 (11)	1.04 (.31)	22.7	0.03
(-91.1, 29.3) ¹¹	8, 7 (7)	20	0.28 (.09)	28 (7)	0.74	22.7	0.07
(-93.7, 29.2) ¹²	2, 1 (21)	42	0.69 (.38)	12 (9)	0.54 (.09)	20.4	0.06

Coordinates represent rounded-average values for georeferenced points within each source. References are as follows: [**1**: (Chmura and Hung 2004); **2**: (Portnoy and Giblin 1997); **3**: (Roman et al., 1997); **4**: (Bricker-Urso et al., 1989); **5**: (Anisfeld et al., 1999); **6**: (Armentano and Woodwell 1975); **7**: (Orson et al., 1990); **8**: (Craft et al., 1993); **9**: (Hatton 1981); **10**: (Nyman et al., 1993); **11**: (Nyman et al., 2006); **12**: (Callaway et al., 1997)]. “n” is the number of salt marsh cores, with the number of freshwater and brackish cores in bold/italic. The average number of depth interval samples per core is in parentheses. BD, %OM, and Accretion are reported as grand means with standard deviations in parentheses. References 2 and 11 used grand means reported in the source. Temperature and grain size measurements are from the geographic methods previously described.

Table 3.2-Tide Gage Information:

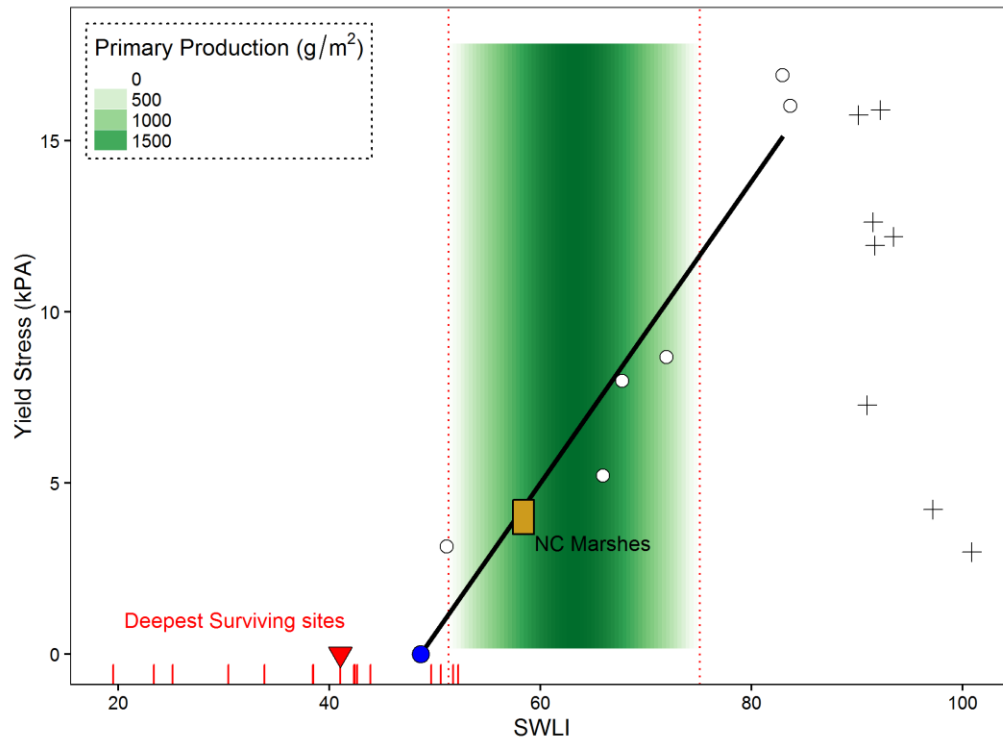
Lon/Lat	GageID	Maximum Range (m)	rSLR (mm/y)
(-67, 44.9)	8410140	8.09	2.11
(-63.6, 44.7)	970-011	-	3.12
(-70.7, 41.5)	8447930	1.22	2.81
(-71.3, 41.5)	8452660	1.84	2.72
(-73.2, 41.2)	8467150	3.13	2.81
(-75.1, 39.9)	8545240	2.74	2.93
(-75.5, 35.8)	8652587	0.56	3.84
(-89.3, 30.3)	8747437	1.21	4.1
(-90.1, 30)	8761927	0.21	4.71
(-91.4, 29.4)	8764311	1.17	9.65
(-90, 29.3)	8761724	0.84	9.05
(-90, 29.3)	8761724	0.84	9.05
(-95.3, 28.9)	8772440	1.12	4.43
(-97, 28)	8774770	0.43	5.33

Rates of relative sea level rise are derived from the NOAA National Water Level Observation Network combined with gages from the Permanent Service for Mean Sea Level (CO-OPS 2013b). Datum information for each site was taken from contemporary measurements (CO-OPS 2013a). For simulations in Canadian sites, tidal range was provided in Chmura and Hung 2004.

Data analyses were performed with the R statistical computing language v. 3.3.0 (R Core Team 2016). Geospatial analyses were carried out with the various geospatial tools available within the R computing environment. Geospatial data classes and methods were implemented with the *sp*, *maptools*, and *rgdal* packages (Pebesma and Bivand 2005; Bivand et al., 2013; Bivand and Lewin-Koh 2014; Bivand et al., 2014). Geostatistical models were developed with the *gstat* package (E. J. Pebesma 2004). To speed up computation, the dynamic sedimentary model was written and compiled using the *Rcpp* package (Eddelbuettel and François 2011; Eddelbuettel 2013).

3.2.2 A Common Frame of Reference:

Figure 3.2-SWLI vs. Marsh Characteristics:



The green region represents areas of primary production for *S. alterniflora* based on the measurements of Morris et al., 2002. Red vertical dotted lines are the roots of the parabola. The points in the red rugplot are the lowest-lying individual observations of marshes (McKee et al., 1988), with the median signified by the triangular marker. Yield stresses vs. SWLI have a rising limb (open symbols) and falling limb (crosses) (Brain et al., 2012). The black line is a linear regression of the rising limb of yield stresses, and the line's intercept is marked in blue. The brown box (not included in the regression) covers the region of values observed in (Brain et al., 2015), with elevation data provided in Kemp et al., 2009 and the Beaufort, NC tidal datum (gage #8656483) (CO-OPS 2013a) used to calculate SWLI.

Many of the processes being modeled were measured relative to the tidal range of the North Inlet, SC. To put sites with different tidal ranges into the same frame of reference, the standardized water level index (SWLI) was used. The SWLI of an elevation is its proportional distance between lowest and highest astronomical tides (Horton and Edwards 2006). This frame of reference seems to be effective in describing other marsh properties dictated by relative elevation. Note the proximity of the lower bound of *S. alterniflora* primary production (Morris

et al., 2002), the intercept of the yield stress relation (Brain et al, 20012), and the lower-bound of *S. alterniflora* survival (McKee and Patrick 1988). This consonance of evidence from multiple sources describing separate processes seems to point to SWLI as a common variable dictating behavior across all of them.

In this study, processes originally parameterized based on depth below mean high water at the North Inlet (D_{ni}) (e.g. accretion rates, primary production, and roots to shoots ratio) were assumed to be equivalent in sites with the same SWLI. For example, a given site's accretion is determined by converting the depth below mean high water at the site being studied to SWLI, then solving for D_{ni} using the tidal datum information for Charleston Harbor (gage #8665530, (CO-OPS 2013a)), and finally calculating accretion based on the formula for accretion relative to D_{ni} (Eq. 3.15).

3.2.3 Model Organization:

Like previous dynamic models of the marsh sediment column, sedimentation is modeled as the accumulation of a discrete sediment cohort within each time step (Morris and Bowden 1986; Fagherazzi et al., 2012), and over the course of the model's run, the thickness of each cohort evolves based on the many processes affecting it (biomass production/mortality, organic matter decay, and compaction). The end result is a model that was intentionally derivative of the OIMAS-N model (Mudd et al., 2009; Kirwan and Mudd 2012), because OIMAS-N has made the most extensive effort to account for all belowground processes, and the purpose of this study is to test the representativeness of current theory against actual data. Consequently, much of this section will be a re-iteration of previous work. Where possible, the most recent experimental data was used to model these dynamics (Mudd et al., 2009; Kirwan and Mudd 2012; Brain et al., 2012; Brain et al., 2015). For ease of comparison with the work of previous authors, notation

styles were preserved where possible. This will lead to inconsistent styling within this paper, but should make it easier to read in the context of the literature.

3.2.5 Modeling Primary Production

Annual peak aboveground biomass (B_p) [g/m^2] (Eq. 3.1) is based on the parabola-shaped quadratic regression of primary production rates with respect to depth below mean high water in the North Inlet, SC (Morris et al., 2002) (Fig. 3.2), with a correction factor based on long-term regional temperature (Kirwan and Mudd 2012). T_{ni} stands for the reference temperature at the North Inlet, T is the temperature at the site being modeled, and σ_b is a factor for proportionate changes in production based on temperature. The value of this constant and others, as well as reference information is presented in Table 3.4.

Temporal and spatial variation in biomass was directly copied from the formulations of Mudd et al., 2009. Daily aboveground biomass (B_{ag}) [g/m^2] (Eq. 3.2) was calculated as a sinusoidal function with the assumption that aboveground production has an annual maximum of B_p and an annual minimum of zero. B_{ag} determines total belowground biomass (B_{bg}) [g/m^2] by the linear relationship of the roots to shoots ratio with respect to D_{ni} (Eq. 3.3) (Mudd et al., 2009). Belowground biomass production is spatially modeled as an exponential decay with respect to depth (Eq. 3.4) (Mudd et al., 2009), with γ_z (Table 3.2) modifying the rate of that decline. Therefore, belowground biomass within a specific cohort at a given time step is the definite integral of Eq. 3.4 for b_{bg} with respect to depth.

3.2.5 Modeling Mortality and Decay

The addition of new decaying organic material to a given cohort is based on the mortality rate. The equation for mortality was drawn directly from the methods presented in Kirwan and Mudd 2012. The aboveground mortality rate (M_{ag}) [$\text{g}/\text{m}^2 \cdot \text{d}$] is the result of subtracting the

derivative of B_{ag} from the growth rate (Mudd et al., 2009; Kirwan and Mudd 2012) (Eq. 3.5). Peak growth rate is directly proportional to peak standing biomass (B_p) based on a proportionality coefficient (v_{Gp}), and here we assume a minimum growth rate of zero. Growth rate is offset from standing biomass based on the assumption that peak growth occurs at the end of July (Morris 2002). The offset parameter for growth rate (ϕ_A) was selected assuming peak growth on July 31st. To determine the total mass of new organic material added to the pool of decaying material within each time step, the definite integral of Eq. 3.5 was calculated over the time step of interest.

Modeling of decay is also directly taken from Kirwan and Mudd 2012. Decay of both labile and refractory organic pools (Eq. 3.7 and 3.8) are modeled as linear differential equations. Addition to each decay pool is based on the fraction of refractory material (χ_r) present in the dying biomass (m) found in each cohort. It is assumed that the proportion of m to M_{ag} is equivalent to the proportion of b_{bg} to B_{ag} .

Decay rates (k_r , k_i) are assumed to be variable with respect to both depth and temperature (Eq. 3.6). Rates of decay are assumed to decline as depth in the sediment column increases, with a constant (μ) modifying that rate. When modeling decay for a sediment cohort, the integrated average of the decay rate is used for the depth interval of the cohort. Just as B_p is modified by ambient temperature, so too is the decay rate, with deviation from the reference temperature T_{ni} modifying rates of decay by a factor of σ_k . Kirwan and Mudd 2012 applied a σ_k value of $.25 \text{ }^\circ\text{C}^{-1}$. This value would lead to cessation of decay in the northernmost cores of this study, and more recent experiments suggest a more modest rate of 3-6% increase in decay rates per degree of temperature increase (Kirwan et al., 2014). For this study, we applied a value of $.05 \text{ }^\circ\text{C}^{-1}$.

3.2.6 Modeling Compaction and Accretion

A framework for predicting void ratios has been developed by previous authors (Eq. 3.9-3.14) (Brain et al., 2012; Brain et al., 2015), by assuming that a marsh's geotechnical properties vary as a function of percent %OM and SWLI. Although compaction has been a component in other dynamic models (Mudd et al., 2009), this framework was selected because it is the only one of its kind, based on geotechnical measurements of actual marsh soils.

Recent research has shown that marsh surface sediments demonstrate compression behavior similar to overconsolidated soils (Eq. 3.14) (Brain et al., 2011). This means that initial changes in void ratio (e) as a function of effective stress (σ') relative to a reference void ratio (e_1) are relatively small and are described by the recompression coefficient (C_r). Once effective stress surpasses the yield stress (σ'_y), however, changes in void ratio as a function of effective stress are much larger and are predicted by the compression coefficient (C_c). The formulas for geotechnical parameters that vary as a function of percent organic matter (Eq. 3.9-3.12) were taken directly from Brain et al., 2015. The linear response of yield stress as a function of SWLI (Eq. 3.13; Fig. 3.2) was based on a linear regression of points traced from Brain et al., 2012.

Taken together, the void ratio, particle mass, and specific gravity of particulate material (G_s) determine the volume of a sediment cohort. As sedimentation, diagenesis, and belowground biomass production progress, the overburden on a sediment cohort changes, as does its organic content, ultimately changing the void ratio. Overburden is calculated under the assumption that the sediment column is in hydrostatic conditions and effective stress is the buoyant weight of overlying material. Buoyant weight is calculated using particle densities based on the specific gravity relationship (Eq. 3.12). Additionally, due to the compression framework being logarithmic, calculations are made assuming a minimum .01 kPa of overburden pressure. A

simulated loss on ignition value for organic material in a cohort was determined by summing belowground biomass, labile, and refractory pools, then subtracting the percent ash value supplied by Morris and Bowden 1986. Given the SWLI of the marsh surface, vertical effective stress, and estimated loss on ignition for a cohort, an updated void ratio is calculated after each time step.

Vertical accretion was estimated to be proportionate to depth below mean high water following the same functional relationship proposed by Morris et al., 2002 (Eq. 3.15). With the same formula and coefficients as Kirwan et al., 2007, the variable “ C_{ss} ” was applied to emulate the effect of variable suspended sediment concentrations across sites. An additional variable OM_0 is also declared before the simulation, determining what fraction of newly deposited material is organic. All of the initially deposited organic material is assumed to be refractory carbon. Using the OM_0 value, the SWLI, and the assumed overburden of .01 kPa, the void ratio of the initial deposit is calculated. That void ratio is then used to determine the volume of sediment added to the initial deposit as a result of vertical accretion.

Table 3.3-Equations:

A. Controls on above and belowground biomass production	
Equation 3.1-Peak Biomass:	$B_p = (155D_{ni} - 1.855D_{ni}^2 - 1354) \cdot [1 + (T - T_{ni}) \cdot \sigma_b]$
Equation 3.2-Aboveground Biomass Production:	$B_{ag} = \frac{B_p}{2} \left[1 + \cos\left(\frac{2\pi[jd - \phi_B]}{365}\right) \right]$
Equation 3.3-Roots to Shoots Ratio:	$\frac{B_{bg}}{B_{ag}} = \theta_{bg} \cdot D_{ni} + D_{mbm}$
Equation 3.4-Belowground Biomass vs. Depth:	$b_{bg} = \frac{B_{bg}}{\gamma_z} \exp\left(\frac{-z}{\gamma_z}\right)$
B. Controls on Mortality and Decay	
Equation 3.5-Mortality of Aboveground Biomass:	$M_{ag} = \frac{B_p \cdot v_{Gp}}{2} \left[1 + \cos\left(\frac{2\pi[jd - \phi_B - \phi_A]}{365}\right) \right] + \frac{B_p \pi}{365} \sin\left(\frac{2\pi[jd - \phi_A]}{365}\right)$
Equation 3.6-Decay Rate of a Pool of Organic Material:	$k_i = [1 + (T - T_{ni}) \cdot \sigma_k] \cdot k_{i,0} \cdot \exp\left(\frac{z}{\mu}\right)$
Equation 3.7-Rate of Change in Labile OM:	$\frac{dC_l}{dt} = -k_l \cdot C_l + m \cdot (1 - \chi_r)$
Equation 3.8-Rate of Change in Refractory OM:	$\frac{dC_r}{dt} = -k_r \cdot C_r + m \cdot \chi_r$
C. Controls on Compaction and Accretion	
Equation 3.9-Reference Void Ratio:	$e_1 = \frac{12.8408}{1 + \exp\left(-\frac{LOI - 30.7401}{10.4283}\right)}$
Equation 3.10-Recompression Index:	$C_r = .0026 + .0134 \cdot \exp(.069 \cdot LOI)$
Equation 3.11-Compression Index:	$C_c = \frac{4.1349}{1 + \exp\left(-\frac{LOI - 26.6509}{7.4981}\right)}$
Equation 3.12-Specific Gravity:	$G_s = 2.7288 - 0.0139 \cdot LOI$
Equation 3.13-Yield Stress:	$\sigma'_y = 44.09 \cdot SWLI - 21.455$
Equation 3.14-Void Ratio:	$e = e_1 - C_r \cdot (\log_{10} \sigma' - \log_{10} \sigma'_y) \quad \log_{10} \sigma' \leq \log_{10} \sigma'_y$ $e = e_1 - C_c \cdot (\log_{10} \sigma' - \log_{10} \sigma'_y) \quad \log_{10} \sigma' > \log_{10} \sigma'_y$
Equation 3.15-Rate of Vertical Accretion:	$\frac{d\eta}{dt} = D_{ni} \cdot (C_{ss} \cdot .00009 + .000015 \cdot B_{ag})$

Table 3.4-Variables and Constants:

Assigned Inputs			
T		°C	Determined
η_0	0.7	SWLI	Assumed
HAT; LAT; MHW		M	NOAA COOPS
rSLR		m/yr	NOAA COOPS
Variables			
χ_r		Fraction	
OM ₀		Fraction	
C _{ss}		(g•yr)/m ³	
Constants			
ϕ_A	212	julian days	Morris et al., 2002
ϕ_B	56	julian days	Mudd et al., 2009
v_{Gp}	0.0138	day ⁻¹	""
θ_{Bg}	-6.8	m ⁻¹	""
D _{mbm}	4.8	Dimensionless	""
γ_z	0.11	m ⁻¹	""
σ_k	0.05	°C ⁻¹	Kirwan et al., 2014
σ_B	0.06	°C ⁻¹	Kirwan and Mudd 2012
$k_{r,0}$	0.001	yr ⁻¹	""
$k_{l,0}$	2	yr ⁻¹	""
μ	0.4	m ⁻¹	""
Ash	.0344	Fraction	Morris and Bowden 1986
T _{ni}	14.24	°C	Assumed

3.2.7 Model Comparison and Fitting

For comparison with each core site, the simulation is run for a 300 year period using the following inputs: temperature, initial elevation (η_0), tidal datum (highest astronomical tide (HAT), lowest astronomical tide (LAT), mean high water (MHW)), and rSLR (Table 3.4). The variables for sediment availability (C_{ss}), initial organic matter content (OM₀), and refractory fraction of dead belowground biomass (χ_r) are unknown and were inferred by optimizing the root mean square error (RMSE) of the model's percent organic matter profile vs. the percent organic matter profile of the actual sediment core. Optimization was carried out using the bounded (L-

BFGS-B) method (Byrd et al., 1995) of the “optim” function in the R statistical computing language’s “stats” library (R Core Team 2016). We allowed the bounded algorithm to search within the following ranges for each variable (OM_0 : .1%-50%), (C_{ss} : 1-100), (χ_r : .0001-.99).

To allow for direct comparison for RMSE between simulated cohorts and experimental core data, simulation results were resampled to the same depth resolution as the core slices. Resampled average percent organic matter values were weighted by the dry bulk density of the cohort and by percent intersection of the sediment cohort with the core slice. Since the dynamic model only describes processes affecting vertical accretion and compaction, analysis was limited to the top half meter of cores drawn from the literature. Deeper sequences might reflect lateral marsh migration.

3.3 Results

3.3.1 Compilation Data

Integrated averages of whole core BD and %OM were compared, where the averages span from the surface to the maximum depth less than 50 cm (Table 3.1). Porosity was calculated using %OM and Eq. 3.12 to predict particle density, then subtracting BD/G_s from a unit volume. Mineral density (MD), dry organic density (OMD), and void ratio were all calculated with simple algebra.

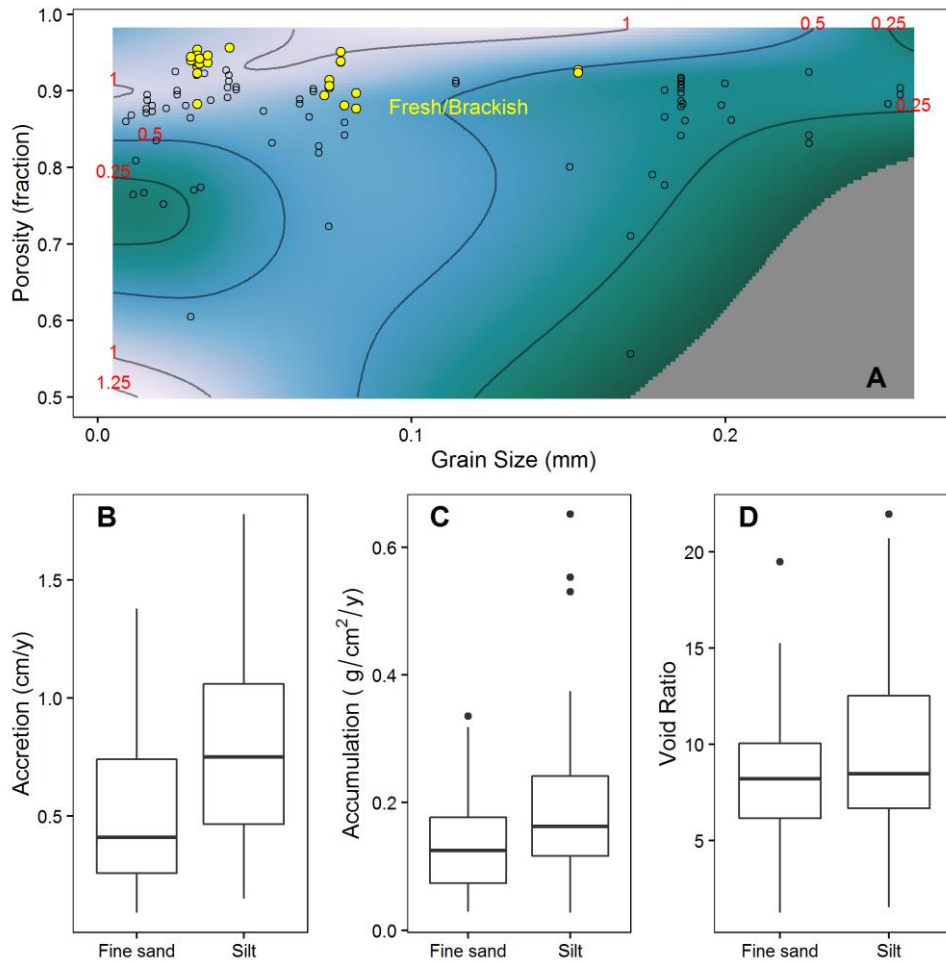
Within the sites selected for this study, vertical accretion rates vary as a function of porosity, salinity, and grain size (Fig. 3.3). A spline fit of accretion as a function of grain size and porosity (Fig. 3.3A) shows that the highest rates of vertical accretion occur in silty (<.0625 mm) estuarine environments with highly porous sediments. Among these rapidly accreting sites, the most rapid are brackish/freshwater (salinity <15 ppt). The linear trend of accretion as a function of void ratio (the ratio of void volume to solid volume) shows a weak positive

correlation (Fig. 3.4E), suggesting that porosity is an occasionally contributing, but not a governing factor for increasing accretion rates.

Broken into silt vs. fine sand groups, mean accretion is higher in marshes from silty environments (Fig. 3.3B). The difference in total mass accumulation (Fig. 3.3C) shows that much of this difference in vertical accretion is accounted for by the increased mass of sediment being deposited. Void ratio has nearly the same median and lower quartile between silt and fine sand sites, but silt sites have a larger maximum and interquartile range (IQR). These lines of evidence indicate that environments with lower sediment grain sizes often foster higher rates of material accumulation, and a subset of those sites (many of them with low salinities) have higher void ratios, combining to provide especially increased rates of vertical accretion in this subpopulation of marshes.

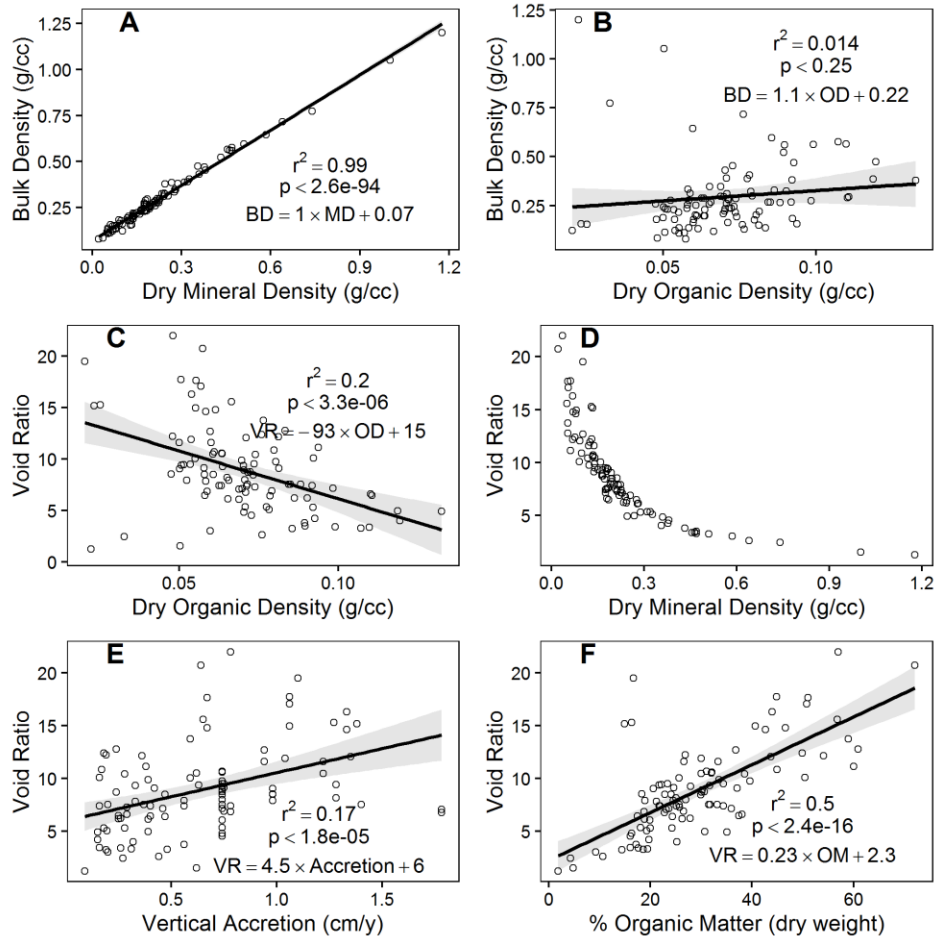
BD is strongly determined by MD (Fig. 3.4A), but there is no significant relationship between OMD and BD (Fig. 3.4B). This is probably due to the substantial difference in particle densities between the two substances. The strong determination of BD by MD does not lead to well-behaved relationships with respect to void ratio, however. It is difficult to say if there is a negative linear relationship between OMD and void volume (Fig. 3.4C) due to low r^2 and apparent heteroskedasticity of void volume in this regression. Void ratio grows increasingly variable as MD decreases (Fig. 3.4D). With the exception of the three tidal fresh marshes of Orson et al., 1990, which have high void ratios at less than 20% OM, generally cores follow the trend of increasing void ratio as %OM increases (Fig. 3.4F), but residuals around the line show that void ratios can vary by a factor of two.

Figure 3.3-Factors Affecting Accretion:



A: Contour map of accretion [cm/y] (labels in red) as a function of Grain size and porosity. **B-D:** Box and whisker plots. Whiskers extend to furthest value within 1.5 * IQR + the hinge.

Figure 3.4 Bivariate Soil Relationships:



Bivariate relationships between integrated core variables. Linear equations, p-values, and r^2 values are reported, but significance values may be overstated due to violations of statistical assumptions.

3.3.2 Model Parameter Results

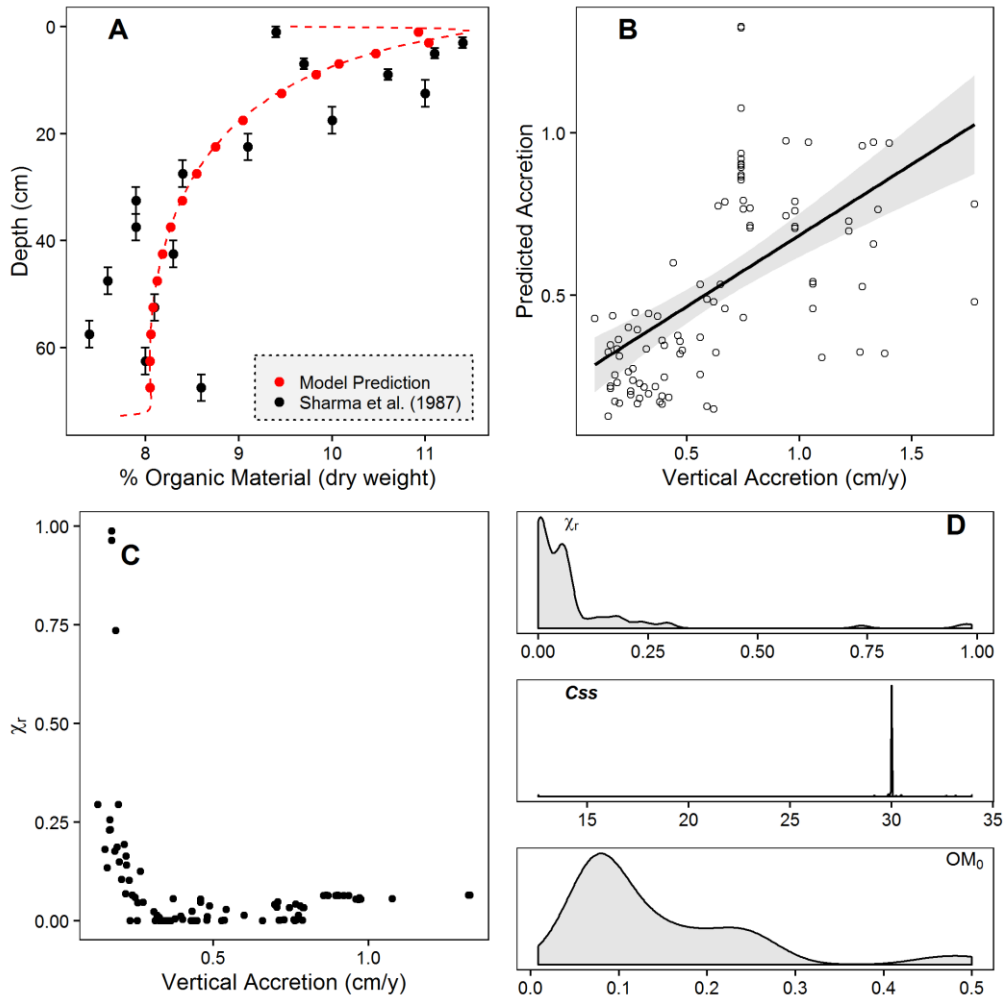
The model's effectiveness was first evaluated based on its performance against the Bread and Butter Creek #4 core taken at the North Inlet (Sharma et al., 1987), which was used to validate the OIMAS-N model (Mudd et al., 2009). The two models display similar behavior, with this model returning an RMSE of .697 vs. OIMAS-N's .68. The shape of the profile is similar as well, with a near surface maximum %OM that declines to a stable value near the bottom (Fig. 3.5A). In addition to providing a reasonable %OM profile, the average cumulative accretion rate over the 300 year simulation is .243 cm/y, which is quite similar to the accretion rate of .27 cm/y estimated for the area (Vogel et al., 1996). Model optimization inferred χ_r was less than 1%, which is much lower than the 15% determined for the OIMAS-N model. The addition of the OM_0 factor as a term for the model is likely to account for this difference.

In most cases, the inferred variables found by optimization returned seemingly reasonable values. C_{ss} wasn't particularly variable. Although values ranged from 12.6-33.96, the vast majority (95/99) of the cores had values between 29 and 31. It's possible that the C_{ss} factor, despite representing a conceptual notion of ambient suspended sediment concentration, is overridden by D_{ni} as the top of the tidal frame is approached. Average rates over the 300 year time frame of the simulation spanned from .1275 to 1.328 cm/y, with a median value of .53 cm/y. These predicted accretion rates broadly fall in line with empirical observations at the study sites (Table 3.1), and predicted vs. actual accretion rates were positively correlated ($r = .57$; Fig. 3.5B). Given that average vertical accretion rates were not directly controlled-for, it is surprising that there is this much agreement with the empirical measurements.

Aside from three sites that had improbably high inferred χ_r values (greater than 70% at "Inlet1" Roman et al., 1997; "Halifax4" Chmura and Hung 2004, and "Sybill1" Anisfeld et al.,

1999), χ_r values were all less than 30%, with roughly a third of all cores having predicted χ_r values of less than 1% (Fig. 3.5D). The strong variation in χ_r was a function of predicted vertical accretion (Fig. 3.5C), with sites predicting low accretion rates (<.25 cm/y) typically presenting higher inferred χ_r values (median: 17.9%; IQR: 13.8) than those with greater rates (median: 1.4%; IQR: 5.44). It is likely that χ_r and OM_0 trade-off in their relative contribution to the inventory of organic matter in simulations with low accretion rates. Inferred OM_0 values have a median at 9.67%, with a right-skewed distribution (Fig. 3.5D). Without measurements of %OM for ambient estuarine sediments, it is difficult to say if these are reasonable estimates for loading of allochthonous organic material. Consequently, it is impossible to say if the balance between χ_r and OM_0 is modeling the relative contributions of allochthonous vs autochthonous organic deposition.

Figure 3.5-Model Performance and Inferred Variables:



A: Comparison of model output after optimization for Bread and Butter Creek #4 (Sharma et al., 1987). Individual red points denote resampled model values used to match resolution of the sediment core samples and calculate RMSE. Bars on the sediment sample points indicate the range of the depth interval. Model parameter values: $OM_0 = 7.1\%$; $C_{ss} = 29.999$; $\chi_r = 0.826\%$. **B:** Comparison of determined accretion rates for sediment cores drawn from the literature vs. predicted average accretion rates from 300 year simulations. **C:** χ_r varying with respect to vertical accretion inferred by the model. **D:** Kernel density smooths of the distributions of the inferred variables (χ_r , C_{ss} , and OM_0) after optimization of RMSE fits to %OM profiles drawn from the literature.

3.3.3 Across Site Performance

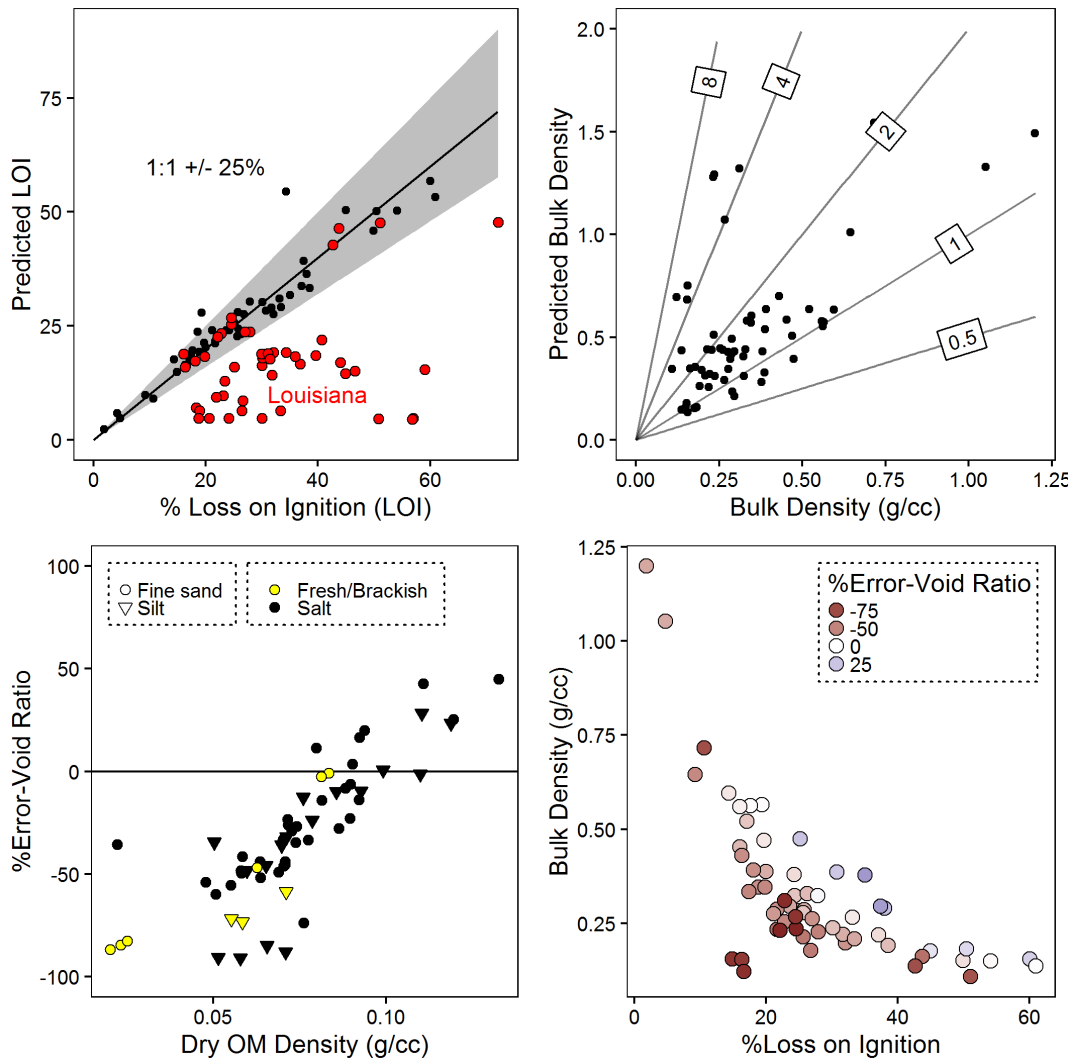
Predictions of integrated average %OM for 61 of the 99 simulated cores fall within 25% of the actual value (Fig. 3.6A). Therefore, this model largely succeeds in replicating the %OM profiles of the majority of cores examined in this study. For this discussion, this majority will be described as “successful” cores. Cores that are not successful are the result of optimization failing to converge on a combination of variables that suitably describe the down-core profile of organic matter. Of the 38 cores that were not successful, 28 of them were taken in Louisiana (out of 40 cores from Louisiana). It is possible that the regional model parameters (e.g. the high rate of relative sea level rise, low tidal range (Table 3.2)) for the 300 year simulation in these Louisiana cores are not conducive to long term marsh establishment. Alternatively, there may be processes sustaining many Louisiana marshes that are not adequately accounted for in the model.

For the successful cores, the model generally has a tendency to overestimate average BD (Fig. 3.6B). Roughly a third fall within 25% of actual BD values. At 51 sites, however, the model predicts bulk densities greater than actually measured, with 13 predicting bulk densities that more than double the expected value. Since accretion rates remain proportionate between actual and modeled sites (Fig. 3.5B), overestimates in BD and concomitant underestimates in void ratio lead to substantial overestimates of material accumulation.

A combination of successful sites with silt sediments and/or low salinity show the greatest relative underestimation in void ratios, indicating that sites with the highest actual porosities have the greatest relative underestimate of void ratio when simulated (Fig. 3.6C). Looked at from another angle, the sites with the lowest actual bulk densities have the highest relative overestimate of bulk density (Fig. 3.6B). Relative error in void ratio among successful cores was linearly related to measured OMD (Fig. 3.6C). This means that relative error in

estimates of void ratio increases orthogonally relative to the overarching hyperbolic trend followed by BD vs. %OM (Fig. 3.6D). This systematic error indicates that the compaction model only successfully predicts void ratios within a narrow band of organic matter densities around .08-.11 g/cm³.

Figure 3.6-Systematic Model Errors:



A: Average %OM for individual cores vs. predicted average %OM based on 300 year dynamic sedimentary simulation. Cores gathered from Louisiana are in red. The 1:1 ratio is marked by a black line, and +/- 25% of the 1:1 ratio is shown by the grey ribbon underlying it. **B:** Average bulk density (g/cc) vs. predicted bulk density of sites falling within the ribbon in Fig. 3.6A. Labeled lines show what multiple of the actual value is present at the predicted value intersecting the line. **C:** %Relative error in simulated void ratio vs. measured dry organic density using the same subset as 6B. **D:** Average %OM vs. bulk density colored by relative error in predicted void ratio using the same subset of sites from 6B/C.

3.4 Discussion

The goal of this study was to purposefully find points of failure in the current modeling framework for dynamic marsh sedimentation, and see if there are specific ways in which our models can be improved. After confronting the model with a diverse set of cores, two major categories of failure emerged. There were sites where model optimization failed to converge upon a set of variables that would yield a modeled %OM profile that resembled measured %OM profiles. Also, there were sites where %OM profiles could be emulated, but compression modeling led to systematic error in estimated void ratio.

3.4.1 Failed Convergence

Cores where optimization failed were almost entirely found in Louisiana. It has previously been noted that dynamic marsh sedimentary models do not tend to reach stable solutions when rates of sea level rise are large and tidal frames are small (Kirwan et al., 2016). Furthermore, many of the sites that could not be simulated were collected in regions where marsh collapse was an ongoing phenomenon (Nyman et al., 1993), indicating that there might not actually be a stable set of parameters in that region. Nevertheless, there are some potentially important aspects of these natural systems that are not accounted for in the model. This potential for a failure of imagination may lead us to an excessively pessimistic prognosis. For one thing, our model assumes that marshes currently reside under the same conditions they were formed. Rates of sea level rise applied in this model are constant, and sedimentary response to inundation is constant. In reality, many marshes experience ephemeral periods of rapid lateral expansion due to a brief surfeit of sediment, then persist in a mildly erosional environment (Kirwan 2011; Fagherazzi 2013).

Also, vegetation may have an outsized role in these environments. Vegetative accretion occurs in the model by altering the mass and compressibility of the sediment cohorts as belowground organic material accumulates. This parameterization glosses over several potentially relevant natural processes. The strict assumption of sedimentary biomass only being produced belowground (Eq. 3.4) runs contrary to observation. In some inundation conditions, *S.alterniflora* root matter can accumulate vertically by growing from inundated aboveground stems (Nyman et al., 2006). Instead of reflecting the inputs of allochthonous and autochthonous sediments, it is possible that the trade-offs between the OM_0 vs χ_x terms (Fig. 3.5C-D) are the result of belowground biomass production deviating from the expected vertical spatial pattern.

Vegetation may play an additional role in compaction by altering the buoyant weight of the sediments. The model assumes that void spaces are saturated with water, but really marsh sediments have two fluid phases: pore water in the sediments and air in the cells of the coarse roots and rhizomes (vascular aerenchyma) (Adam 1993). The air-filled aerenchymae have buoyant particle density (Davey et al., 2011), and marsh plants may produce more aerenchymae in inundated conditions (Burdick 1989; Maricle and Lee 2002). In a sufficiently low-mineral environment, this can yield neutrally buoyant or floating marsh sediment columns (Swarzenski et al., 1991). Since marsh porosity is modeled as a function of compression, it is impossible for this model to conceptualize a marsh that is under no effective stress.

3.4.2 Compression Error

The balance of material accumulation vs. relative elevation has been the primary focus of dynamic sedimentary modeling of marshes (Kirwan et al. 2010; Kirwan and Mudd 2012). Void spaces, despite comprising the majority of emergent wetland elevation, are strangely absent from the discussion. We attempted to describe the significant variability of void spaces observed in the

literature (Fig. 3.3; Fig. 3.4) through a previously derived geotechnical framework (Brain et al., 2012) and found a systematic trend in error (Fig. 3.6C-D). It is our suspicion that this is primarily due to an unaccounted for variability in the consolidation and compressibility of different organic materials.

Consider %OM as the ratio of organic mass to mineral mass. Since these two materials differ so strongly with respect to specific gravity and compressibility, it makes intuitive sense that their relative proportion should have a first order control on e_1 and the compression indices (Brain et al., 2012). Despite substantial variability around the trend, this relationship is readily observed when comparing void ratio to %OM (Fig. 3.4F). Systematic error in void ratios along the gradient of organic matter densities (Fig. 3.6C), on the other hand, suggests that there is an important secondary control on compaction. It is possible that organic matter density reflects the relative proportion of the different pools of organic matter present in the marsh core, and their differences in density and compressibility.

Recent research involving CT-scans on marsh cores (Davey et al., 2011) has allowed for remarkably detailed investigation of the structure and wet particle density (ρ_{wet}) of belowground materials. It has been clearly demonstrated that the ρ_{wet} of organic material varies along a continuum, but may be divided into three operationally defined groups: coarse roots and rhizomes ($\rho_{\text{wet}} \sim .74$ g/cc), peat ($\rho_{\text{wet}} \sim 1.13$ g/cc), and particulates ($\rho_{\text{wet}} > 1.23$ g/cc) (Davey et al., 2011). This order of increasing ρ_{wet} may parallel the order of primary production and diagenesis. As diagenesis progresses, the cellular structure of the roots and peats will break down, consolidating them and decreasing their compressibility. This evolution in the properties of organic matter means that e_1 , and the compression indices should vary depending on the relative abundances of roots, peat, and particulates.

Low organic matter density may be the result of a higher ratio of roots to partially decayed organic matter, while high organic matter density suggests the inverse relationship. Average void ratio does not appear to be strongly determined by organic matter density when compared across cores (Fig. 3.4C), but the effect of organic content on compressibility may be masked by the influence of overburden in high mineral density cores (3.4D) in addition to the overarching influence of %OM (3.4F). If this relationship were true, then conditions of low overburden would yield a higher void ratio for low organic density soils due to the abundance of porous roots. On the other hand, there would be a lower void ratio for high organic density soils due to the abundance of compact peat. This additional control would counterbalance the systematic error observed in the present model (Fig. 3.6C).

Both low-salinity and low grain size marshes frequently had highly underestimated void ratios in our model (Fig. 3.6C). Such environmental differences may further modify compressibility of marsh soils, but the evidence is less demonstrative. Fresh water marshes are known to have low bulk densities (Craft 2007), and have rapid rates of vertical accretion in part due to their higher void volumes (Fig. 3.3A), but it is difficult to say what mechanism would be responsible for their exceptional porosity. Marshes from regions with silty sediments have the capacity to present exceptionally high void ratios as well (Fig. 3.3D). Surface sediment deposits in both lacustrine and marine sediments have shown a tendency for porosity to be low when grain sizes are low (Wu and Wang 2006; Richardson and Briggs 1993), indicating that differences in consolidation may play a factor. In the absence of any clear trends, however, it is difficult to address these potential factors with any confidence.

3.4.3 Recommendations for future research

Further work is required to find modeling parameters that can replicate the organic matter profiles of many marsh cores in Louisiana using environmental variables derived from the region. This is important, because the majority of estuarine emergent wetlands in the conterminous United States are found in the Gulf of Mexico (Dahl and Stedman 2013), and rSLR is especially rapid in that region (Table 3.2), suggesting a highly uncertain future for a vast number of wetlands.

Uncertainty regarding the content and compressibility of marsh organic material points to a need for more extensive characterization of marsh sediments. Although CT-scanning (Davey et al., 2011) and oedometry (Brain et al., 2012) have yielded tremendous new insights into the field, other simple and affordable methods should be adopted as well. Despite the simplicity of pycnometer measurements, only a handful of specific gravity estimates have been made for marsh soils (Brain et al., 2015; Craft et al., 1993; Delaune et al., 1983). Also, the possibility of buoyant roots affecting overburden necessitates the measurement of the buoyant weight of wet sediments. Regardless of what new measurements are adopted, we need to continue applying and reporting legacy measurements of loss on ignition and dry bulk density as well. Consistency of methodology over the course of forty years is what made this study possible.

Perhaps with additional insight from new measurements on the abundance and mechanical behavior of organic material in marsh sediments, the next big conceptual leap in modeling the marsh sedimentary column will involve explicitly linking the production and diagenesis of belowground biomass to its geotechnical properties. The operational pools of “labile” vs. “refractory” organic carbon have had some speculative basis, but are lacking in their

connection to tangible materials. If we can clear that conceptual hurdle, the systematic errors we see in void ratio estimation may be mitigated.

3.5 Conclusions

Dynamic models of marsh sedimentation are critical tools for understanding the behavior of marshes as well as predicting their survival over the course of global change. This study reveals glaring weaknesses in the current modeling paradigm, demonstrating a failure to characterize broad regions (mostly in Louisiana) and a failure to fully explain the spectrum of soil void volumes as a function of vertical compression. As a result, only 21/99 marsh cores were reasonably replicated by simulations. This casts doubt on our current capacity to adequately predict the behavior of these dynamic systems as environmental conditions change.

Processes controlling compaction are just as important in dictating marsh elevation as those determining material accumulation. In most instances where simulation could successfully emulate percent organic matter profiles, sediment bulk density was overestimated. Error in simulated void ratio was systematically correlated with organic matter density, suggesting that the geotechnical properties of organic matter vary with its abundance. We posit that this systematic deviation of the model from reality is the result of differences in the consolidation and compressibility of live roots vs. decaying organic material. Differences in salinity and sediment grain size may have additional influence on material densities, but that relationship is less clear.

REFERENCES

- Adam, P. *Saltmarsh ecology*. Cambridge University Press, 1993.
- Anisfeld, S.C., M.J. Tobin, and G. Benoit. 1999. "Sedimentation Rates in Flow-Restricted and Restored Salt Marshes in Long Island Sound." *Estuaries* 22 (2). Springer Science Business Media: 231. doi:[10.2307/1352980](https://doi.org/10.2307/1352980).
- Armentano, T.V., and G.M. Woodwell. 1975. "Sedimentation Rates in a Long Island Marsh Determined by 210Pb Dating." *Limnol. Oceanogr.* 20 (3). Wiley-Blackwell: 452–56. doi:[10.4319/lo.1975.20.3.0452](https://doi.org/10.4319/lo.1975.20.3.0452).
- Bivand, R.S., E. Pebesma, and V. Gomez-Rubio. 2013. *Applied Spatial Data Analysis with R, Second Edition*. Springer, NY. <http://www.asdar-book.org/>.
- Bivand, R., and N. Lewin-Koh. 2014. *Maptools: Tools for Reading and Handling Spatial Objects*. <http://CRAN.R-project.org/package=maptools>.
- Bivand, R., T. Keitt, and B. Rowlingson. 2014. *Rgdal: Bindings for the Geospatial Data Abstraction Library*. <http://CRAN.R-project.org/package=rgdal>.
- Brain, M.J., A.C. Kemp, B.P. Horton, S.J. Culver, A.C. Parnell, and N. Cahill. 2015. "Quantifying the Contribution of Sediment Compaction to Late Holocene Salt-Marsh Sea-Level Reconstructions, North Carolina, USA." *Quaternary Research* 83 (1). Elsevier BV: 41–51. doi:[10.1016/j.yqres.2014.08.003](https://doi.org/10.1016/j.yqres.2014.08.003).
- Brain, M.J., A.J. Long, S.A. Woodroffe, D.N. Petley, D.G. Milledge, and A.C. Parnell. 2012. "Modelling the Effects of Sediment Compaction on Salt Marsh Reconstructions of Recent Sea-Level Rise." *Earth and Planetary Science Letters* 345-348 (September). Elsevier BV: 180–93. doi:[10.1016/j.epsl.2012.06.045](https://doi.org/10.1016/j.epsl.2012.06.045).
- Buczowski, B.J., J.A. Reid, C.J. Jenkins, J.M. Reid, S.J. Williams, and J.G. Flocks. 2006. "UsSEABED: Gulf of Mexico and Caribbean (Puerto Rico and U.S. Virgin Islands) Offshore Surficial Sediment Data Release." U.S. Geological Survey Data Series 146. Woods Hole Science Center, Woods Hole, MA: U.S. Geological Survey, Coastal and Marine Geology Program. <http://pubs.usgs.gov/ds/2006/146/>.
- Burdick, D.M. 1989. "Root Aerenchyma Development in *Spartina Patens* in Response to Flooding." *American Journal of Botany* 76 (5). Botanical Society of America: 777. doi:[10.2307/2444425](https://doi.org/10.2307/2444425).
- Byrd, R. H., Lu, P., Nocedal, J. and Zhu, C. (1995) A limited memory algorithm for bound constrained optimization. *Scientific Computing*, 16. *SIAM J*: 1190–1208.
- Callaway, J.C., R.D. DeLaune, and W.H. Patrick. 1997. "Sediment Accretion Rates from Four Coastal Wetlands along the Gulf of Mexico". *Journal of Coastal Research*. 13 (1).

- Coastal Education and Research Foundation, Inc.: 181-191. URL:
<http://www.jstor.org/stable/4298603>
- Chmura, G.L., S.C. Anisfeld, D.R. Cahoon, and J.C. Lynch. 2003. "Global Carbon Sequestration in Tidal, Saline Wetland Soils." *Global Biogeochem. Cycles* 17 (4). Wiley-Blackwell: n/a–/a. doi:[10.1029/2002gb001917](https://doi.org/10.1029/2002gb001917).
- Chmura, G.L., and G.A. Hung. 2004. "Controls on Salt Marsh Accretion: A Test in Salt Marshes of Eastern Canada." *Estuaries* 27 (1). Springer Science Business Media: 70–81. doi:[10.1007/bf02803561](https://doi.org/10.1007/bf02803561).
- CO-OPS. 2013. "Tides and Currents Products" National Oceanic and Atmospheric Administration (NOAA); Center for Operational Oceanographic Products and Services (CO-OPS). <https://tidesandcurrents.noaa.gov>
- CO-OPS. 2013. "Sea Levels Online: Sea Level Variations of the United States Derived from National Water Level Observation Network Stations" Department of Commerce (DOC), National Oceanic and Atmospheric Administration (NOAA), National Ocean Service (NOS), Center for Operational Oceanographic Products and Services (CO-OPS). <http://tidesandcurrents.noaa.gov/sltrends/sltrends.html>
- Costanza, R., R. d'Arge, R. De Groot, S. Faber, M. Grasso, B. Hannon, K. Limburg, and S. Naeem. 1997. "The Value of the Worlds Ecosystem Services and Natural Capital." *Nature* 387 (6630). Nature Publishing Group: 253–60. doi:[10.1038/387253a0](https://doi.org/10.1038/387253a0).
- Craft, C. B., E. D. Seneca, and S. W. Broome. 1991. "Loss on Ignition and Kjeldahl Digestion for Estimating Organic Carbon and Total Nitrogen in Estuarine Marsh Soils: Calibration with Dry Combustion." *Estuaries* 14 (2). Springer Science Business Media: 175. doi:[10.2307/1351691](https://doi.org/10.2307/1351691).
- Craft, C.B., E.D. Seneca, and S.W. Broome. 1993. "Vertical Accretion in Microtidal Regularly and Irregularly Flooded Estuarine Marshes." *Estuarine, Coastal and Shelf Science* 37 (4). Elsevier BV: 371–86. doi:[10.1006/ecss.1993.1062](https://doi.org/10.1006/ecss.1993.1062).
- Dahl, T.E. 2000. *Status and Trends of Wetlands in the Conterminous United States 1986 to 1997*. Inventory. Washington D.C.: U.S. Department of the Interior, Fish and Wildlife Service.
- Dahl, T.E. 2006. *Status and Trends of Wetlands in the Conterminous United States 1998 to 2004*. Inventory. Washington D.C.: U.S. Department of the Interior, Fish and Wildlife Service.
- Dahl, T.E. 2009. *Status and Trends of Wetlands in the Conterminous United States 2004 to 2009*. Inventory. Washington D.C.: U.S. Department of the Interior, Fish and Wildlife Service.

- Dahl, T.E., and C.E. Johnson. 1991. *Status and Trends of Wetlands in the Conterminous United States Mid-1970's to Mid-1980's*. Inventory. Washington D.C.: U.S. Department of the Interior; Fish and Wildlife Service.
- Dahl, T.E., and S.M. Stedman. 2013. *Status and Trends of Wetlands in the Coastal Watersheds of the Conterminous United States 2004 to 2009*. Inventory. Washington D.C.: U.S. Department of the Interior, Fish and Wildlife Service, National Oceanic and Atmospheric Administration, National Marine Fisheries Service.
- Davey, E., C. Wigand, R. Johnson, K. Sundberg, J. Morris, and C.T. Roman. 2011. "Use of Computed Tomography Imaging for Quantifying Coarse Roots, Rhizomes, Peat, and Particle Densities in Marsh Soils." *Ecological Applications* 21 (6). Wiley-Blackwell: 2156–71. doi:[10.1890/10-2037.1](https://doi.org/10.1890/10-2037.1).
- DeLaune, R.D., R.H. Baumann, J.G. Gosselink. 1983. "Relationships Among Vertical Accretion, Coastal Submergence, and Erosion in a Louisiana Gulf Coast Marsh." *Journal of Sedimentary Petrology*. 53 (1). The Society of Economic Paleontologists and Mineralogists: 147-157.
- Duarte, C. M., J. J. Middelburg, and N. Caraco. 2005. "Major Role of Marine Vegetation on the Oceanic Carbon Cycle." *Biogeosciences* 2 (1). Copernicus GmbH: 1–8. doi:[10.5194/bg-2-1-2005](https://doi.org/10.5194/bg-2-1-2005).
- Duarte, C.M., W.C. Dennison, R.J.W. Orth, and T.J.B. Carruthers. 2008. "The Charisma of Coastal Ecosystems: Addressing the Imbalance." *Estuaries and Coasts: J CERF* 31 (2). Springer Science Business Media: 233–38. doi:[10.1007/s12237-008-9038-7](https://doi.org/10.1007/s12237-008-9038-7).
- Eddelbuettel, D. 2013. *Seamless R and C++ Integration with Rcpp*. New York: Springer.
- Eddelbuettel, D., and R. François. 2011. "Rcpp: Seamless R and C++ Integration." *Journal of Statistical Software* 40 (8): 1–18. <http://www.jstatsoft.org/v40/i08/>.
- Fagherazzi, S. 2013. "The Ephemeral Life of a Salt Marsh." *Geology* 41 (8). Geological Society of America: 943–44. doi:[10.1130/focus082013.1](https://doi.org/10.1130/focus082013.1).
- Fagherazzi, S., M.L. Kirwan, S.M. Mudd, G.R. Guntenspergen, S. Temmerman, A. Dand, J. van de Koppel, J.M. Rybczyk, E. Reyes, C. Craft, and J. Clough. 2012. "Numerical Models of Salt Marsh Evolution: Ecological, Geomorphic, and Climatic Factors." *Rev. Geophys.* 50 (1). Wiley-Blackwell. doi:[10.1029/2011rg000359](https://doi.org/10.1029/2011rg000359).
- Frayer, W.E., T.J. Monahan, D.C. Bowden, and F.A. Graybill. 1983. *Status and Trends of Wetlands and Deepwater Habitats in the Conterminous United States 1950's to 1970's*. Inventory. St. Petersburg, FL: U.S. Department of the Interior; Fish; Wildlife Service.

- Gedan, K.B., A.H. Altieri, and M.D. Bertness. 2011. "Uncertain Future of New England Salt Marshes." *Marine Ecology Progress Series* 434 (July). Inter-Research Science Center: 229–37. doi:[10.3354/meps09084](https://doi.org/10.3354/meps09084).
- Hatton, R.S. 1981. "Aspects of Marsh Accretion and Geochemistry, Barataria Basin, Louisiana." Master of Science, Louisiana State University.
- Hopkinson, C.S., W. Cai, and X. Hu. 2012. "Carbon Sequestration in Wetland Dominated Coastal Systems a Global Sink of Rapidly Diminishing Magnitude." *Current Opinion in Environmental Sustainability* 4 (2). Elsevier BV: 186–94. doi:[10.1016/j.cosust.2012.03.005](https://doi.org/10.1016/j.cosust.2012.03.005).
- Horton, B.P. and Edwards, R.J. 2006. "Quantifying Holocene Sea Level Change Using Intertidal Foraminifera: Lessons from the British Isles." *Cushman Foundation for Foraminiferal Research, Special Publication*. 40. University of Pennsylvania Scholarly Commons: 97pp. URL: http://repository.upenn.edu/ees_papers/50
- Jenkins, C.J. 1997. "Building Offshore Soils Databases." *Sea Technology* 38 (12): 25–28.
- Jenkins, C.J. 2003. "Data Management of MARGINS Geologic Data, with Emphasis on Efficiency, Quality Control and Data Integration." *MARGINS Newsletter* 10: 8–10.
- Jenkins, C.J. 2002. "Automated Digital Mapping of Geological Colour Descriptions." *Geo-Mar Lett* 22 (4). Springer Science Business Media: 181–87. doi:[10.1007/s00367-002-0111-0](https://doi.org/10.1007/s00367-002-0111-0).
- Kemp, A. C., B. P. Horton, S. J. Culver, D. R. Corbett, O. van de Plassche, W. R. Gehrels, B. C. Douglas, and A. C. Parnell. 2009. "Timing and Magnitude of Recent Accelerated Sea-Level Rise (North Carolina, United States)." *Geology* 37 (11). Geological Society of America: 1035–8. doi:[10.1130/g30352a.1](https://doi.org/10.1130/g30352a.1).
- Kirwan, M.L., G.R. Guntenspergen, A. Dand, J.T. Morris, S.M. Mudd, and S. Temmerman. 2010. "Limits on the Adaptability of Coastal Marshes to Rising Sea Level." *Geophys. Res. Lett.* 37 (23). Wiley-Blackwell. doi:[10.1029/2010gl045489](https://doi.org/10.1029/2010gl045489).
- Kirwan, M. L., G. R. Guntenspergen, and J. A. Langley. 2014. "The Temperature Sensitivity of Organic Matter Decay in Tidal Marshes." *Biogeosciences Discussions* 11 (4). Copernicus GmbH: 6019–37. doi:[10.5194/bgd-11-6019-2014](https://doi.org/10.5194/bgd-11-6019-2014).
- Kirwan, M.L., and S.M. Mudd. 2012. "Response of Salt-Marsh Carbon Accumulation to Climate Change." *Nature* 489 (7417). Nature Publishing Group: 550–53. doi:[10.1038/nature11440](https://doi.org/10.1038/nature11440).
- Kirwan, M. L., and A. B. Murray. 2007. "A Coupled Geomorphic and Ecological Model of Tidal Marsh Evolution." *Proceedings of the National Academy of Sciences* 104 (15). Proceedings of the National Academy of Sciences: 6118–22. doi:[10.1073/pnas.0700958104](https://doi.org/10.1073/pnas.0700958104).

- Kirwan, M. L., A. B. Murray, J. P. Donnelly, and D. R. Corbett. 2011. "Rapid Wetland Expansion During European Settlement and Its Implication for Marsh Survival Under Modern Sediment Delivery Rates." *Geology* 39 (5). Geological Society of America: 507–10. doi:[10.1130/g31789.1](https://doi.org/10.1130/g31789.1).
- Kirwan, M.L., S. Temmerman, E.E. Skeehan, G.R. Guntenspergen, and S. Fagherazzi. 2016. "Overestimation of Marsh Vulnerability to Sea Level Rise." *Nature Climate Change* 6 (3). Nature Publishing Group: 253–60. doi:[10.1038/nclimate2909](https://doi.org/10.1038/nclimate2909).
- Maricle, B.R., and R.W. Lee. 2002. "Aerenchyma Development and Oxygen Transport in the Estuarine Cordgrasses *Spartina Alterniflora* and *S. Anglica*." *Aquatic Botany* 74 (2). Elsevier BV: 109–20. doi:[10.1016/s0304-3770\(02\)00051-7](https://doi.org/10.1016/s0304-3770(02)00051-7).
- McKee, K.L., and W. H. Patrick. 1988. "The Relationship of Smooth Cordgrass (*Spartina Alterniflora*) to Tidal Datums: A Review." *Estuaries* 11 (3). Springer Science Business Media: 143. doi:[10.2307/1351966](https://doi.org/10.2307/1351966).
- Morris, J.T., and W.B. Bowden. 1986. "A mechanistic, numerical model of sedimentation, mineralization, and decomposition for marsh sediments." *Soil Science Society of America Journal* 50 (1) Soil Science Society of America: 96-105. doi:[10.2136/sssaj1986.03615995005000010019x](https://doi.org/10.2136/sssaj1986.03615995005000010019x).
- Morris, J.T., P.V. Sundareshwar, C.T. Nietch, B. Kjerfve, and D.R. Cahoon. 2002. "RESPONSES OF COASTAL WETLANDS TO RISING SEA LEVEL." *Ecology* 83 (10). Ecological Society of America: 2869–77. doi:[10.1890/0012-9658\(2002\)083\[2869:rocwtr\]2.0.co;2](https://doi.org/10.1890/0012-9658(2002)083[2869:rocwtr]2.0.co;2).
- Morris, J.T. and B. Haskin. 1990. "A 5-yr record of aerial primary production and stand characteristics of *Spartina alterniflora*." *Ecology* 71 (6) Wiley Online Library: 2209-2217. doi: [10.2307/1938633](https://doi.org/10.2307/1938633).
- Mudd, S.M., S.M. Howell, and J.T. Morris. 2009. "Impact of dynamic feedbacks between sedimentation, sea-level rise, and biomass production on near-surface marsh stratigraphy and carbon accumulation." *Estuarine, Coastal and Shelf Science* 82(3). Elsevier: 377-389. doi: [10.1080/15320380802547841](https://doi.org/10.1080/15320380802547841).
- Mudd, S.M., A. D'Alpaos, and J.T. Morris. 2010. "How does vegetation affect sedimentation on tidal marshes? Investigating particle capture and hydrodynamic controls on biologically mediated sedimentation." *Journal of Geophysical Research: Earth Surface* 115(F3). Wiley Online Library. doi: [10.1029/2009jf001566](https://doi.org/10.1029/2009jf001566).
- Natural Resources Canada. 2016. "Expedition Database." Geological Survey of Canada. http://ed.gdr.nrcan.gc.ca/grainsize_e.php.
- NCAR-GIS-Program 2012. "Climate Change Scenarios, Version 2.0. Community Climate System Model, June 2004 Version 3.0. (Http://www.cesm.ucar.edu/models/ccsm3.0/) Was Used to Derive Data Products." National Center for Atmospheric Research (NCAR)

- / University Corporation for Atmospheric Research (UCAR).
<http://www.gisclimatechange.org>.
- Nellemann, C., E. Corcoran, C.M. Duarte, L. Valdes, C. De Young, L. Fonseca, and G. Grimsditch. 2009. *Blue Carbon - the Role of Healthy Oceans in Binding Carbon*. Rapid Response Assessment. Arendal, Norway: GRID-Arendal / United Nations Environment Programme (UNEP). <http://www.grida.no/publications/rr/blue-carbon/>.
- Nyman, J.A., R.D. DeLaune, H.H. Roberts, and W.H. Patrick. 1993. "Relationship Between Vegetation and Soil Formation in a Rapidly Submerging Coastal Marsh." *Marine Ecology Progress Series* 96. Inter-Research Science Center: 269–79. doi:[10.3354/meps096269](https://doi.org/10.3354/meps096269).
- Nyman, J.A., R.J. Walters, R.D. Delaune, and W.H. Patrick. 2006. "Marsh Vertical Accretion via Vegetative Growth." *Estuarine, Coastal and Shelf Science* 69 (3-4). Elsevier BV: 370–80. doi:[10.1016/j.ecss.2006.05.041](https://doi.org/10.1016/j.ecss.2006.05.041).
- Orson, R.A, R.L. Simpson, and R.E. Good. 1990. "Rates of Sediment Accumulation in a Tidal Freshwater Marsh." *Journal of Sedimentary Research*, no. 60: 6.
- Pebesma, E.J. 2004. "Multivariable Geostatistics in S: The Gstat Package." *Computers & Geosciences* 30: 683–91.
- Pebesma, E.J., and R.S. Bivand. 2005. "Classes and Methods for Spatial Data in R." *R News* 5 (2): 9–13. <http://CRAN.R-project.org/doc/Rnews/>.
- Portnoy, J. W., and A. E. Giblin. 1997. "Effects of historic tidal restrictions on salt marsh sediment chemistry." *Biogeochemistry* 36 (3) Springer: 275-303. doi: [10.1023/a:1005715520988](https://doi.org/10.1023/a:1005715520988) .
- R Core Team. 2016. *R: A Language and Environment for Statistical Computing*. Vienna, Austria: R Foundation for Statistical Computing. <https://www.R-project.org/>.
- Redfield, A.C. 1972. "Development of a New England Salt Marsh." *Ecological Monographs* 42 (2). JSTOR: 201. doi:[10.2307/1942263](https://doi.org/10.2307/1942263).
- Reid, J.M., J.A. Reid, C.J. Jenkins, M.E. Hastings, S.J. Williams, and L.J. Poppe. 2005. "UsSEABED: Atlantic Coast Offshore Surficial Sediment Data Release." U.S. Geological Survey Data Series 118. Woods Hole Science Center, Woods Hole, MA: U.S. Geological Survey, Coastal; Marine Geology Program. <http://pubs.usgs.gov/ds/2005/118/>.
- Rohatgi, A. 2016. "WebPlotDigitizer - Extract Data from Plots, Images, and Maps." <http://arohatgi.info/WebPlotDigitizer/>.

- Roman, C.T., J.A. Peck, J. R. Allen, J.W. King, and P.G. Appleby. 1997. "Accretion of a New England (USA) salt marsh in response to inlet migration, storms, and sea-level rise." *Estuarine, Coastal and Shelf Science* 45 (6) Elsevier: 717-727. doi:
[10.1006/ecss.1997.0236](https://doi.org/10.1006/ecss.1997.0236).
- Richardson, M.D., and K.B. Briggs. 1993. *On the Use of Acoustic Impedence Values to Determine Sediment Properties*. Edited by U.K. Institute of Acoustics University of Bath. Vol. 15 (2).
- Sharma, P., L.R. Gardner, W.S. Moore, and M.S. Bollinger. 1987. "Sedimentation and Bioturbation in a Salt Marsh as Revealed by 210Pb, 137Cs, and 7Be Studies." *Limnol. Oceanogr.* 32 (2). Wiley-Blackwell: 313–26. doi:[10.4319/lo.1987.32.2.0313](https://doi.org/10.4319/lo.1987.32.2.0313).
- Swarzenski, C.M., E.M. Swenson, C.E. Sasser, and J.G. Gosselink. 1991. "Marsh Mat Flotation in the Louisiana Delta Plain." *The Journal of Ecology* 79 (4). JSTOR: 999. doi:[10.2307/2261094](https://doi.org/10.2307/2261094).
- USGS. 2005. "ATL_CLC: UsSEABED CaLCulated Data for the Entire U.S. Atlantic Coast." U.S. Geological Survey (USGS); University of Colorado. http://pubs.usgs.gov/ds/2005/118/htmldocs/data_cata.htm.
- USGS. 2006. "GMX_CLC: UsSEABED CaLCulated Data for the Entire U.S. Gulf of Mexico and Caribbean (Puerto Rico and U.S. Virgin Islands)." U.S. Geological Survey (USGS); University of Colorado. http://pubs.usgs.gov/ds/2006/146/htmldocs/data_cata.htm.
- Vogel, R. L., B. Kjerfve, and L.R. Gardner. (1996). "Inorganic sediment budget for the North Inlet salt marsh, South Carolina, USA." *Mangroves and Salt Marshes*, 1 (1). Springer: 23-35.
- Wu, W., and S. Wang. 2006. "Formulas for Sediment Porosity and Settling Velocity." *Journal of Hydraulic Engineering*, 858–62. doi:[10.1061/\(ASCE\)0733-9429\(2006\)132:8\(858\)](https://doi.org/10.1061/(ASCE)0733-9429(2006)132:8(858))

APPENDIX A.1: STREAM GAGE SUMMARY

Table A.1.1-Gage Summary Table 1

gage#	Lat	Area (km²)	Rain (m/y)	nYear	nConc	smear	Span	Yield (MT/km²)	τ
1673000	37.77	2,792	1.16	37 (18)	489	1.56	0.57	0.016	-0.08
2035000	37.67	16,193	1.17	38 (19)	710	1.66	0.56	0.045	-0.15
2041650	37.23	3,476	1.16	34 (18)	444	1.22	0.54	0.005	-0.25
2075500	36.64	6,700	1.30	16 (2)	94	2.07	0.90	0.119	-
2085500	36.18	386	1.20	29 (20)	196	1.40	0.68	0.046	-0.18
208524090	36.15	21	1.14	20 (19)	166	1.42	0.65	0.033	0.18
208521324	36.14	203	1.29	16 (12)	63	1.51	0.68	0.059	-0.36
208650112	36.13	3	1.12	23 (19)	168	2.01	0.74	0.086	-0.05
208524975	36.11	256	1.15	19 (18)	150	-	-	0.002	0.01
2085000	36.07	171	1.24	28 (22)	203	1.30	0.56	0.042	-0.34
2096846	35.99	20	1.24	27 (22)	207	1.00	-	0.002	0.03
208700780	35.99	26	1.14	9 (3)	88	1.38	0.75	0.159	-0.33
2087183	35.94	1,997	1.44	14 (1)	131	1.68	0.93	0.013	-
2097464	35.92	22	1.22	27 (22)	200	-	-	0.002	0.00
2116500	35.86	5,905	1.18	19 (7)	353	1.33	0.63	0.080	-0.14
2096960	35.77	3,302	1.26	17 (7)	178	1.42	0.42	0.038	0.14
209782609	35.76	31	1.13	16 (15)	99	1.18	0.62	0.022	0.22
2087580	35.72	54	1.20	13 (12)	175	1.15	0.82	0.012	-0.39
2087500	35.65	2,978	1.43	14 (2)	126	1.58	0.64	0.034	-
214266000	35.39	68	0.98	6 (6)	99	1.38	0.82	0.138	0.33
2124692	35.15	62	1.10	10 (10)	176	1.75	0.56	0.107	0.07
2126000	35.15	3,553	1.24	15 (4)	102	1.34	0.78	0.054	0.67

These are summary descriptions for gages north of the 35th parallel (i.e. north of Georgia). Under nYear, the first number is the total number of years with available sediment data used to train the rating curve regression. The number in parentheses is the number of years intersecting with the time frame of the night lights data set (1992-2014). τ is the non-parametric correlation coefficient between basin-averaged illumination and sediment yield.

Table A.1.2-Gage Summary Table 2

gage#	Lat	Area (km²)	Rain (m/y)	nYear	nConc	smear	Span	Yield (MT/km²)	τ
2331600	34.54	816	1.84	20 (7)	230	1.44	0.48	0.107	0.71
2333500	34.53	396	1.83	17 (7)	273	1.46	0.44	0.113	0.43
2334480	34.13	24	1.35	13 (13)	130	3.70	0.71	2.108	-0.23
2334578	34.10	13	1.34	14 (13)	126	4.07	0.67	0.829	0.18
2217274	34.08	3	1.28	14 (13)	126	2.56	0.87	0.588	-0.08
2334885	34.03	122	1.39	14 (14)	96	-	-	0.096	-0.16
2218565	34.01	15	1.33	13 (12)	120	2.31	0.81	1.095	0.18
2335350	33.97	23	1.38	12 (12)	82	2.36	0.65	1.138	0.54
2335870	33.95	80	1.40	22 (21)	347	1.70	0.81	0.295	0.05
2208150	33.92	80	1.35	14 (13)	81	2.85	0.82	0.580	0.03
2336030	33.91	4	1.24	12 (11)	114	2.36	0.78	0.504	-0.22
2336360	33.87	69	1.32	8 (8)	102	1.94	0.57	0.508	-0.14
2336410	33.84	98	1.42	6 (6)	105	1.89	0.74	0.406	0.20
2336120	33.83	90	1.39	8 (7)	106	1.98	0.88	0.198	-0.14
2207400	33.82	21	1.37	13 (12)	93	2.47	0.92	0.347	-0.15
2336300	33.82	225	1.46	19 (14)	301	1.91	0.55	0.957	0.14
2207385	33.82	45	1.38	13 (12)	85	3.17	0.93	1.024	-0.39
2336240	33.80	71	1.39	9 (8)	90	-	-	0.062	-0.07
2336526	33.79	35	1.44	7 (7)	86	2.48	0.91	0.387	0.14
2207185	33.78	26	1.34	14 (13)	137	2.78	0.87	0.183	-0.23
2207120	33.77	420	1.38	13 (12)	88	2.12	0.64	0.351	-0.03
2207220	33.73	552	1.33	7 (7)	62	1.61	0.93	0.191	-0.24
2203655	33.68	58	1.36	9 (9)	157	1.82	0.82	0.238	0.08
2207335	33.67	673	1.41	9 (9)	114	2.11	0.66	0.215	-0.11
2337500	33.53	92	1.36	11 (9)	196	1.69	0.61	0.102	0.06
2338000	33.48	6,294	1.44	37 (21)	717	1.26	0.33	0.068	-0.43
2338523	33.34	44	1.62	10 (9)	65	-	-	0.002	-0.11
2212600	33.10	187	1.27	14 (2)	76	-	-	0.004	-
2339500	32.89	9,194	-	14 (2)	169	2.29	0.94	0.018	-

These are summary descriptions for gages south of the 35th parallel (i.e. in Georgia). Labeling conventions are the same as table A.1.1

APPENDIX A.2: SEDIMENT RATING CURVES

Figure A.2.1-01673000: PAMUNKEY RIVER NEAR HANOVER, VA

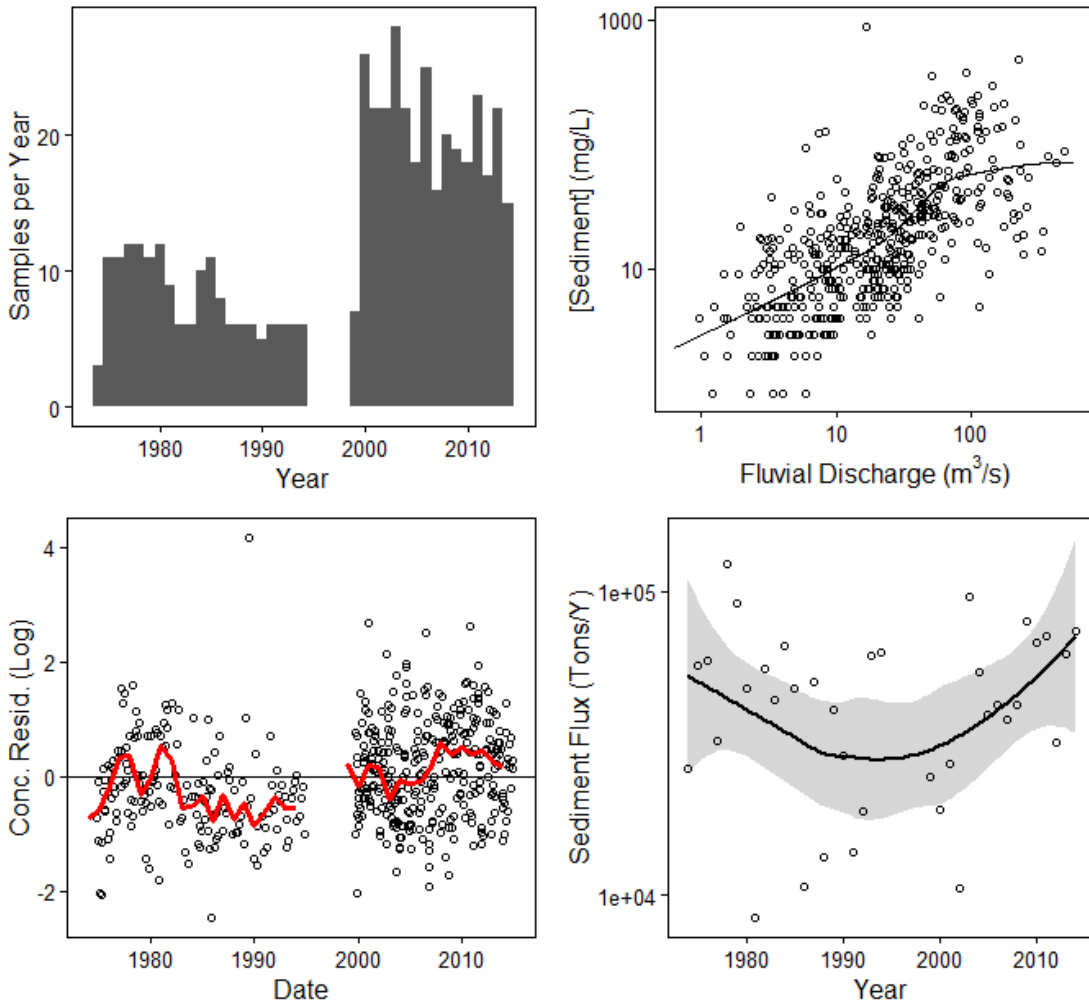


Figure A.2.2-02035000: JAMES RIVER AT CARTERSVILLE, VA

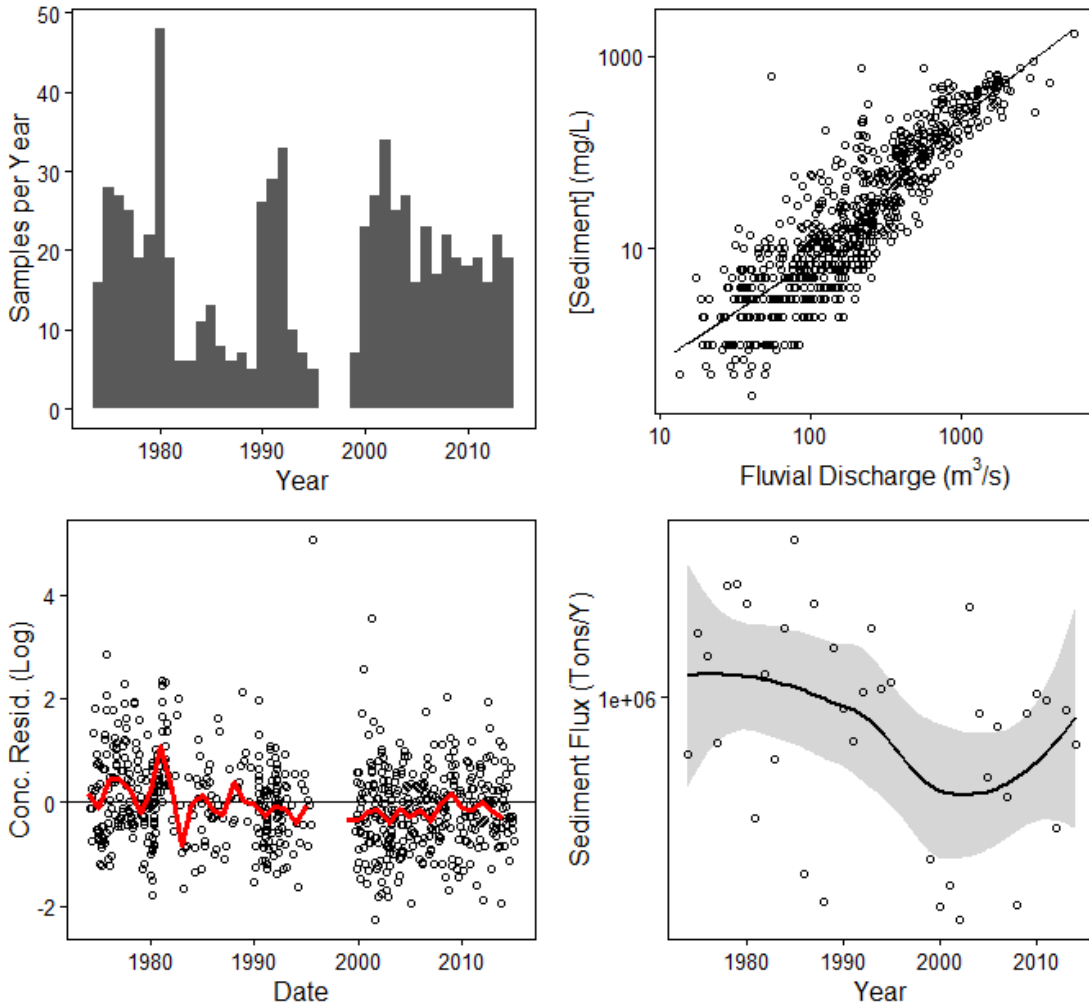


Figure A.2.3-02041650: APPOMATTOX RIVER AT MATOACA, VA

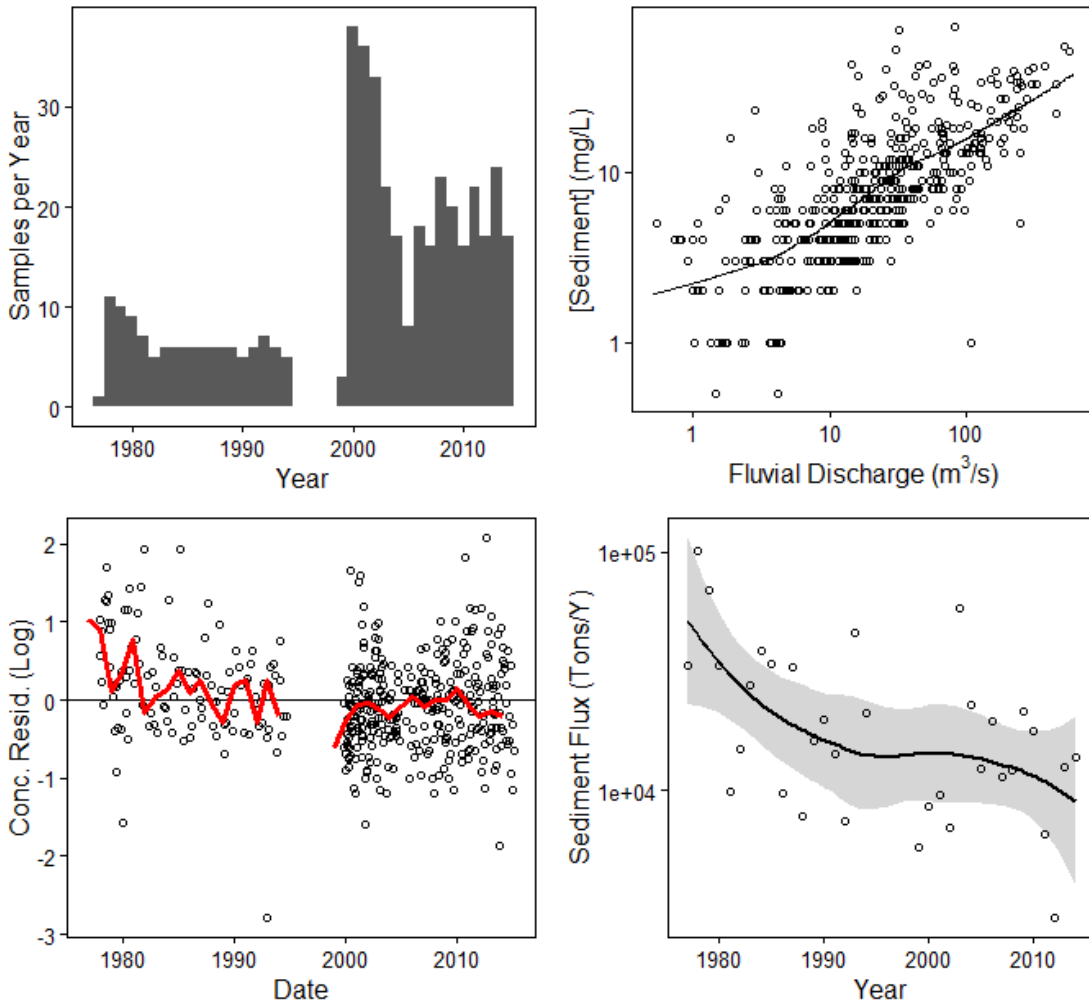


Figure A.2.4-02075500: DAN RIVER AT PACES, VA

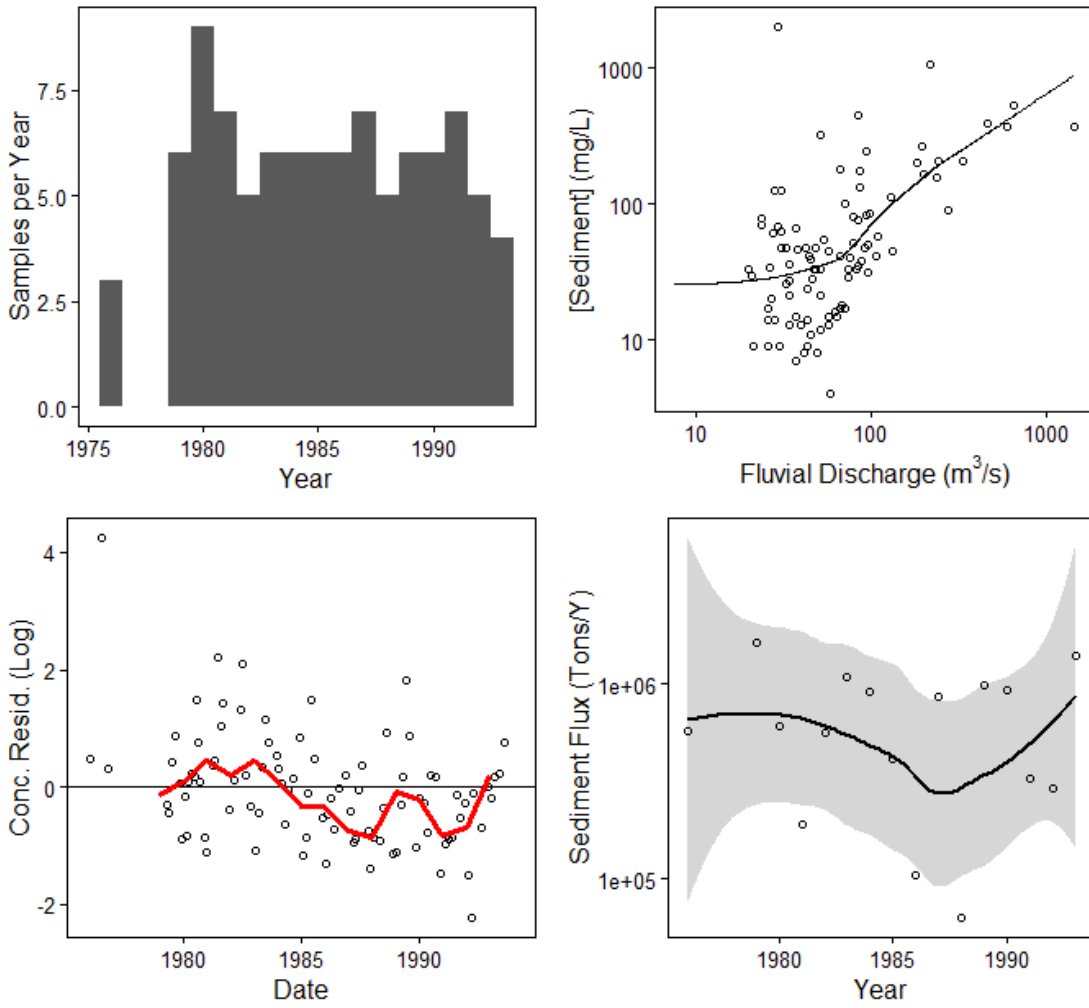


Figure A.2.5-02085500: FLAT RIVER AT BAHAMA, NC

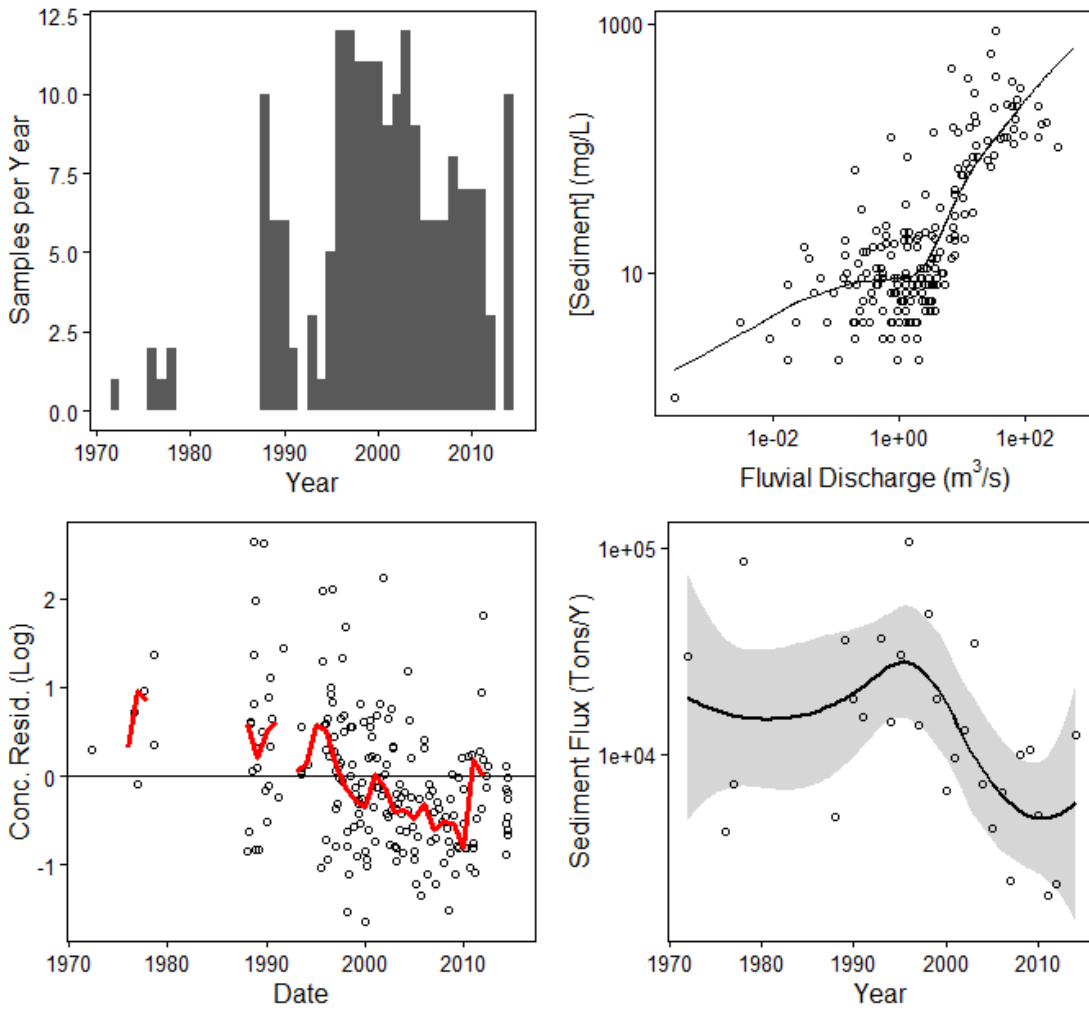


Figure A.2.6-0208524090: MOUNTAIN CREEK AT SR1617 NR BAHAMA, NC

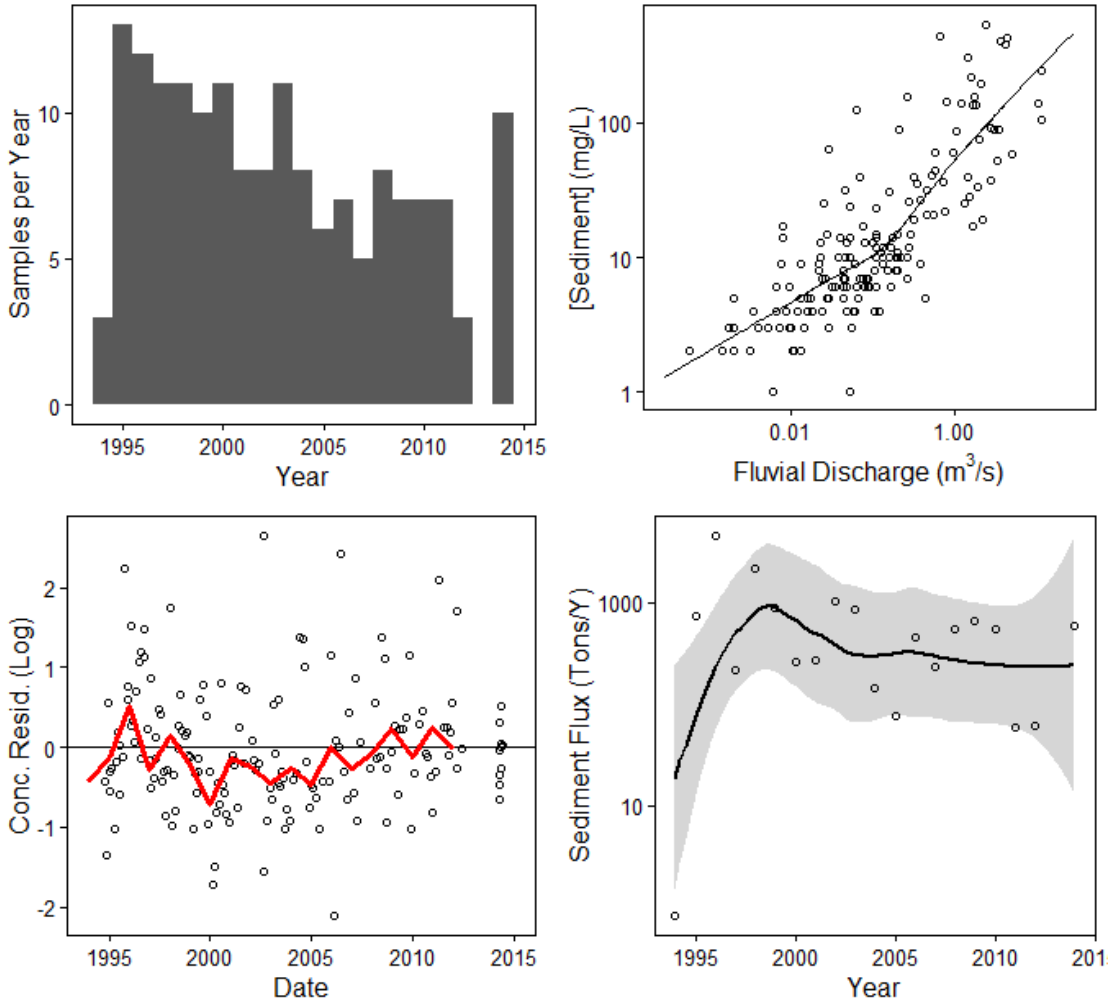


Figure A.2.7-0208521324: LITTLE RIVER AT SR1461 NEAR ORANGE FACTORY, NC

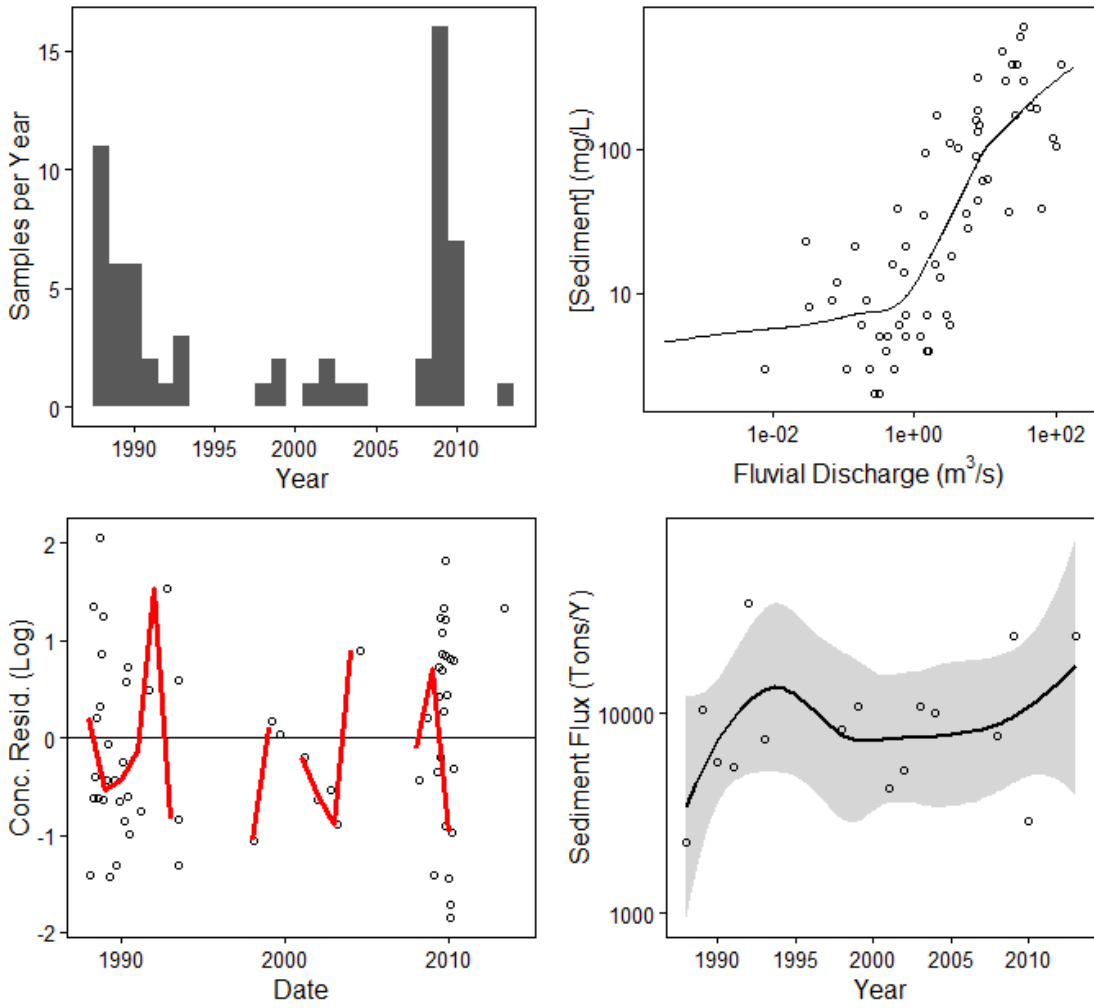


Figure A.2.8-0208650112: FLAT RIVER TRIB NR WILLARDVILLE, NC

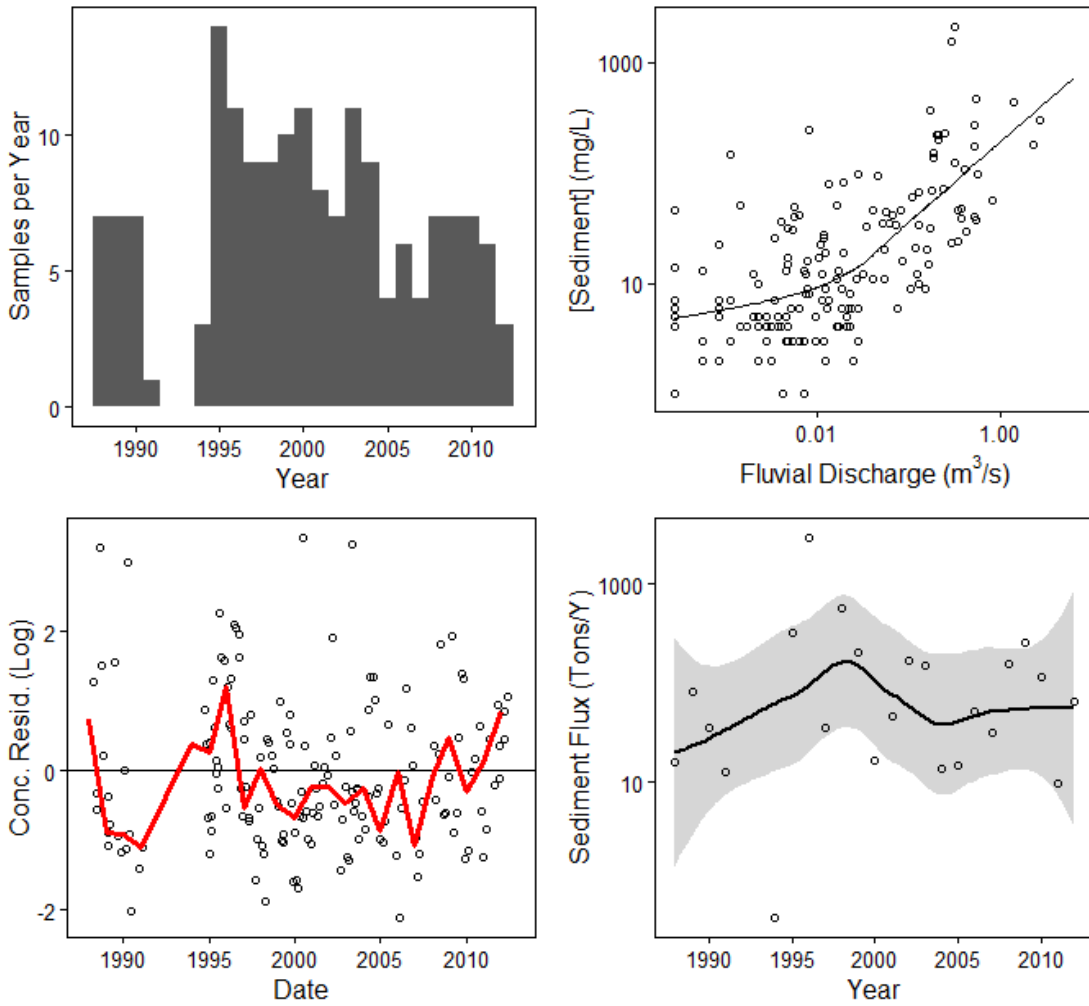


Figure A.2.9-0208524975: LITTLE R BL LITTLE R TRIB AT FAIRNTOSH, NC

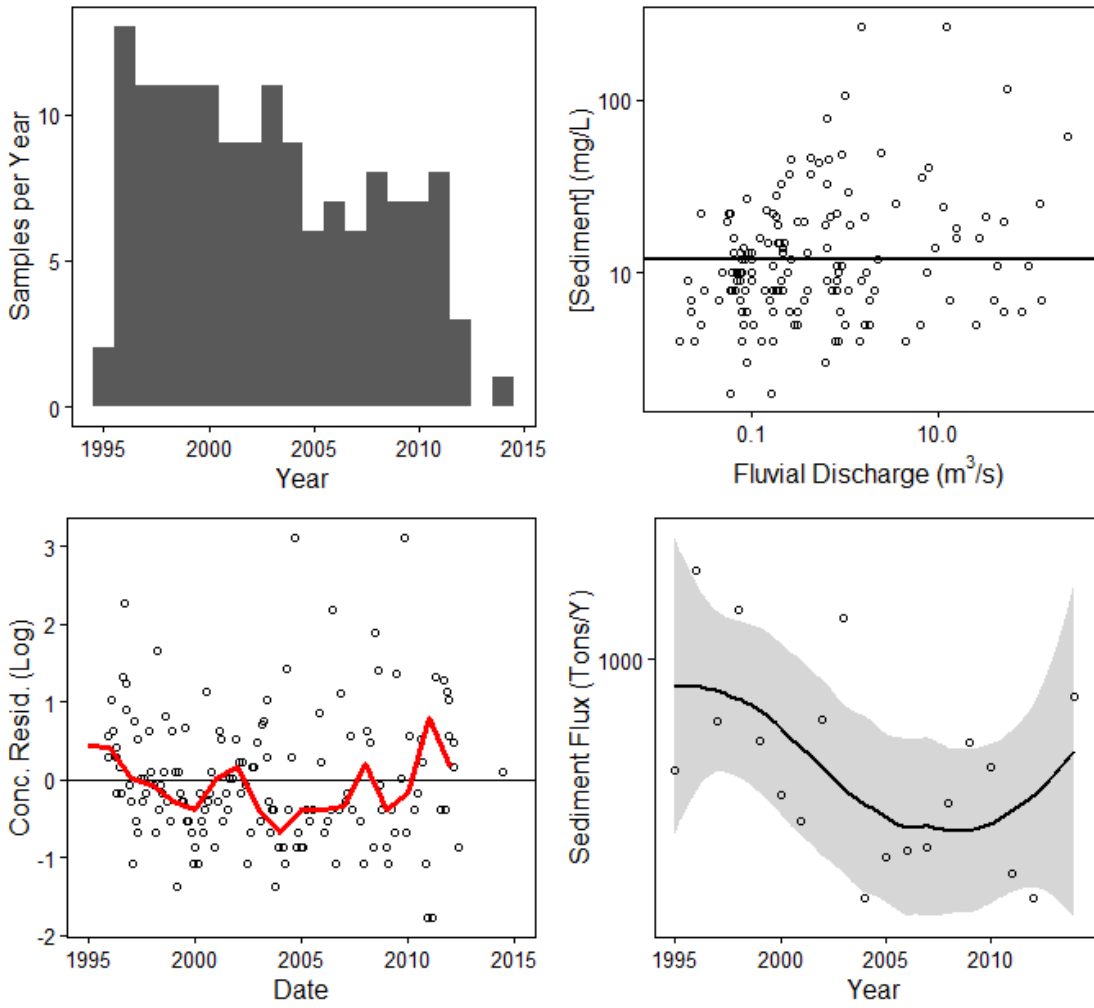


Figure A.2.10-02085000: ENO RIVER AT HILLSBOROUGH, NC

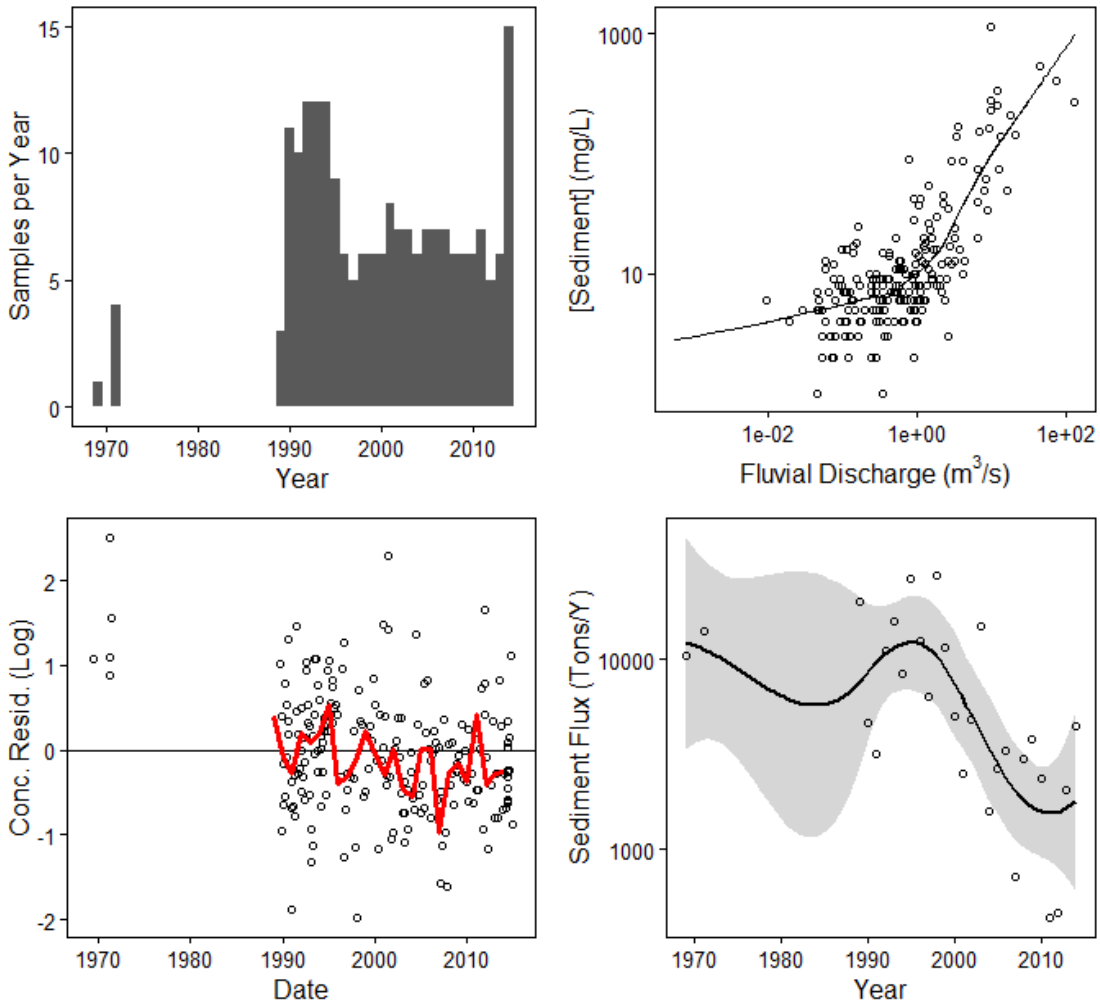


Figure A.2.11-02096846: CANE CREEK NEAR ORANGE GROVE, NC

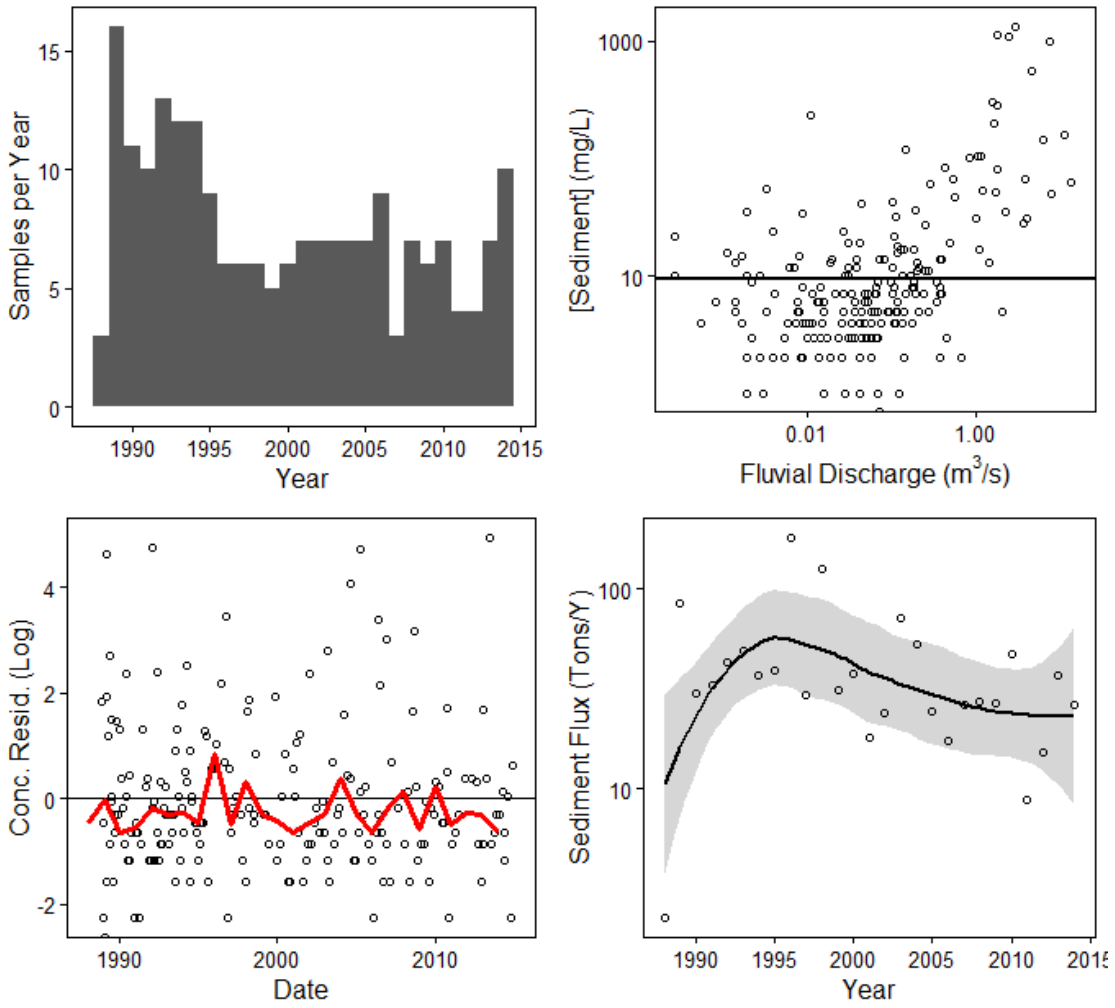


Figure A.2.12-0208700780: LITTLE LICK CR AB SR1814 NR OAK GROVE, NC

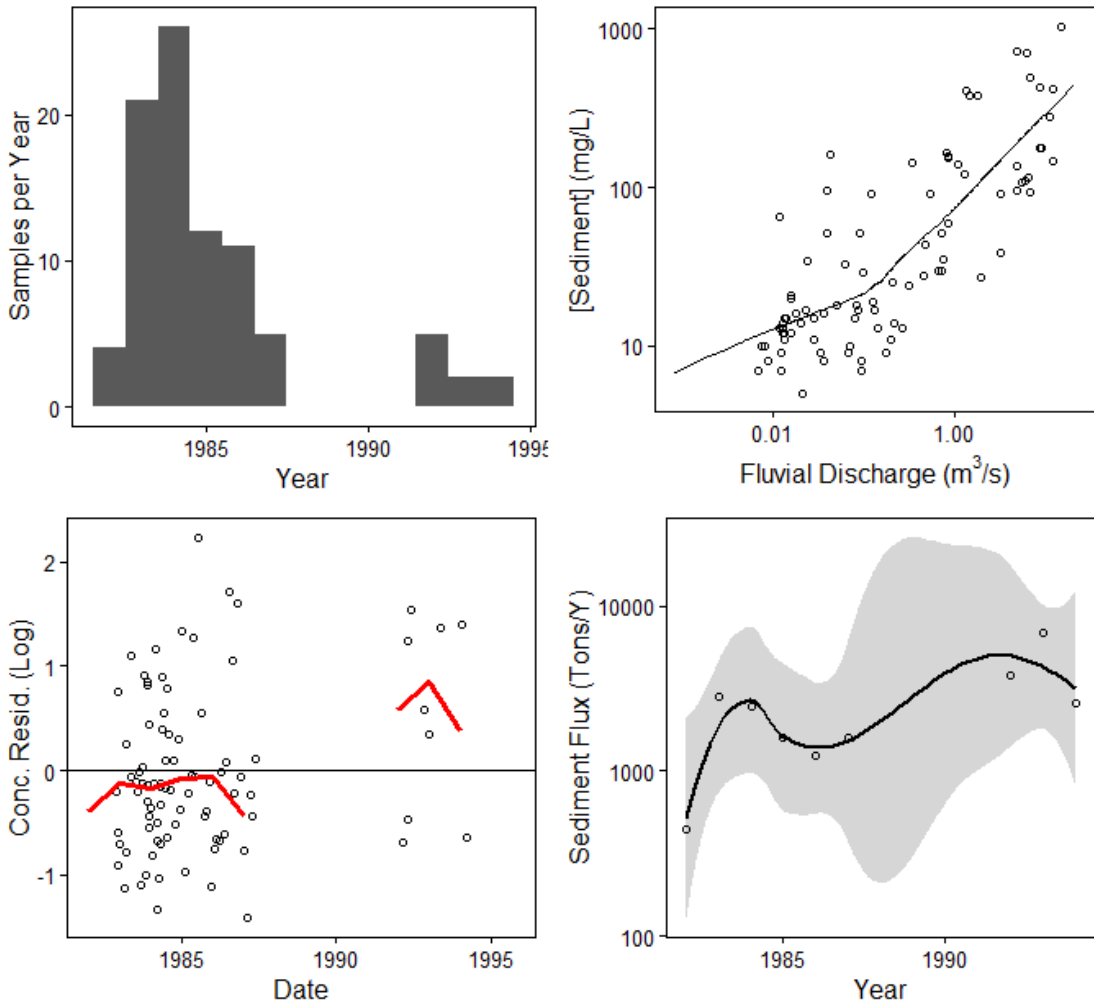


Figure A.2.13-02087183: NEUSE RIVER NEAR FALLS, NC

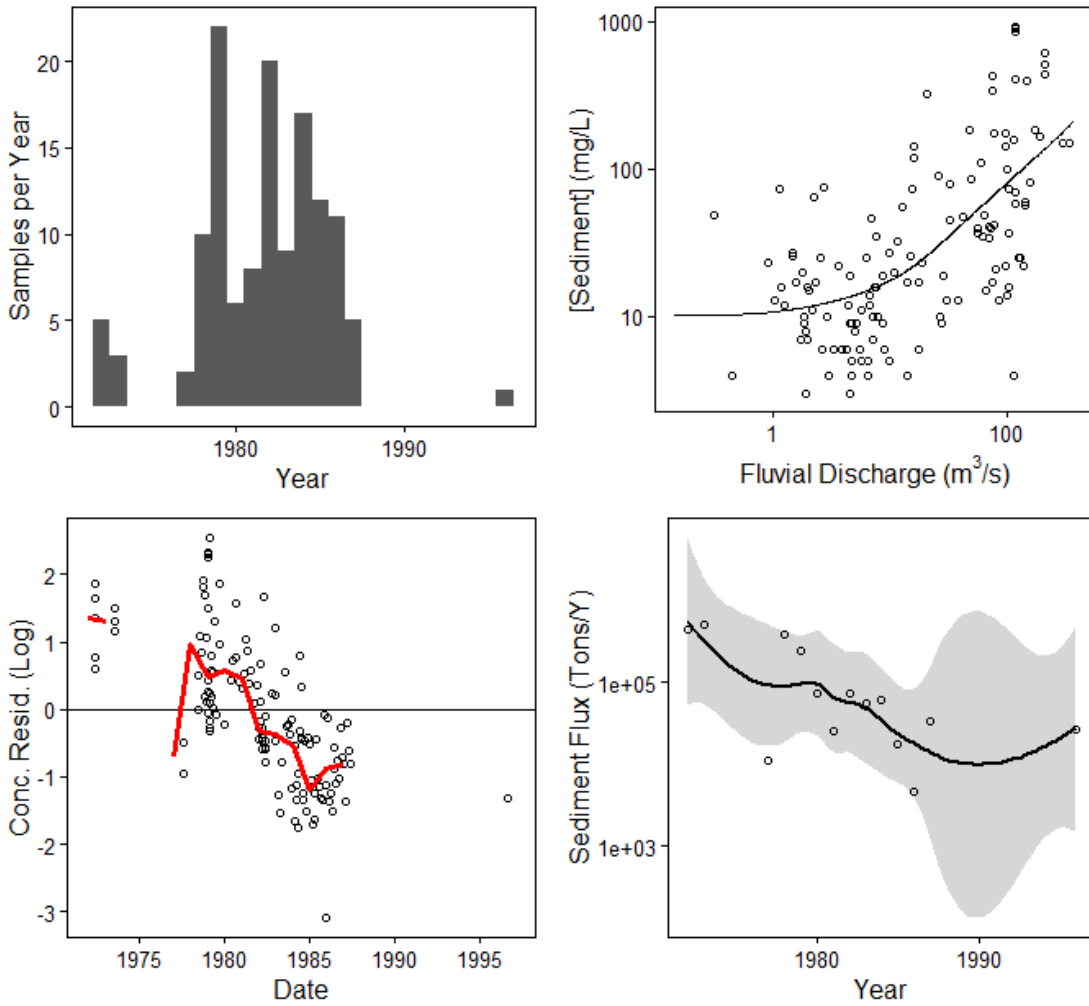


Figure A.2.14-02097464: MORGAN CREEK NEAR WHITE CROSS, NC

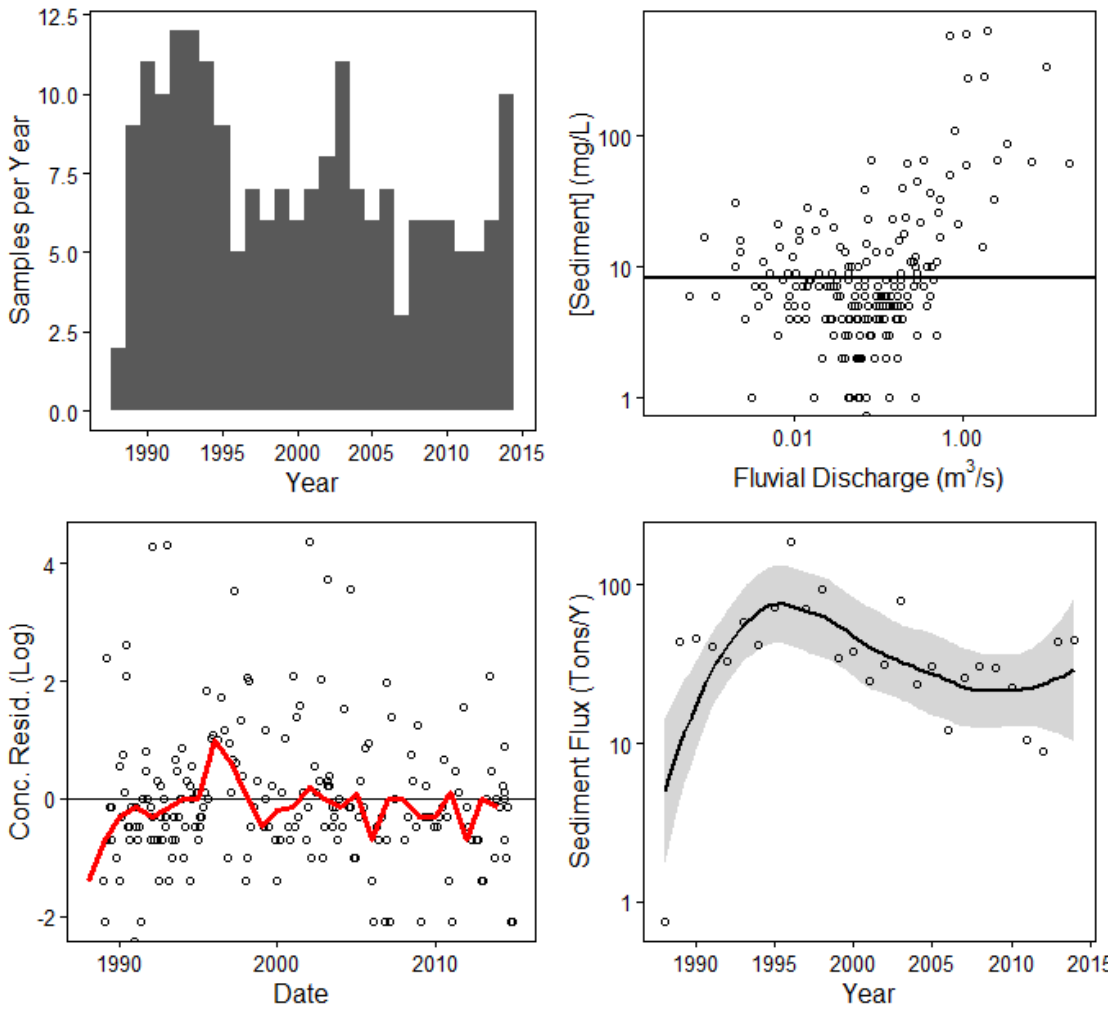


Figure A.2.15-02097517: MORGAN CREEK NEAR CHAPEL HILL, NC

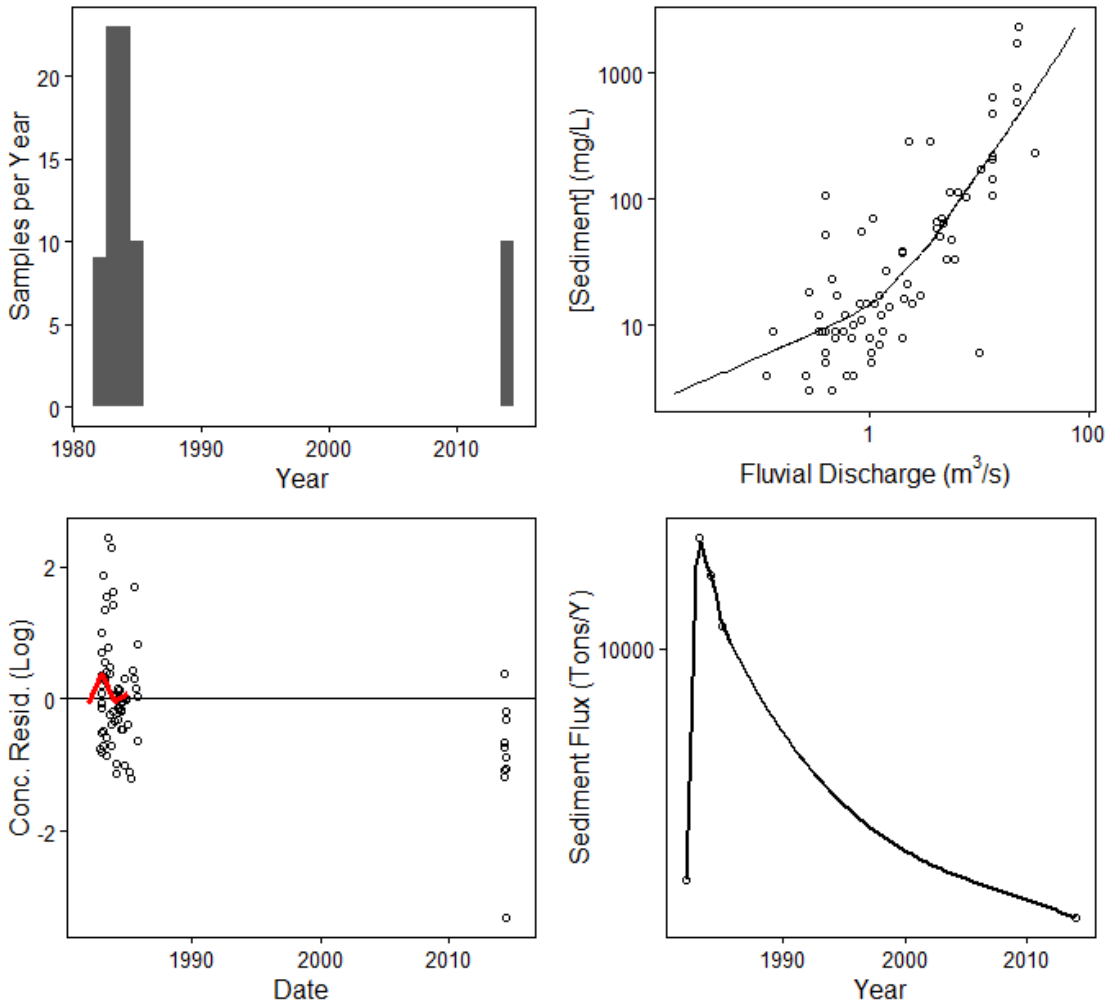


Figure A.2.16-02116500: YADKIN RIVER AT YADKIN COLLEGE, NC

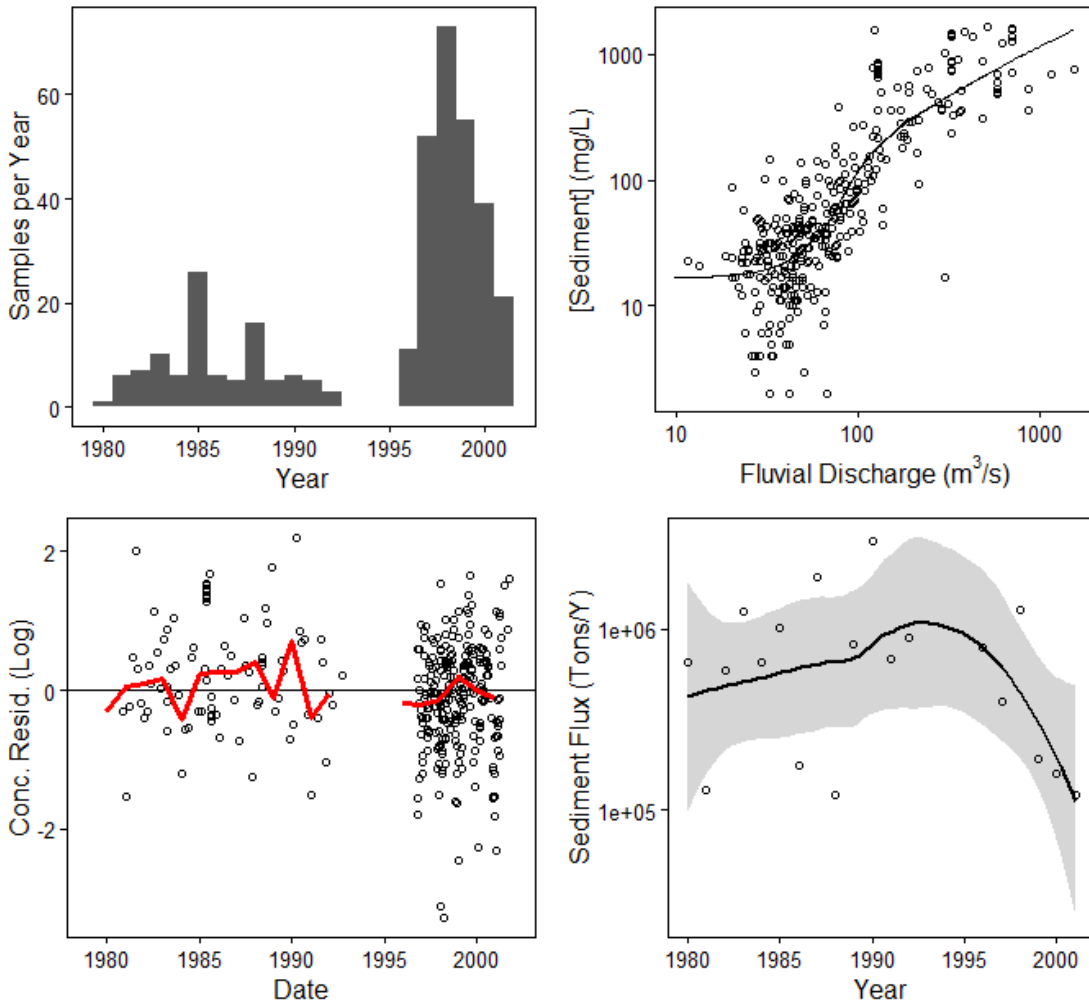


Figure A.2.17-02096960: HAW RIVER NEAR BYNUM, NC

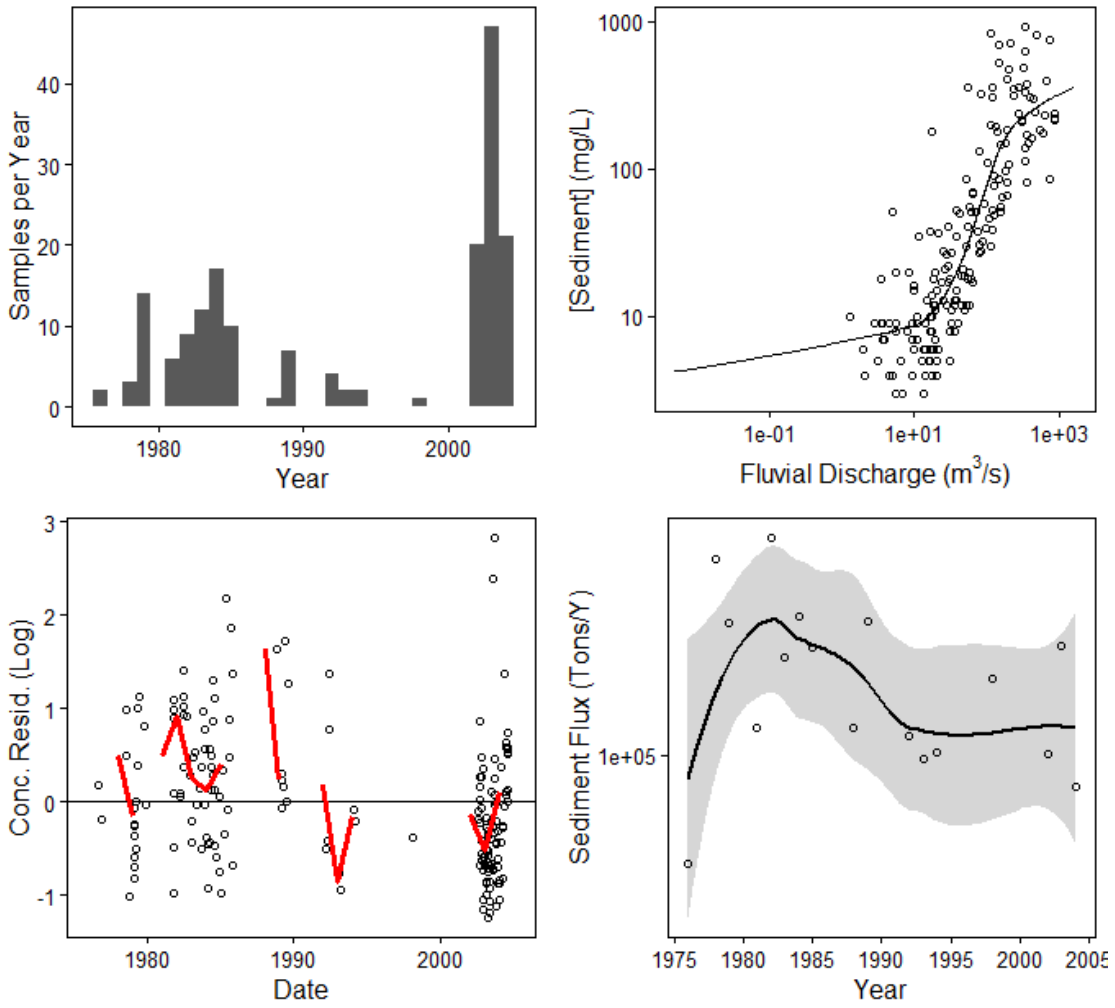


Figure A.2.18-0209782609: WHITE OAK CR AT MOUTH NEAR GREEN LEVEL, NC

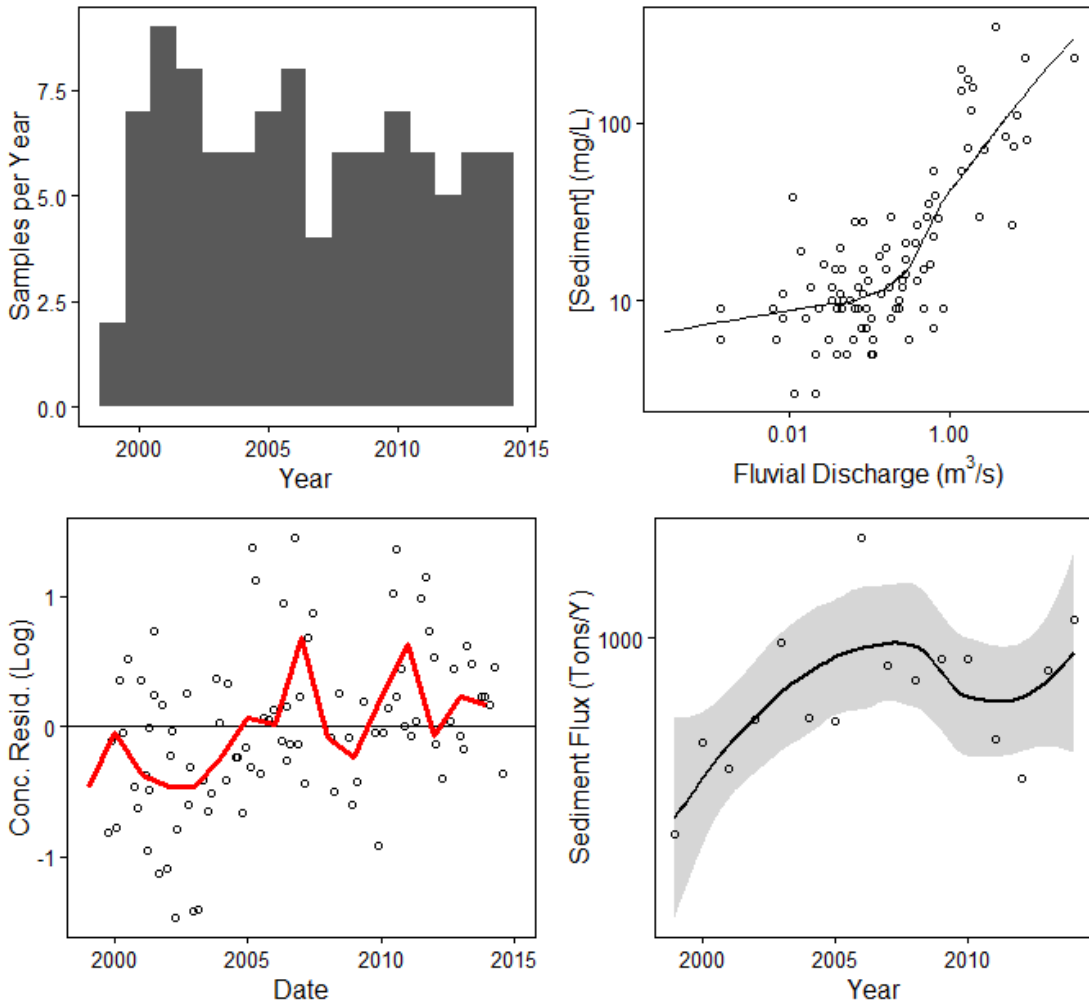


Figure A.2.19-02087580: SWIFT CREEK NEAR APEX, NC

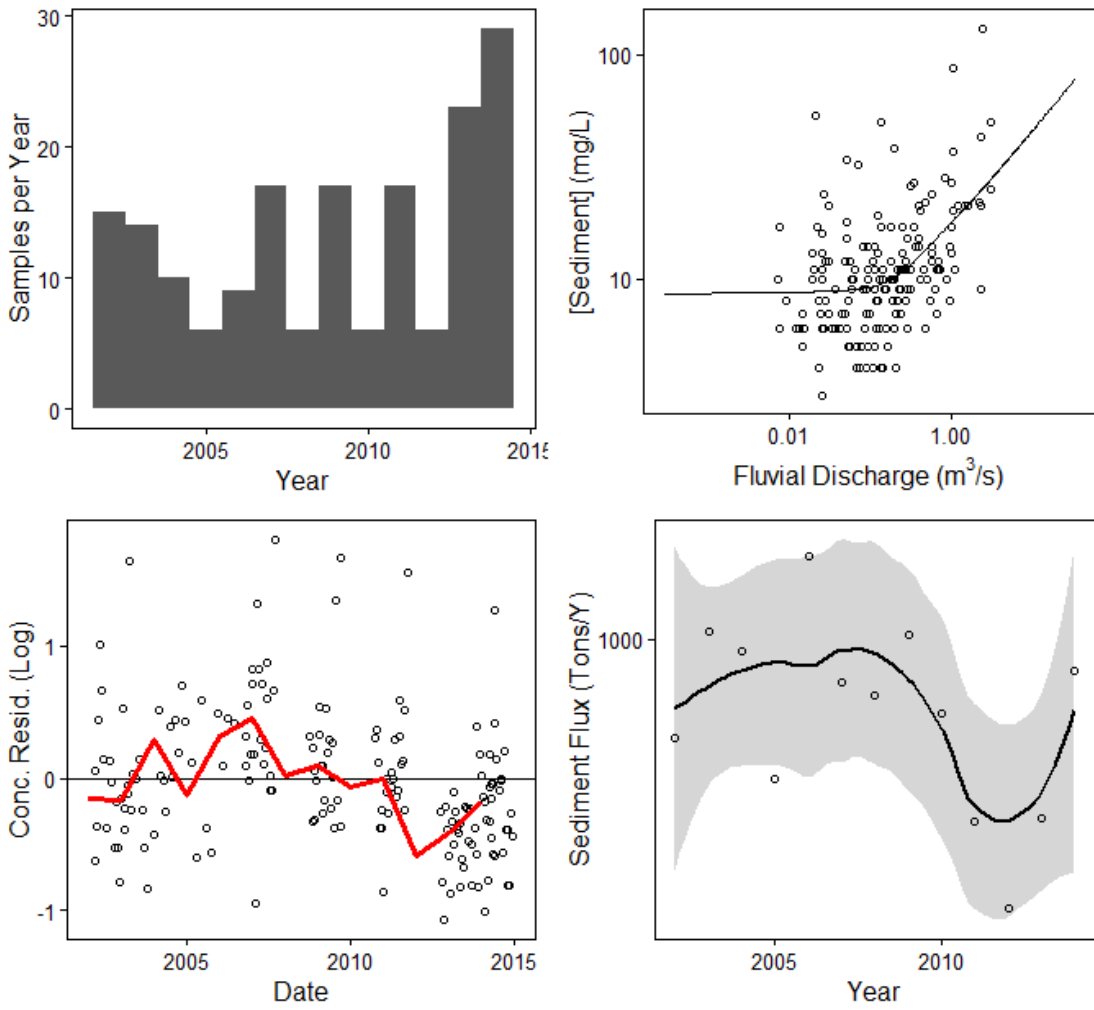


Figure A.2.20-02087500: NEUSE RIVER NEAR CLAYTON, NC

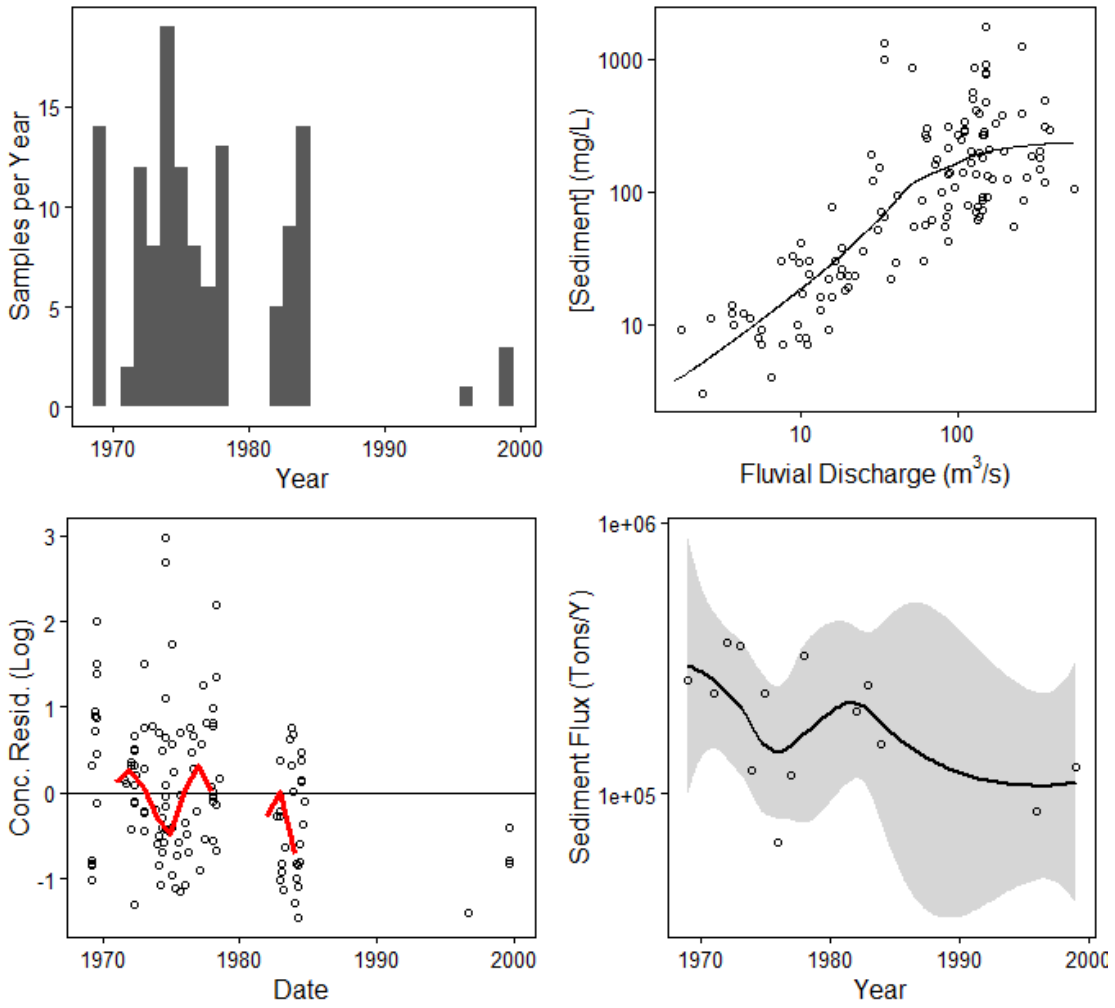


Figure A.2.21-0214266000: MCDOWELL CREEK NR CHARLOTTE, NC (CSW10)

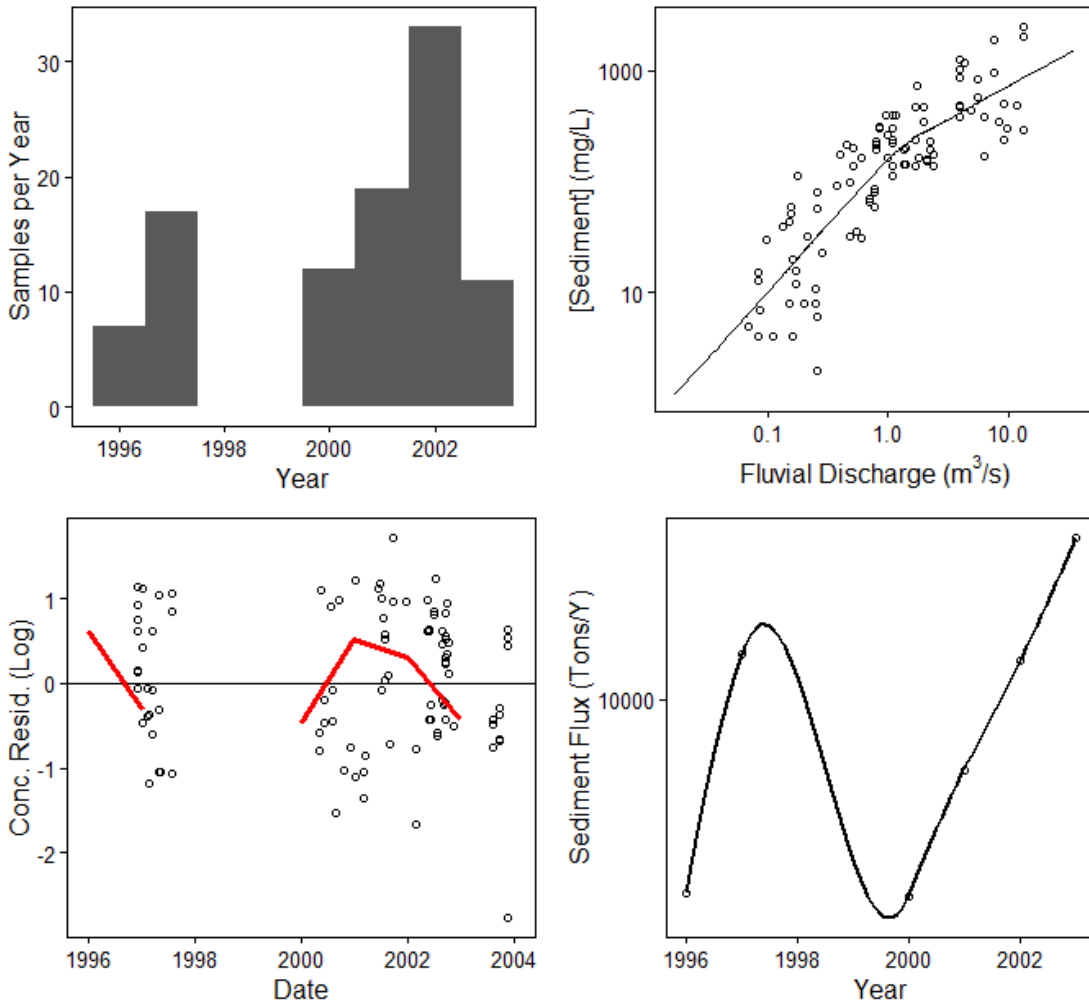


Figure A.2.22-02124692: GOOSE CR AT FAIRVIEW, NC

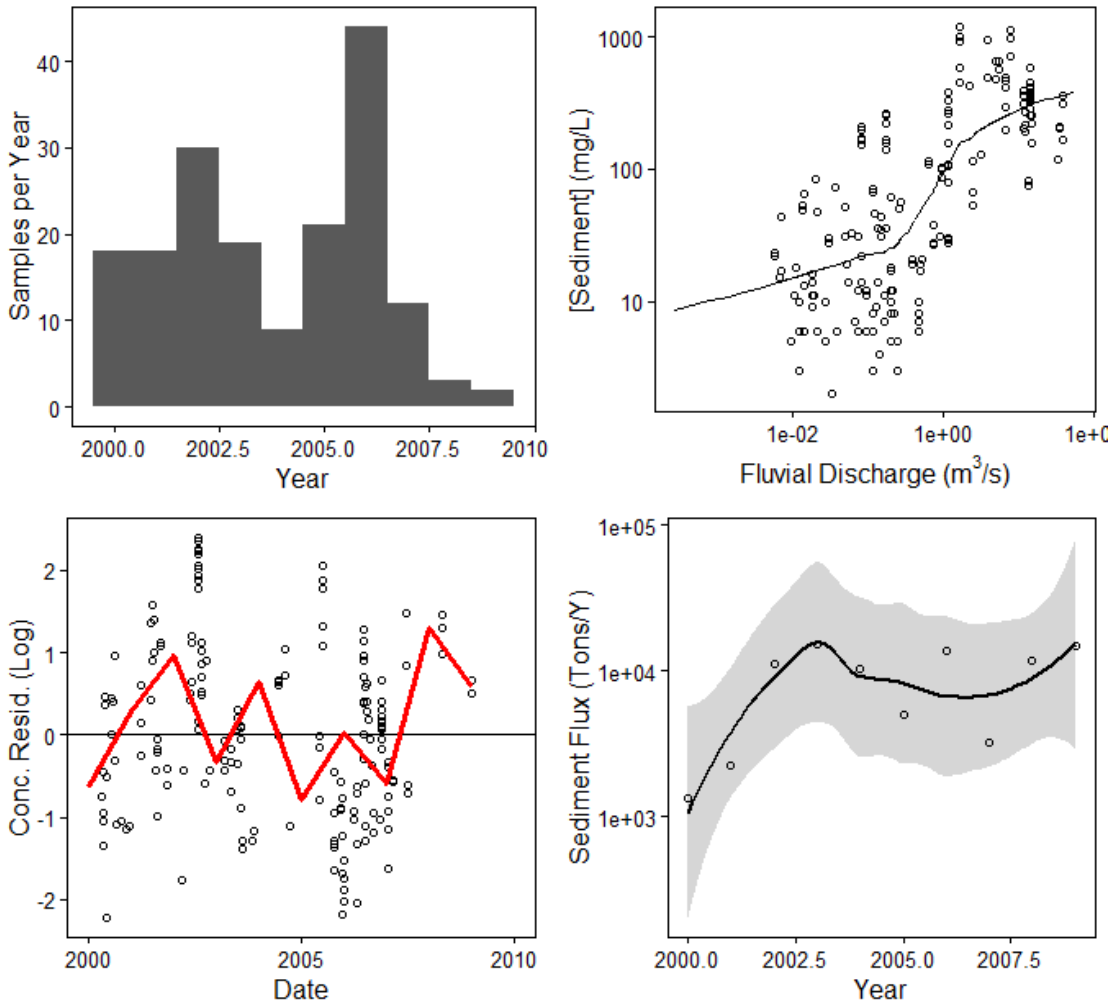


Figure A.2.23-02126000: ROCKY RIVER NEAR NORWOOD, NC

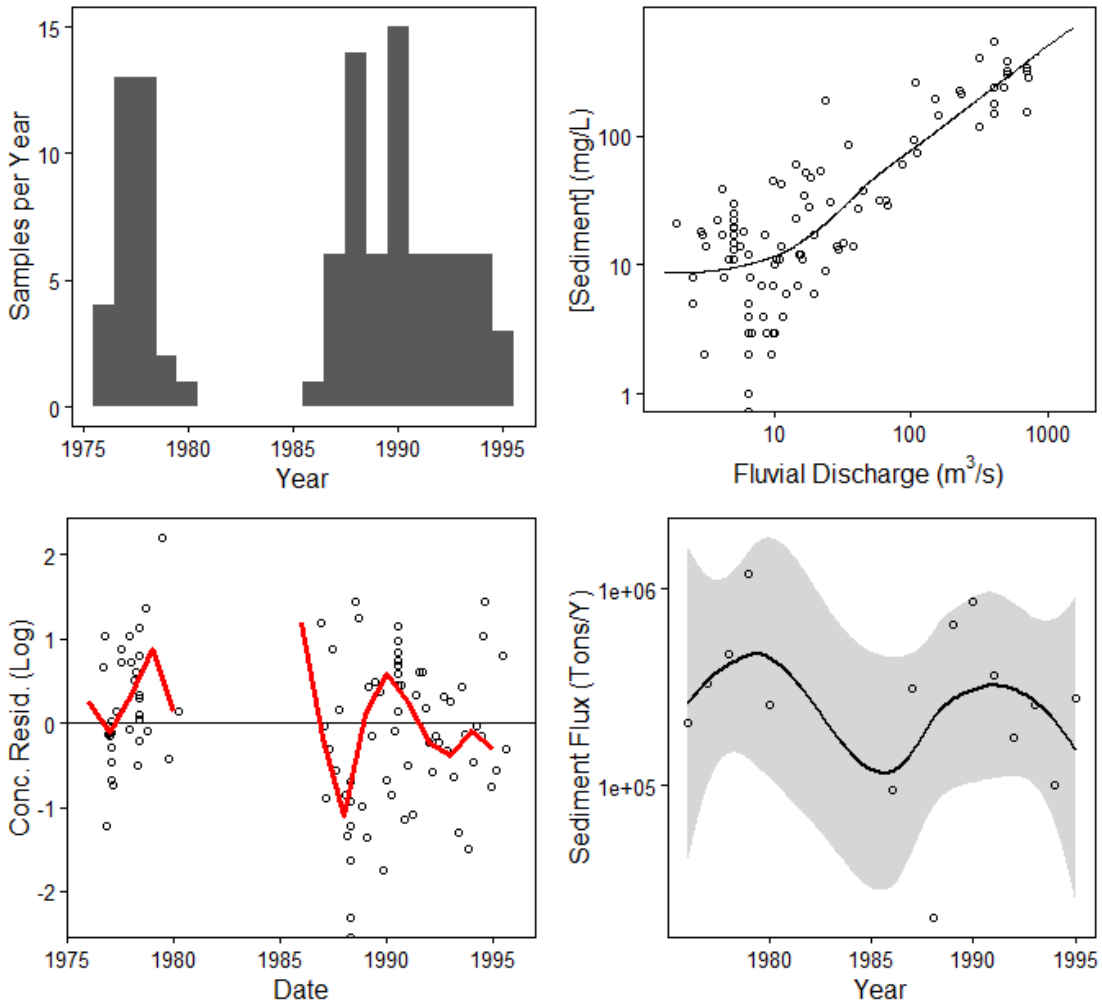


Figure A.2.24-02331600: CHATTAHOOCHEE RIVER NEAR CORNELIA, GA

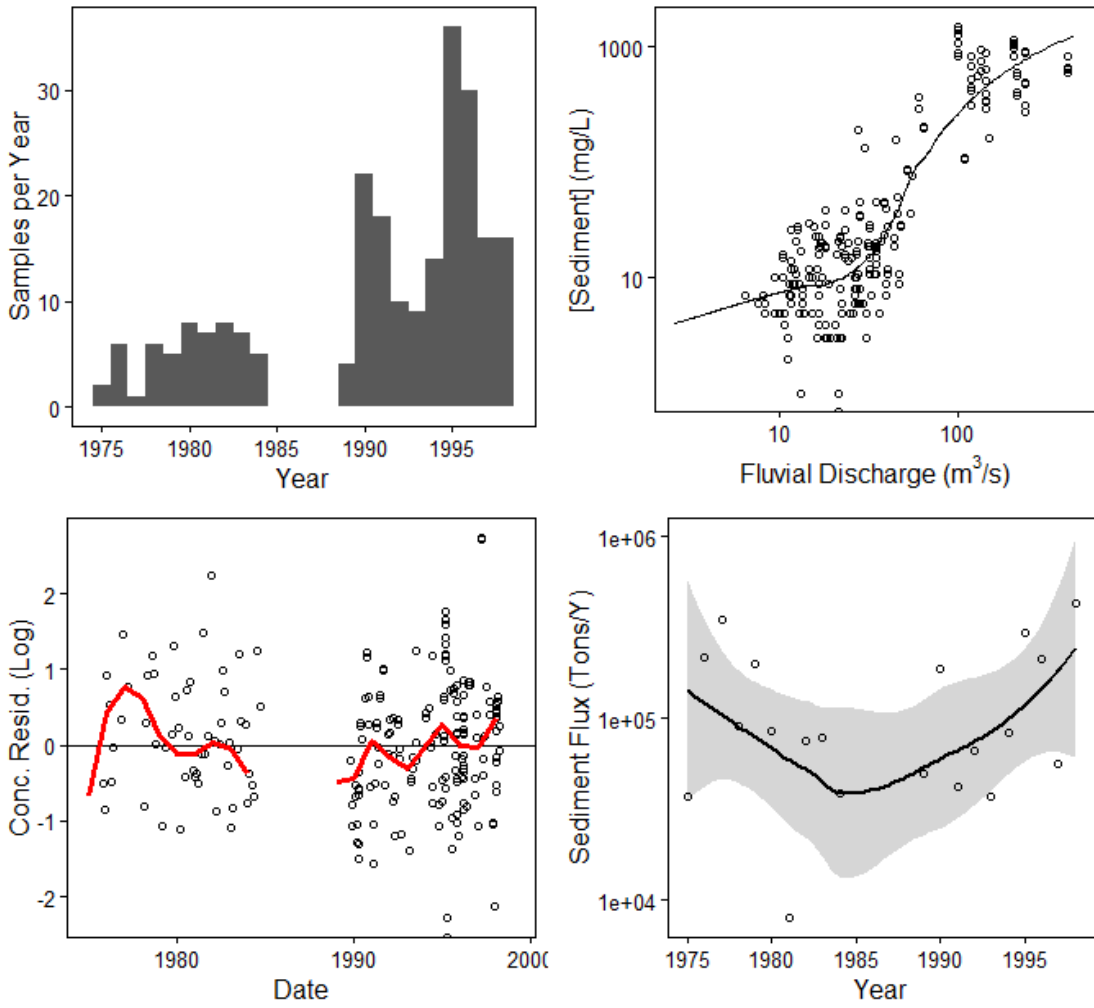


Figure A.2.25-02333500: CHESTATEE RIVER NEAR DAHLONEGA, GA

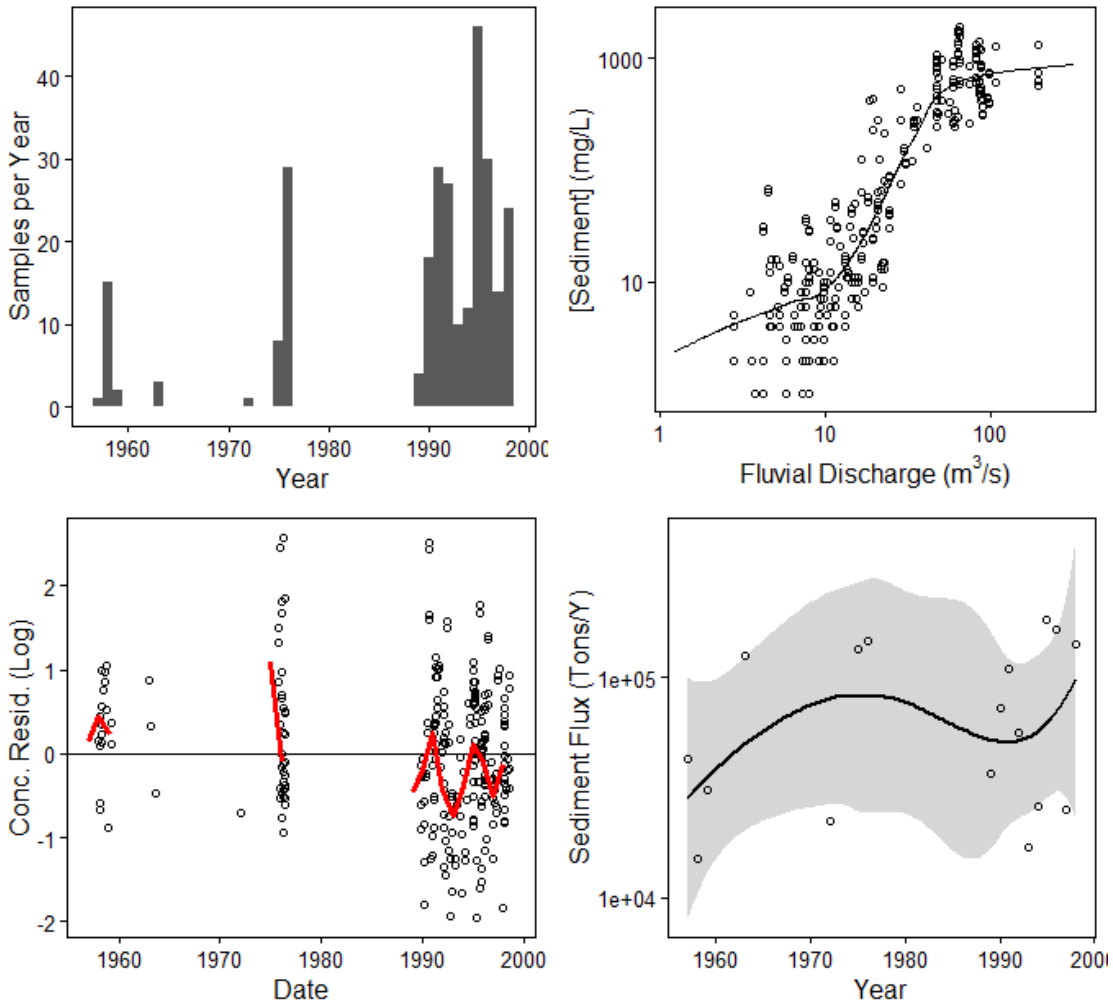


Figure A.2.26-

02334480: RICHLAND CREEK AT SUWANEEN DAM ROAD, NEAR BUFORD,GA

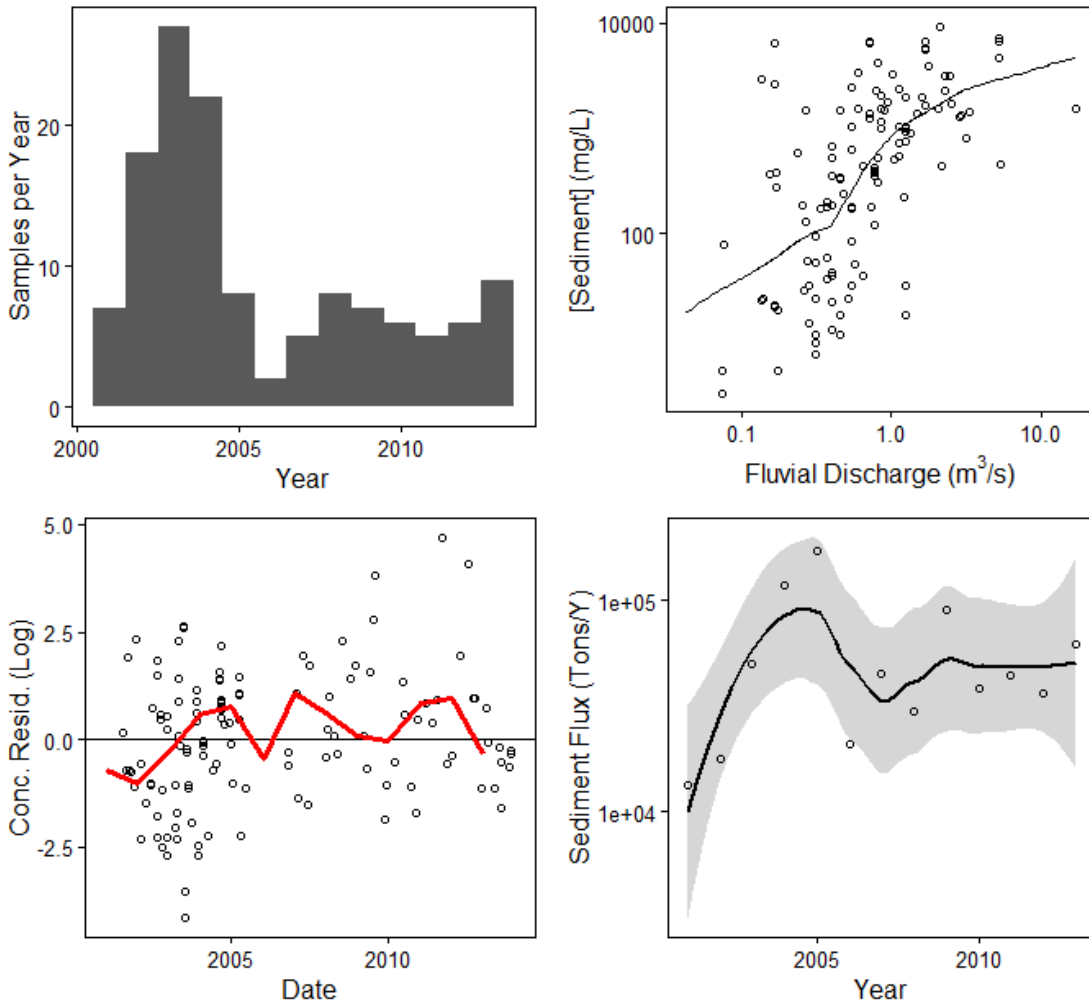


Figure A.2.27-

02334578: LEVEL CREEK AT SUWANEE DAM ROAD, NEAR SUWANEE, GA

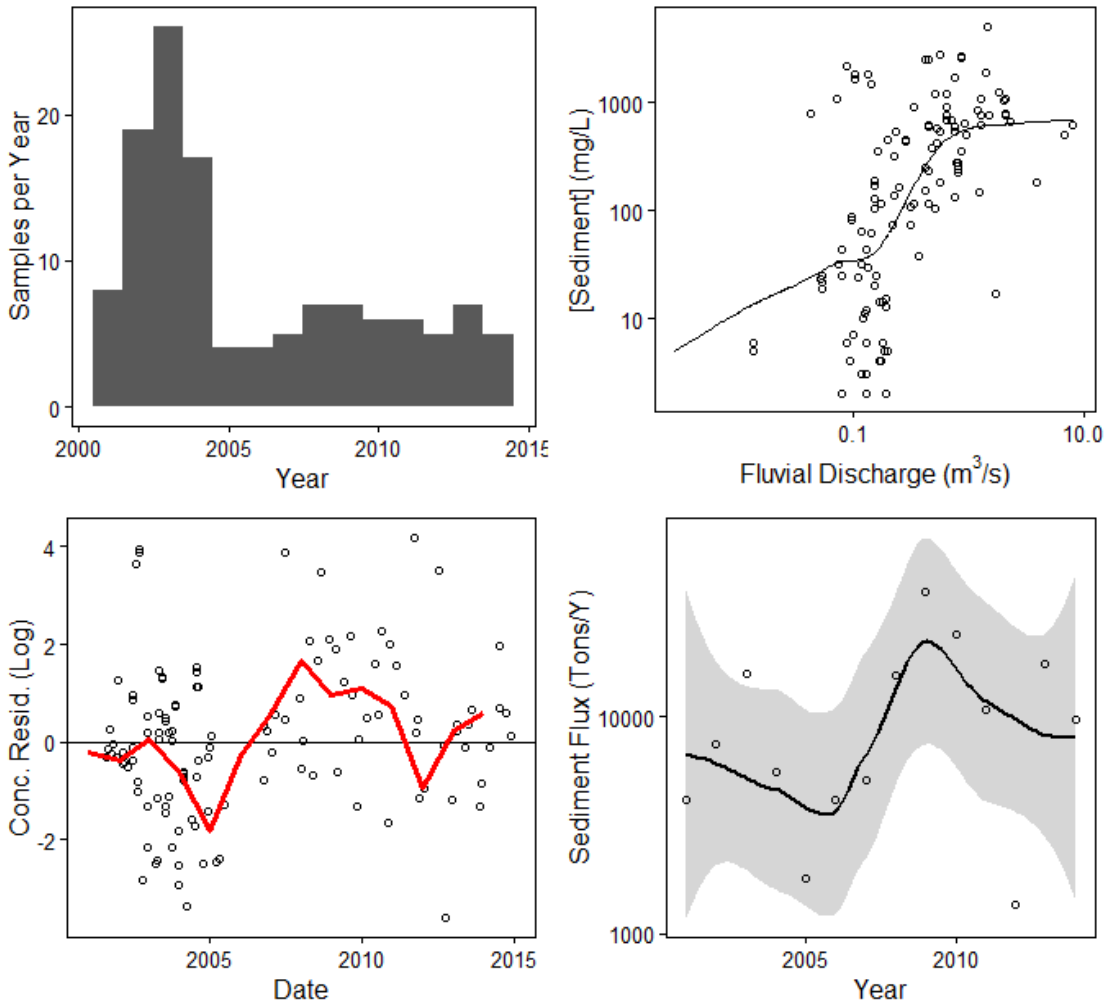


Figure A.2.28-

02217274: WHEELER CREEK AT BILL CHEEK ROAD, NEAR AUBURN, GA

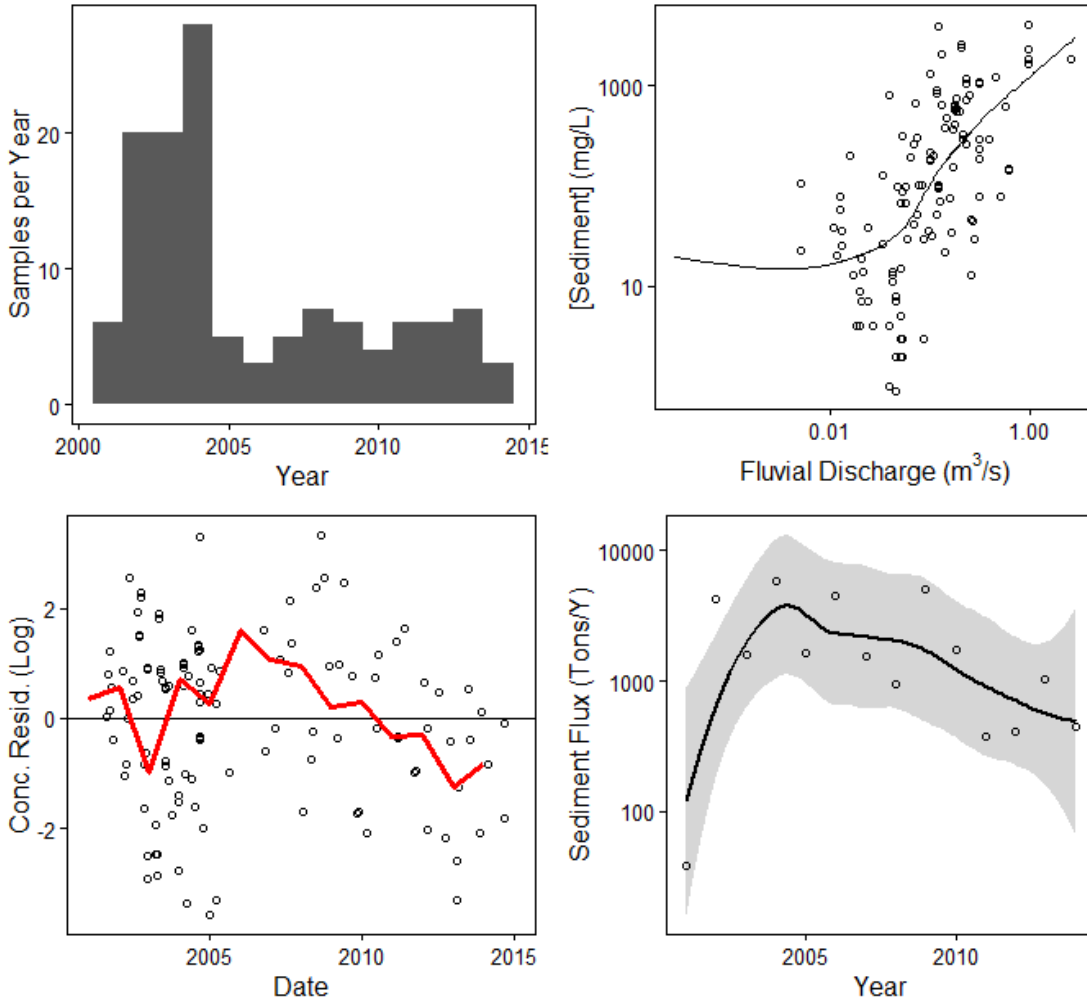


Figure A.2.29-02334885: SUWANEE CREEK AT SUWANEE, GA

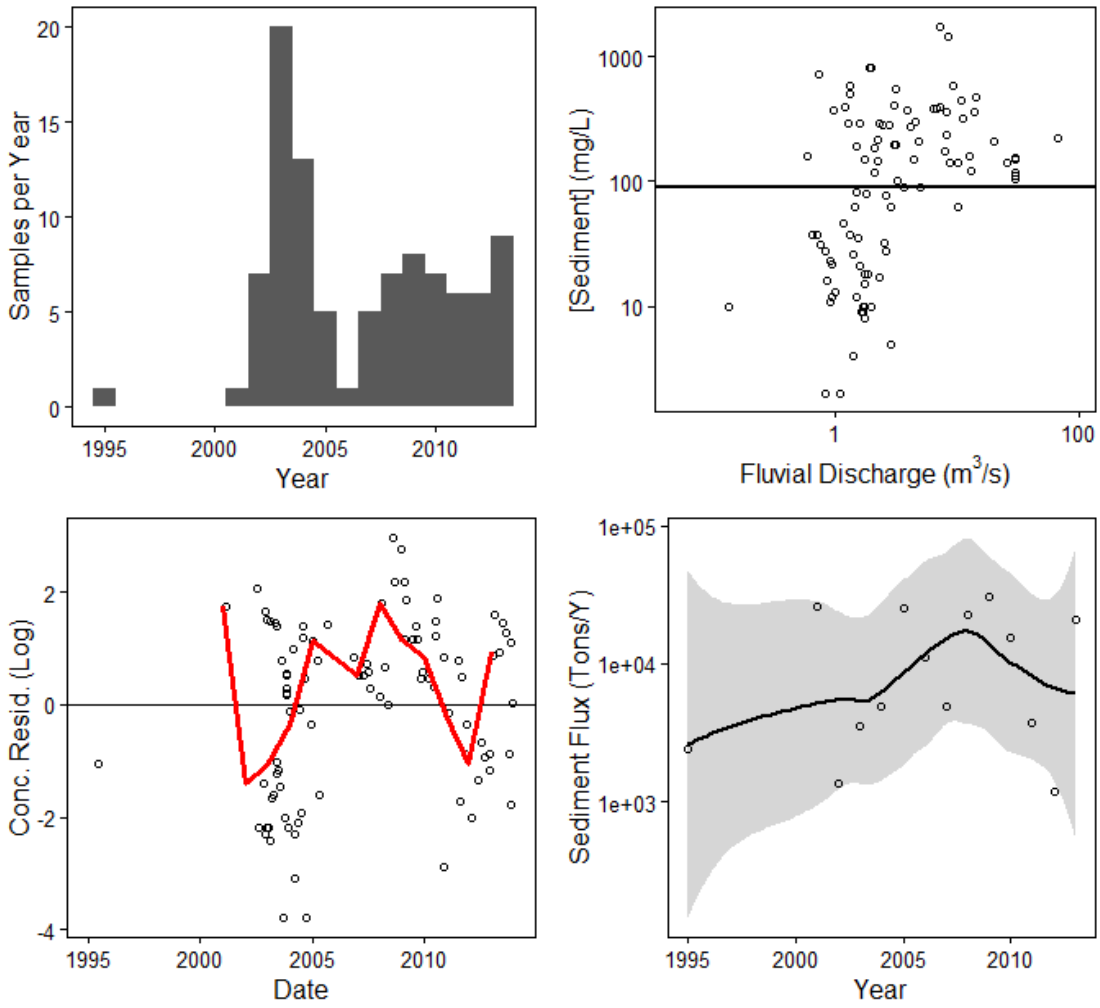


Figure A.2.30-02218565: APALACHEE RIVER AT FENCE ROAD, NEAR DACULA, GA

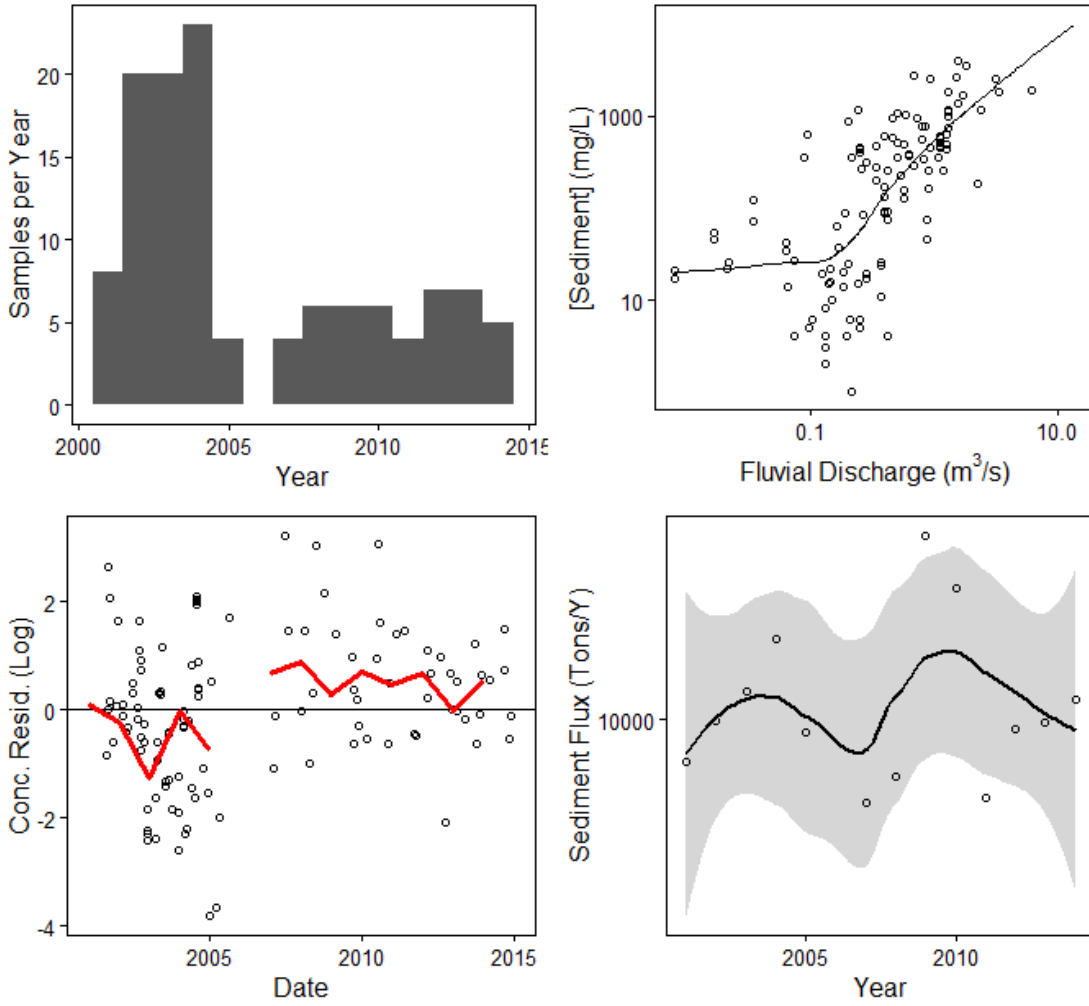


Figure A.2.31-02335350: CROOKED CREEK NEAR NORCROSS, GA

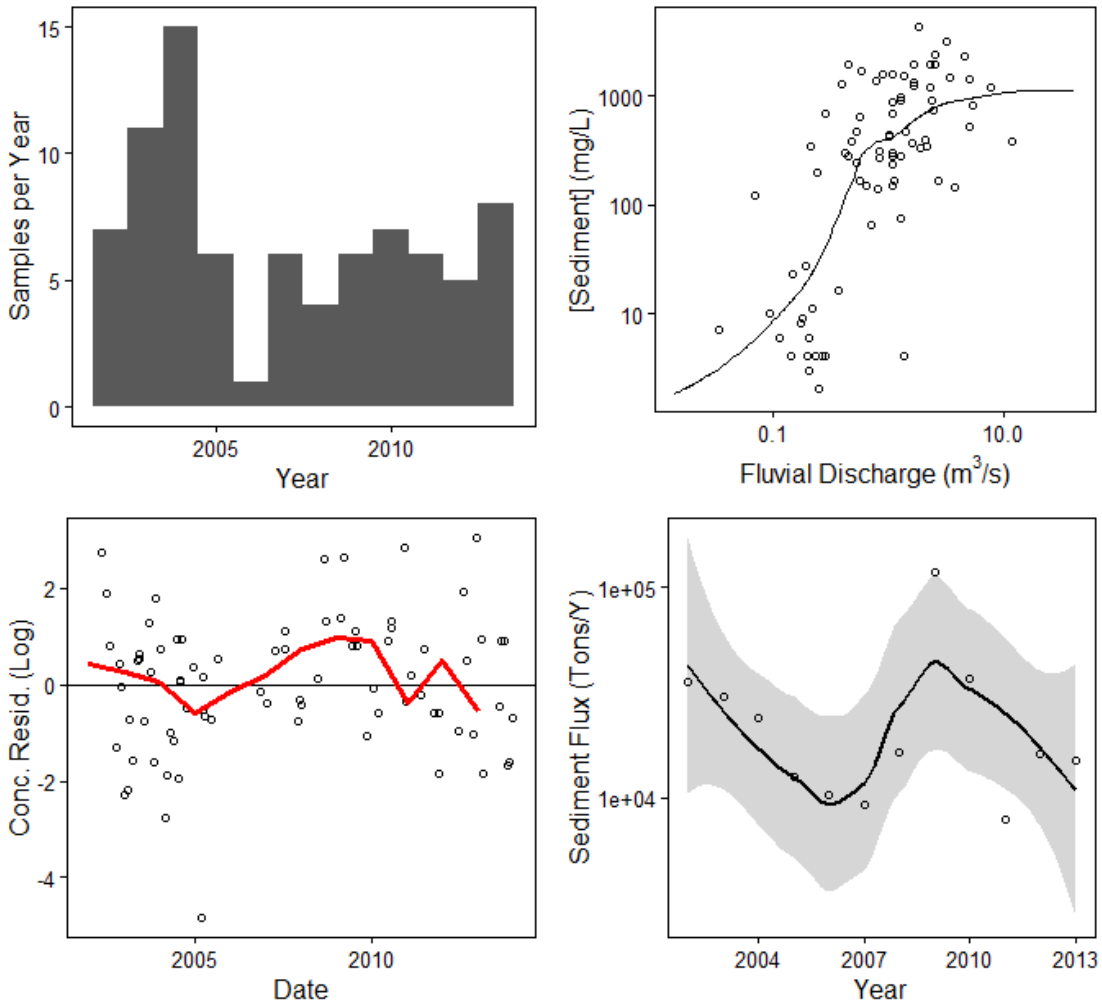


Figure A.2.32-02335870: SOPE CREEK NEAR MARIETTA, GA

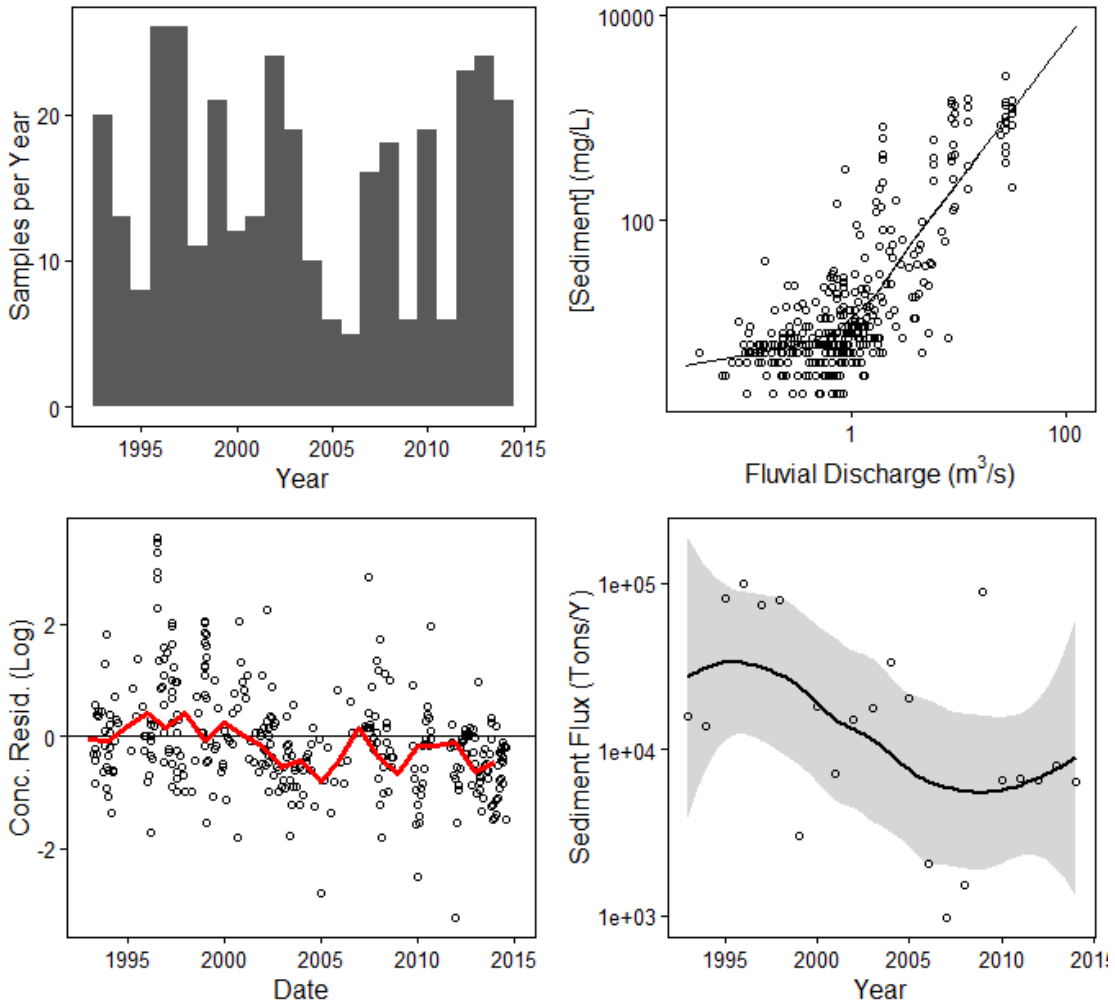


Figure A.2.33-

02208150: ALCOVY RIVER AT NEW HOPE ROAD, NEAR GRAYSON, GA

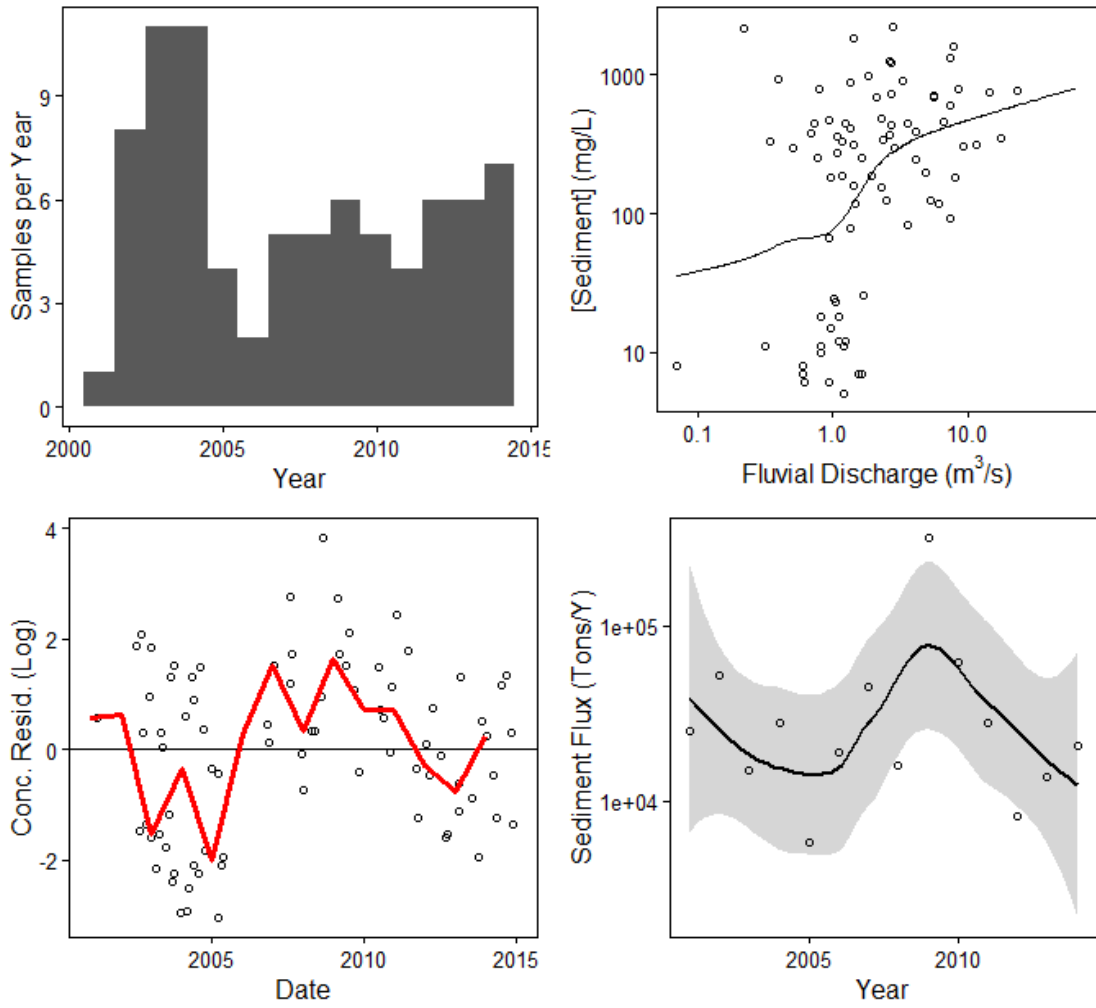


Figure A.2.34-

02336030: N.F. PEACHTREE CREEK AT GRAVES RD, NR DORAVILLE,GA

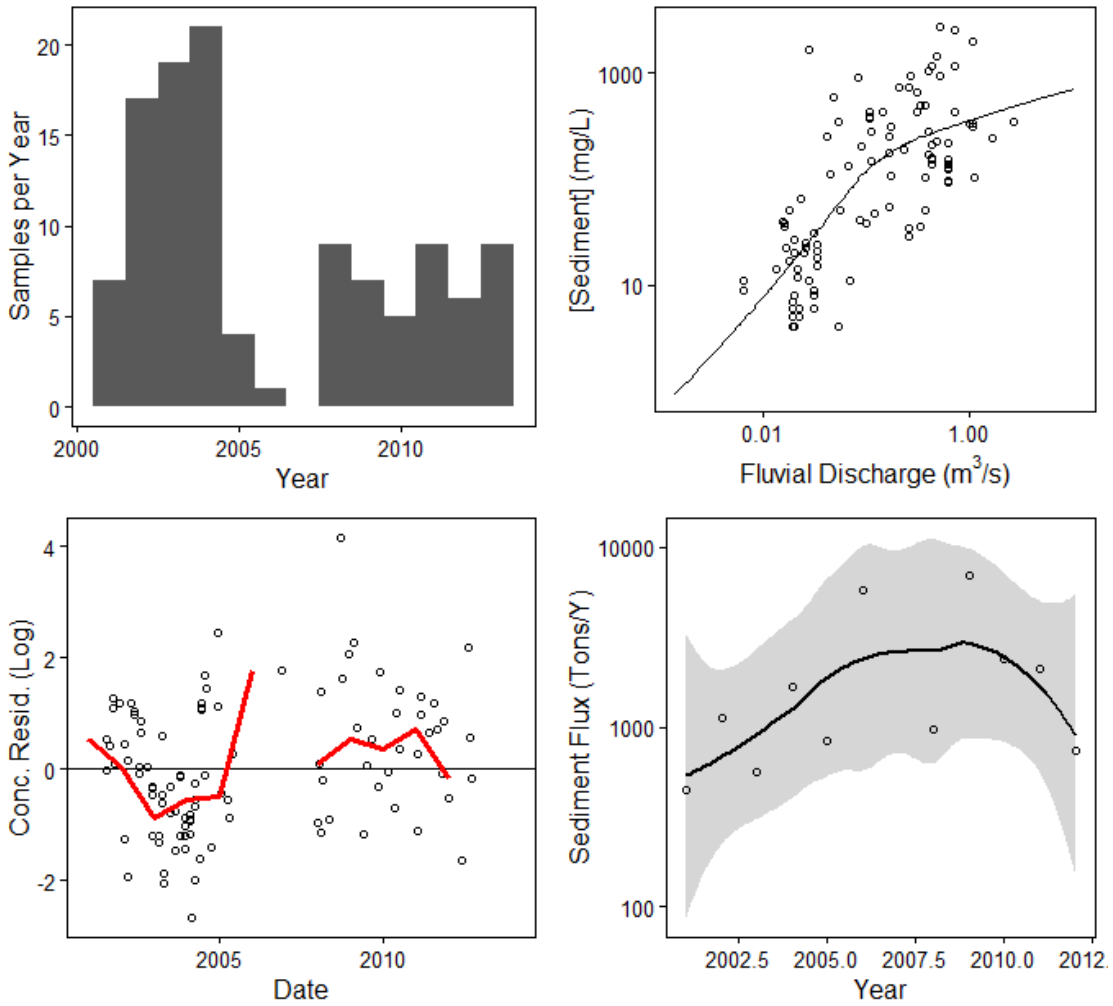


Figure A.2.35-

02336360: NANCY CREEK AT RICKENBACKER DRIVE, AT ATLANTA, GA

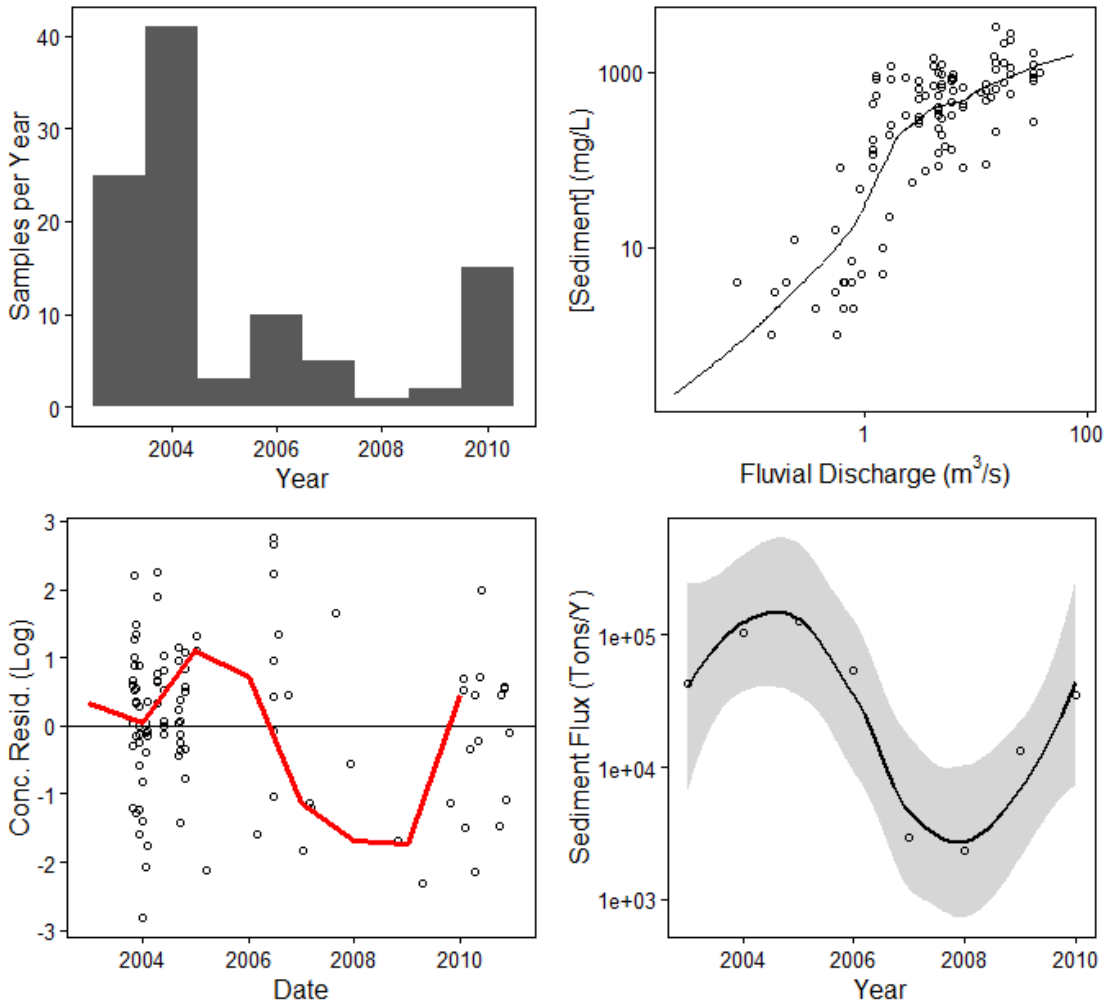


Figure A.2.36-

02336410: NANCY CREEK AT WEST WESLEY ROAD, AT ATLANTA, GA

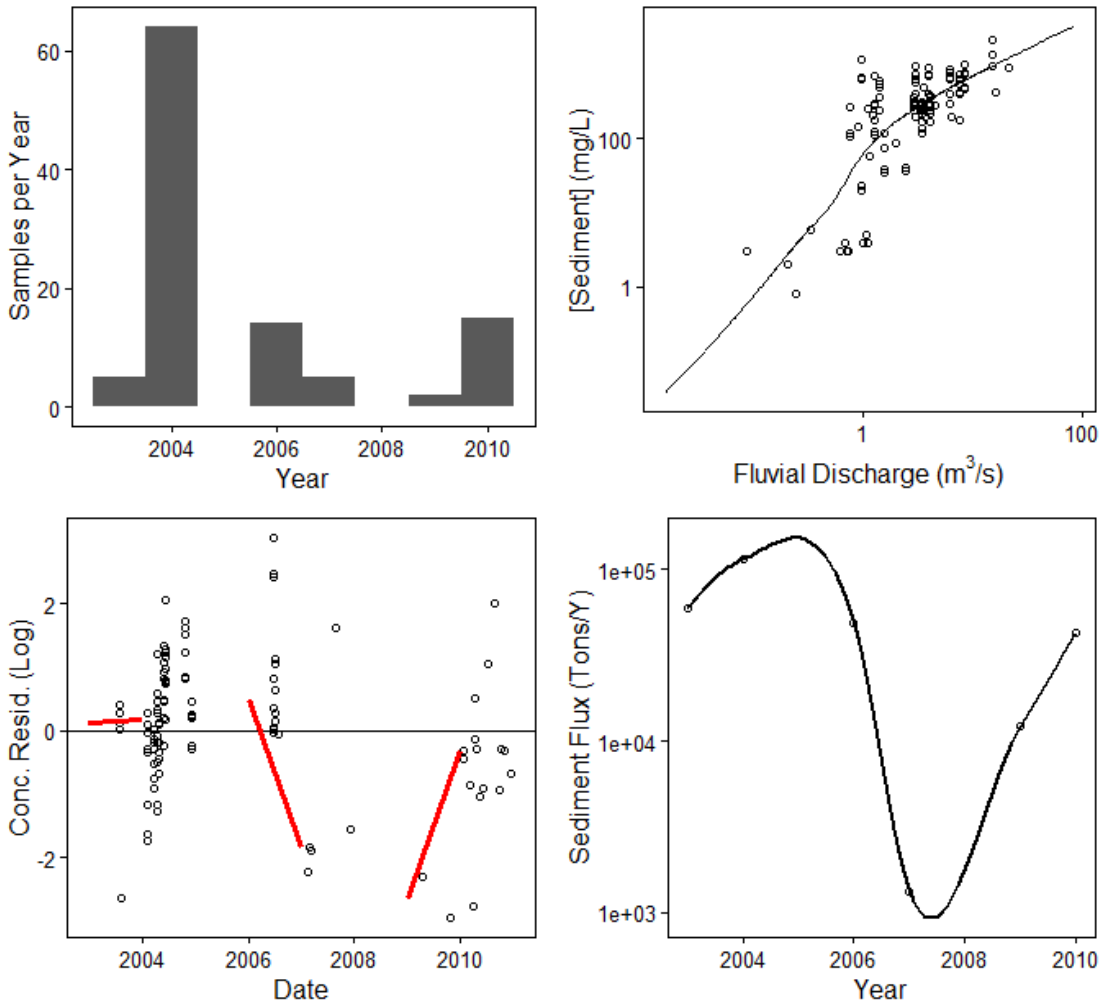


Figure A.2.37-

02336120: N.F. PEACHTREE CREEK, BUFORD HWY, NEAR ATLANTA, GA

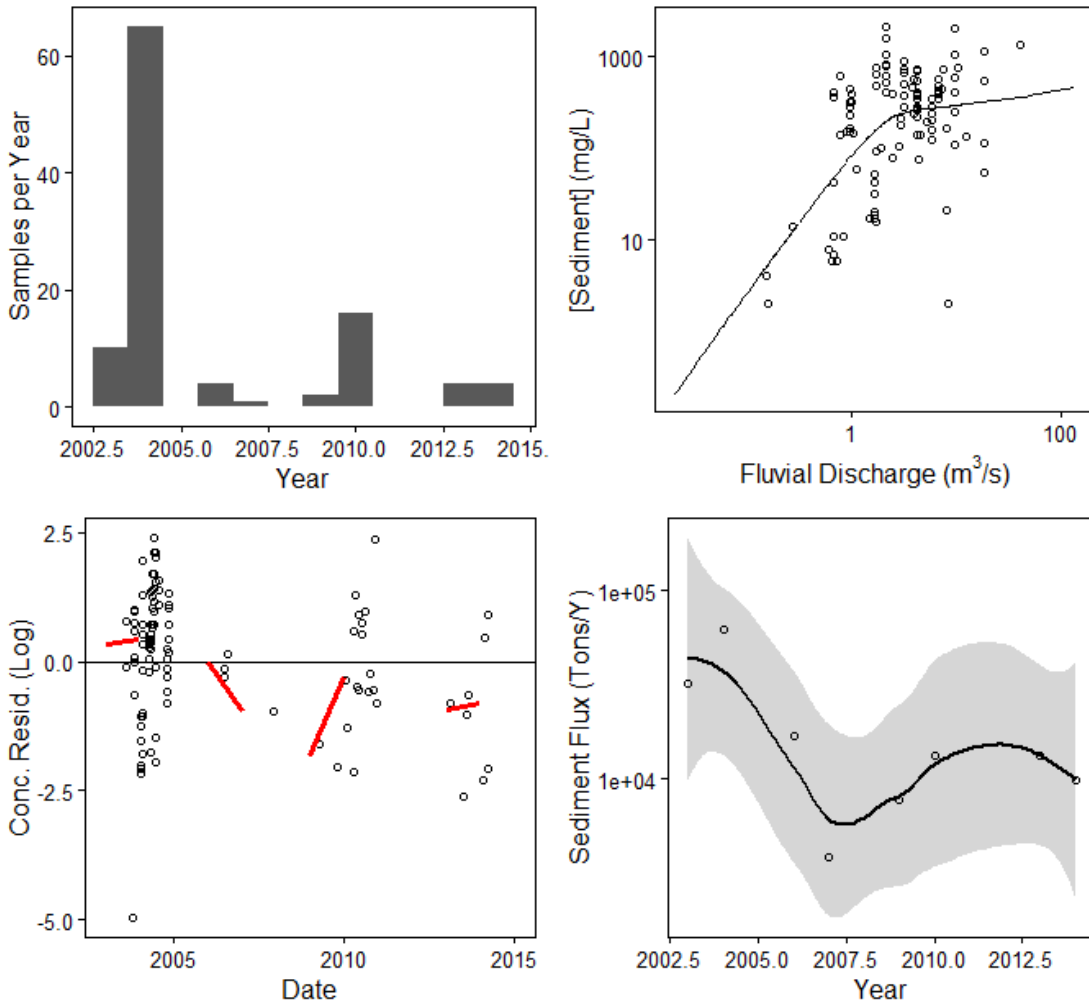


Figure A.2.38-

02207400: BRUSHY FORK CREEK AT BEAVER ROAD, NR LOGANVILLE, GA

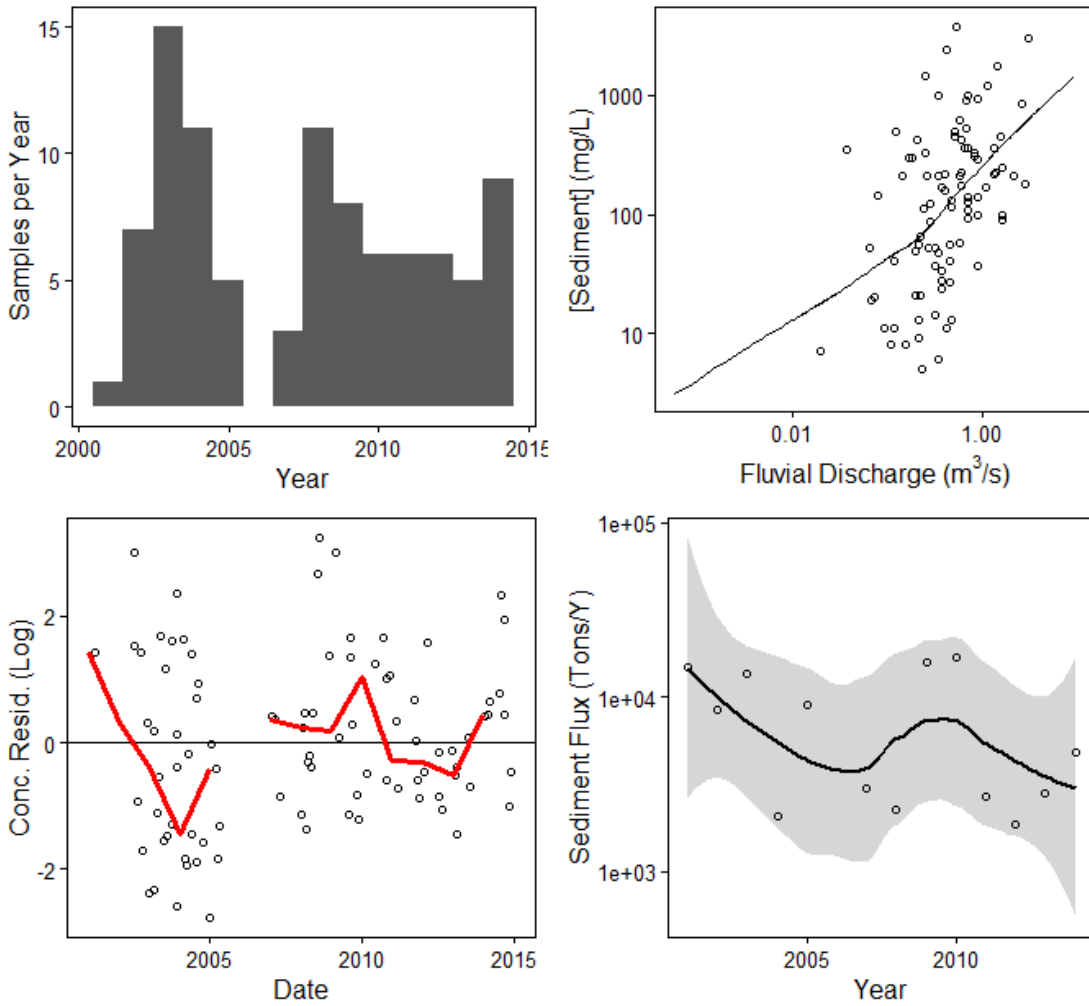


Figure A.2.39-02336300: PEACHTREE CREEK AT ATLANTA, GA

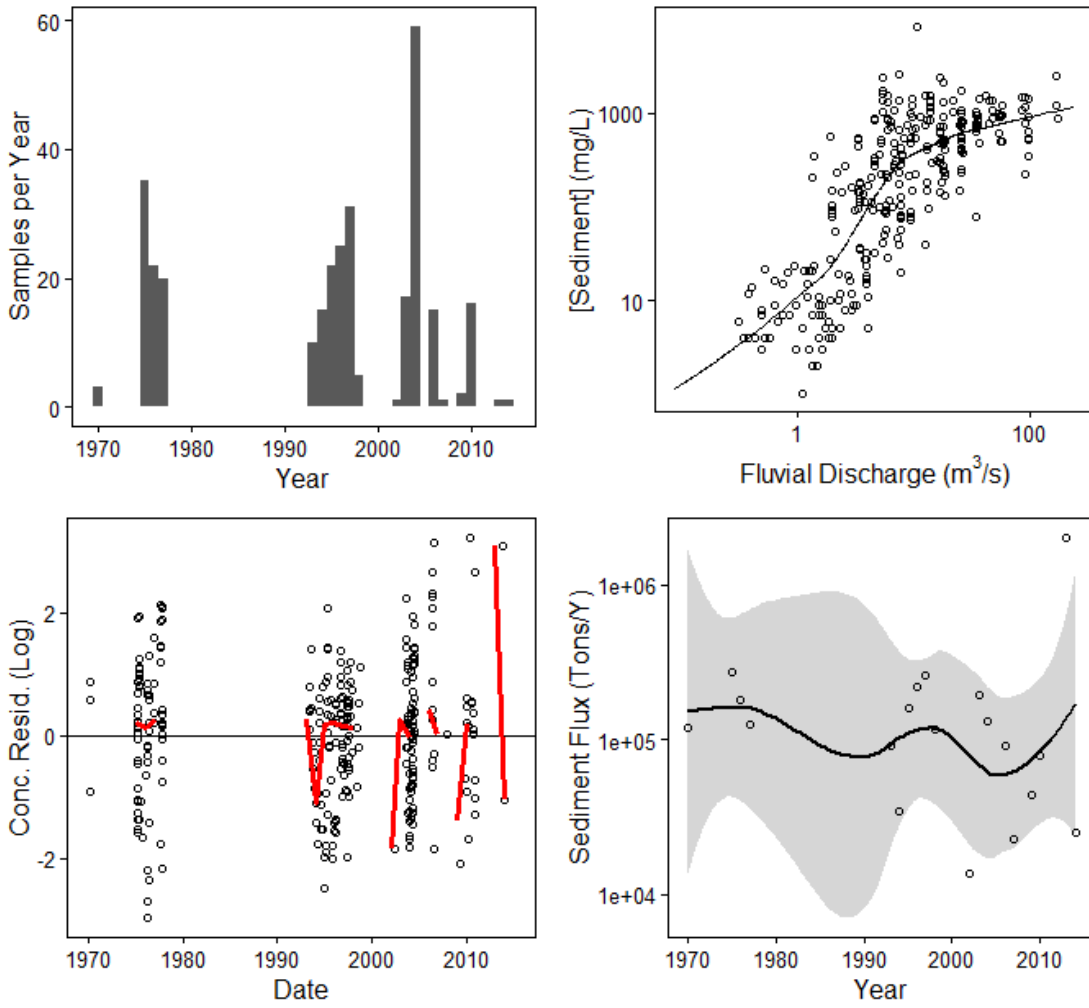


Figure A.2.40-

02207385: BIG HAYNES CREEK AT LENORA ROAD, NR SNELLVILLE, GA

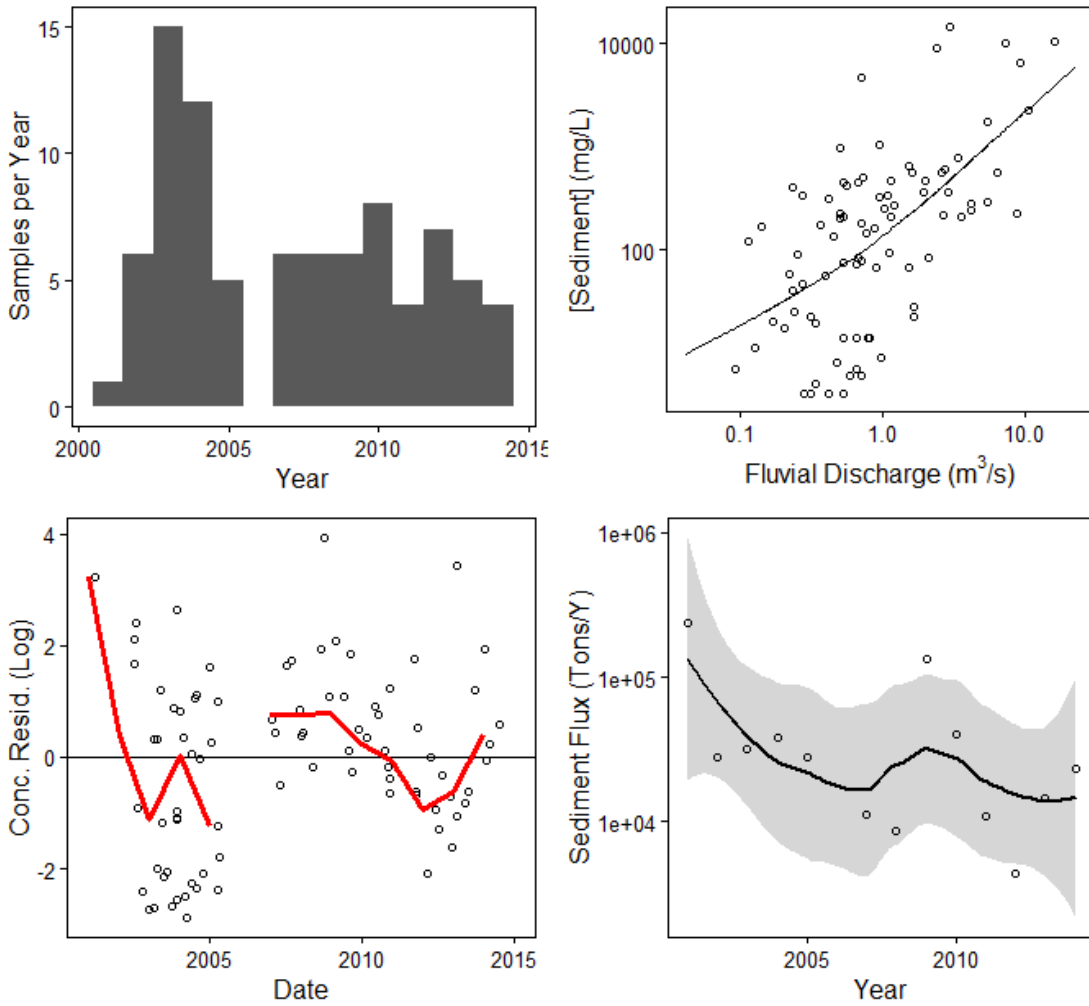


Figure A.2.41-

02336240: S.F. PEACHTREE CREEK JOHNSON RD, NEAR ATLANTA, GA

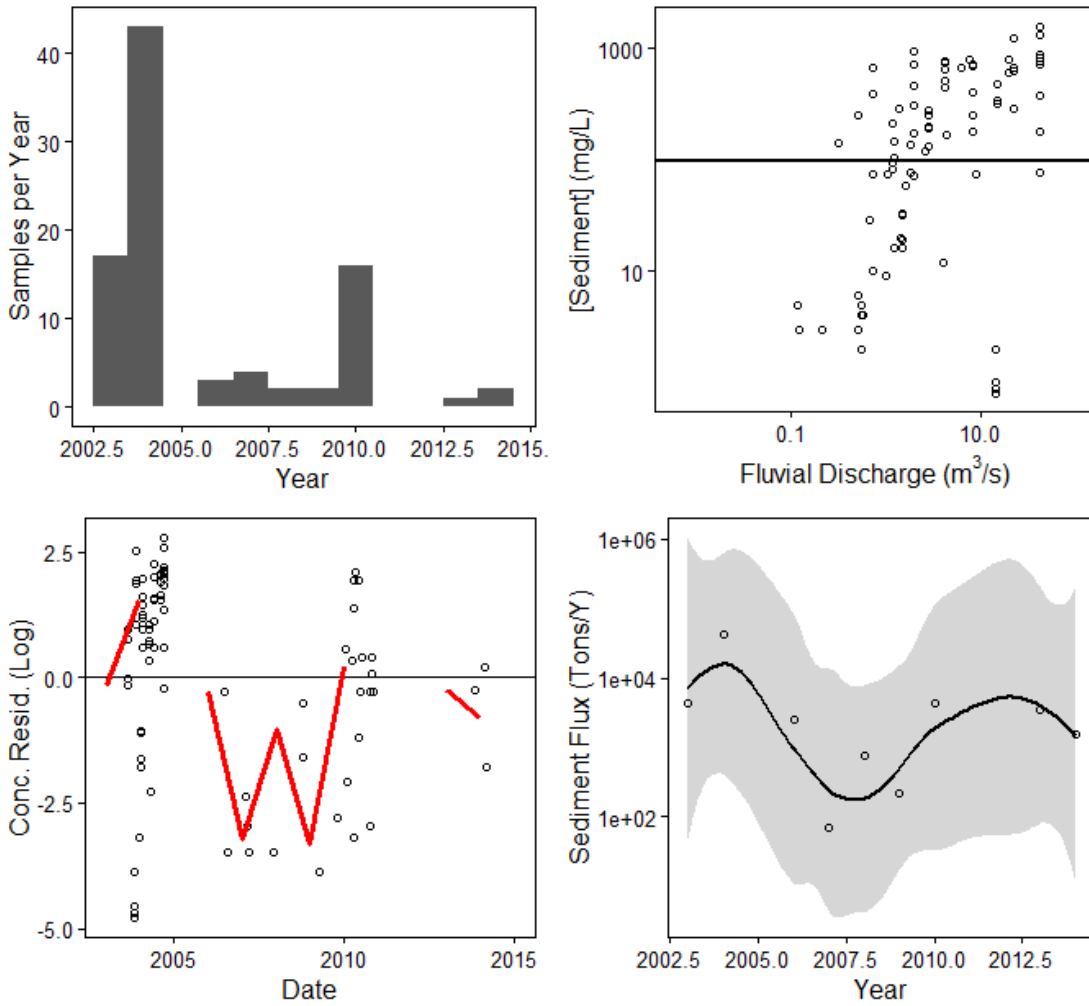


Figure A.2.42-

02336526: PROCTOR CREEK AT JACKSON PARKWAY, AT ATLANTA, GA

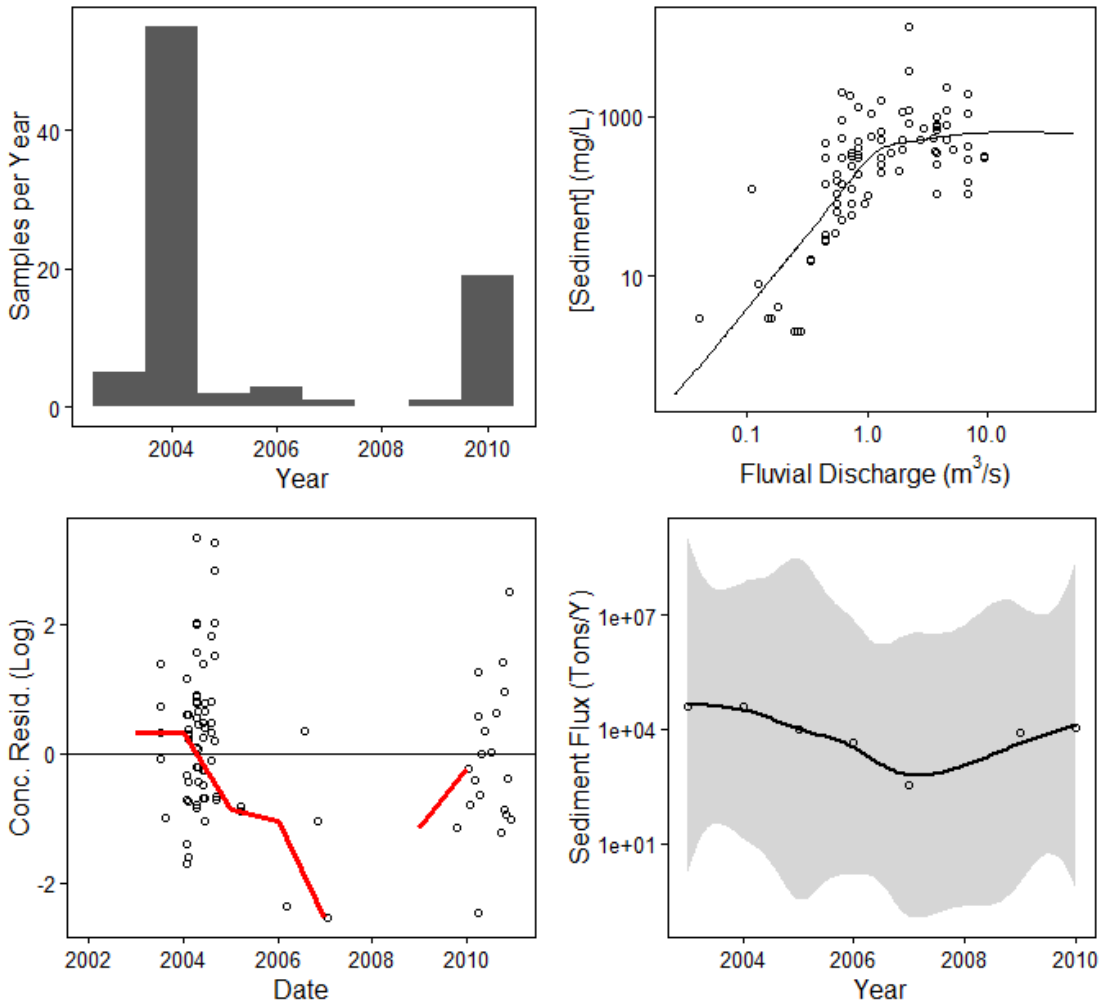


Figure A.2.43-

02207185: NO BUSINESS CREEK AT LEE ROAD, BELOW SNELLVILLE,GA

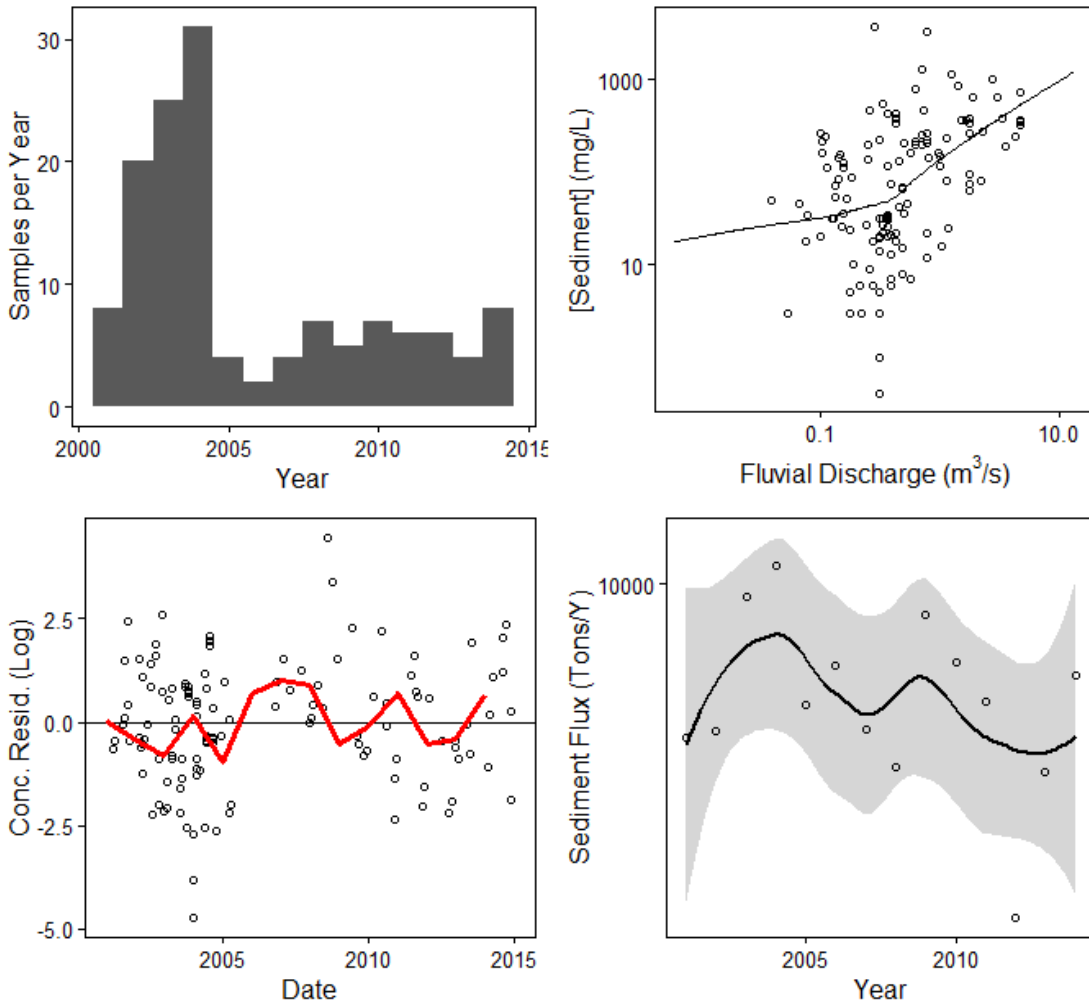


Figure A.2.44-02207120: YELLOW RIVER AT GA 124, NEAR LITHONIA, GA

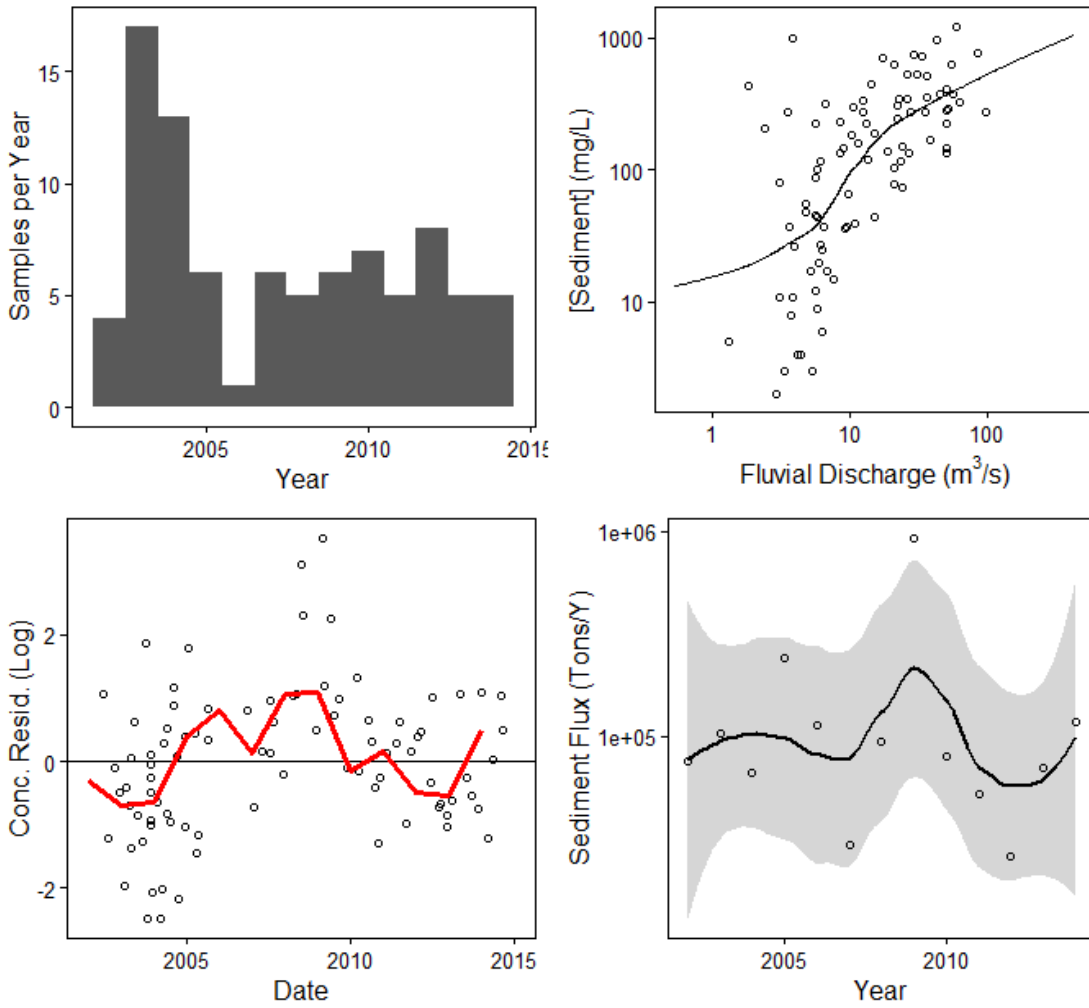


Figure A.2.45-

02207220: YELLOW RIVER AT PLEASANT HILL ROAD, NR LITHONIA,GA

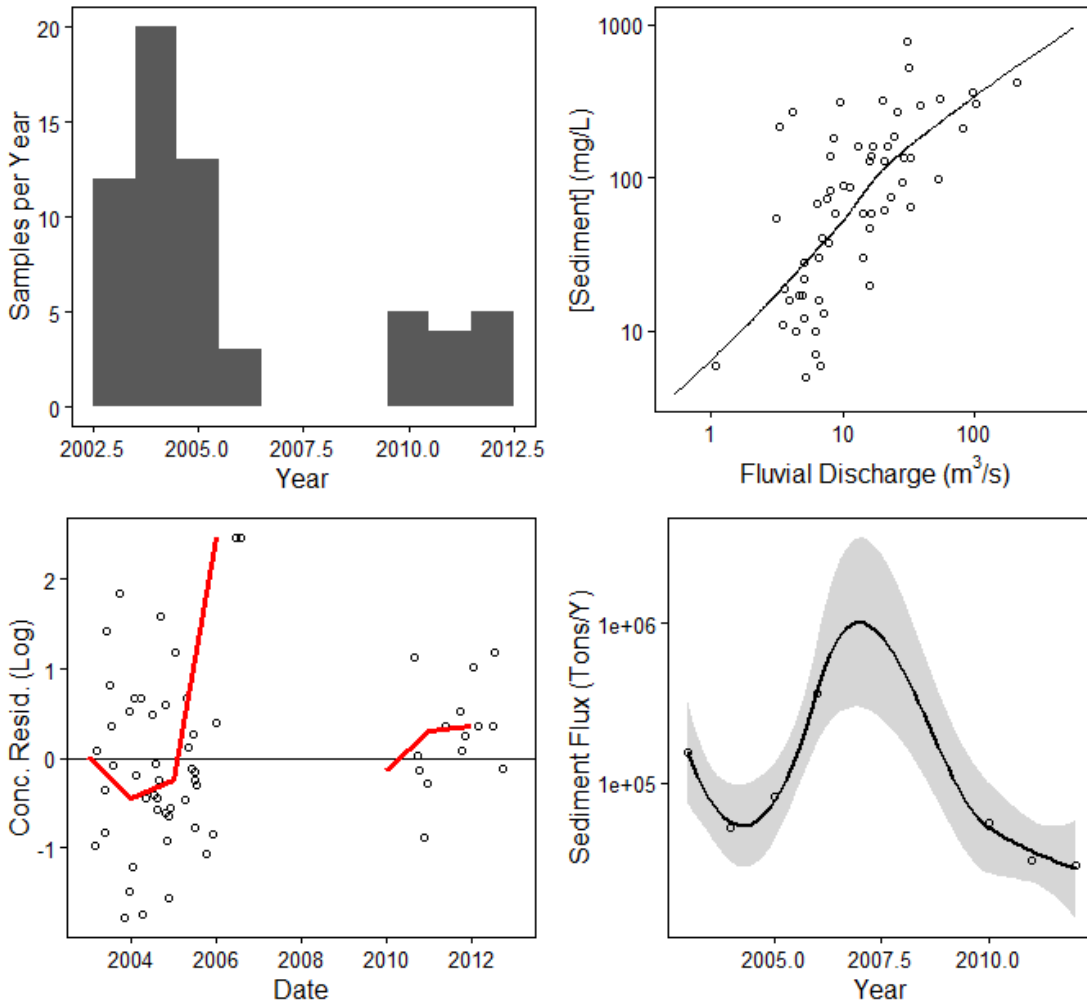


Figure A.2.46-

02203655: SOUTH RIVER AT FORREST PARK ROAD, AT ATLANTA, GA

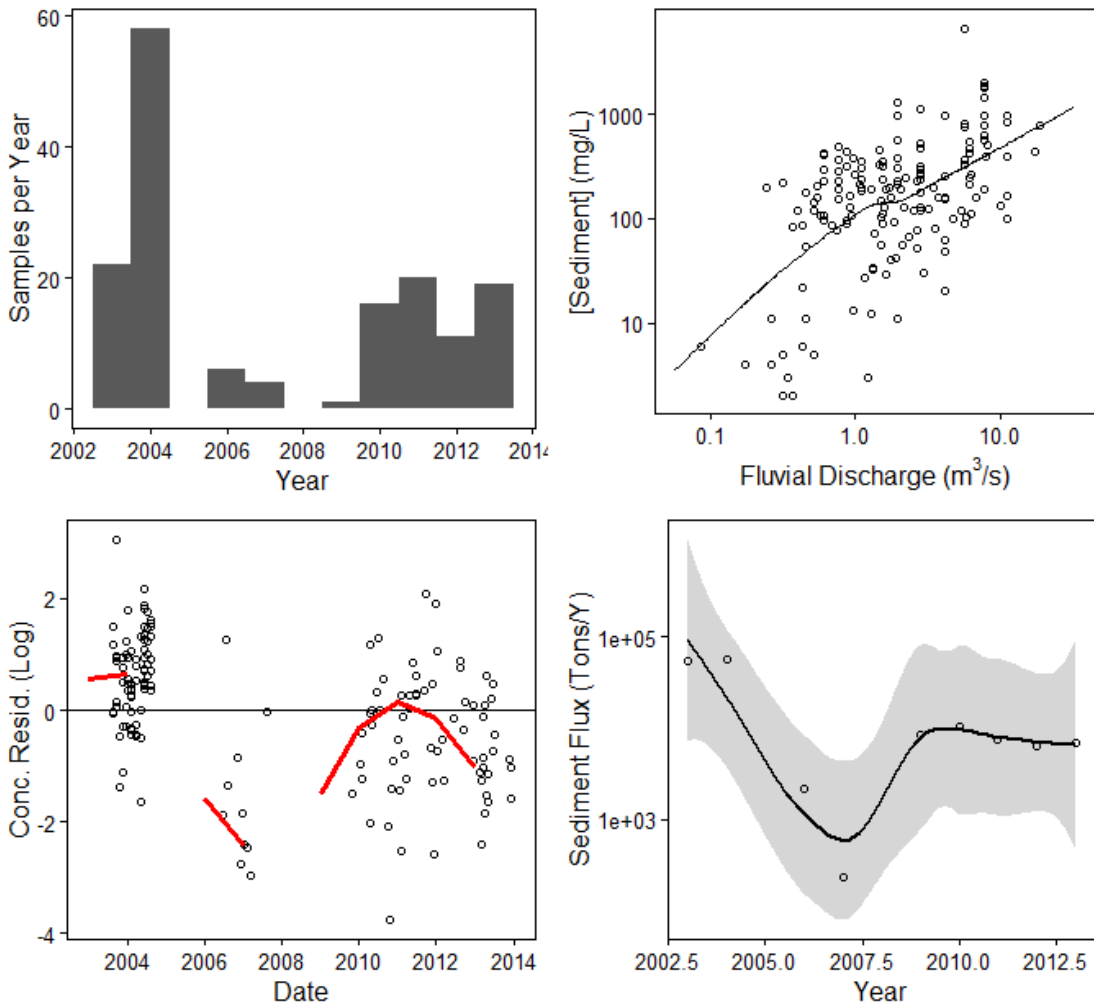


Figure A.2.47-

02207335: YELLOW RIVER AT GEES MILL ROAD, NEAR MILSTEAD, GA

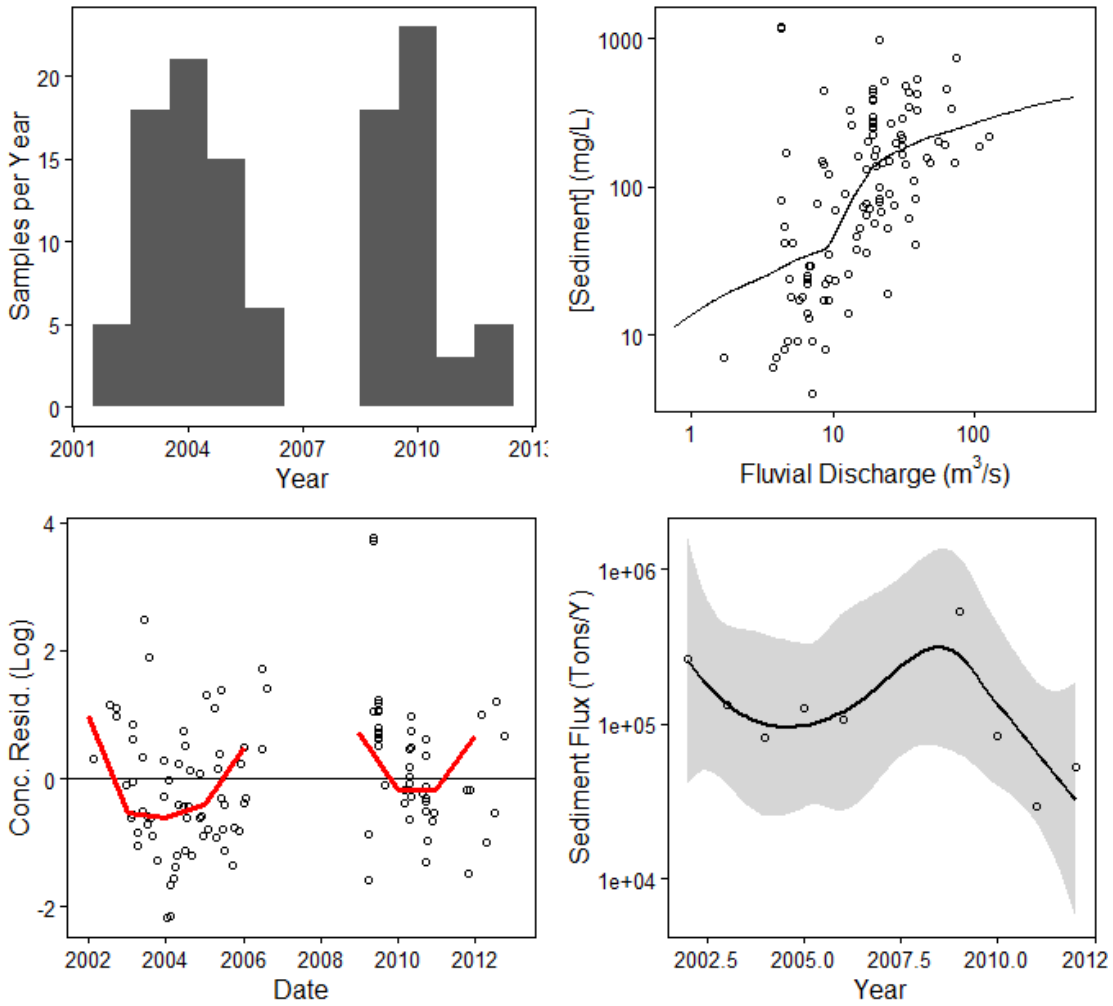


Figure A.2.48-02337500: SNAKE CREEK NEAR WHITESBURG, GA

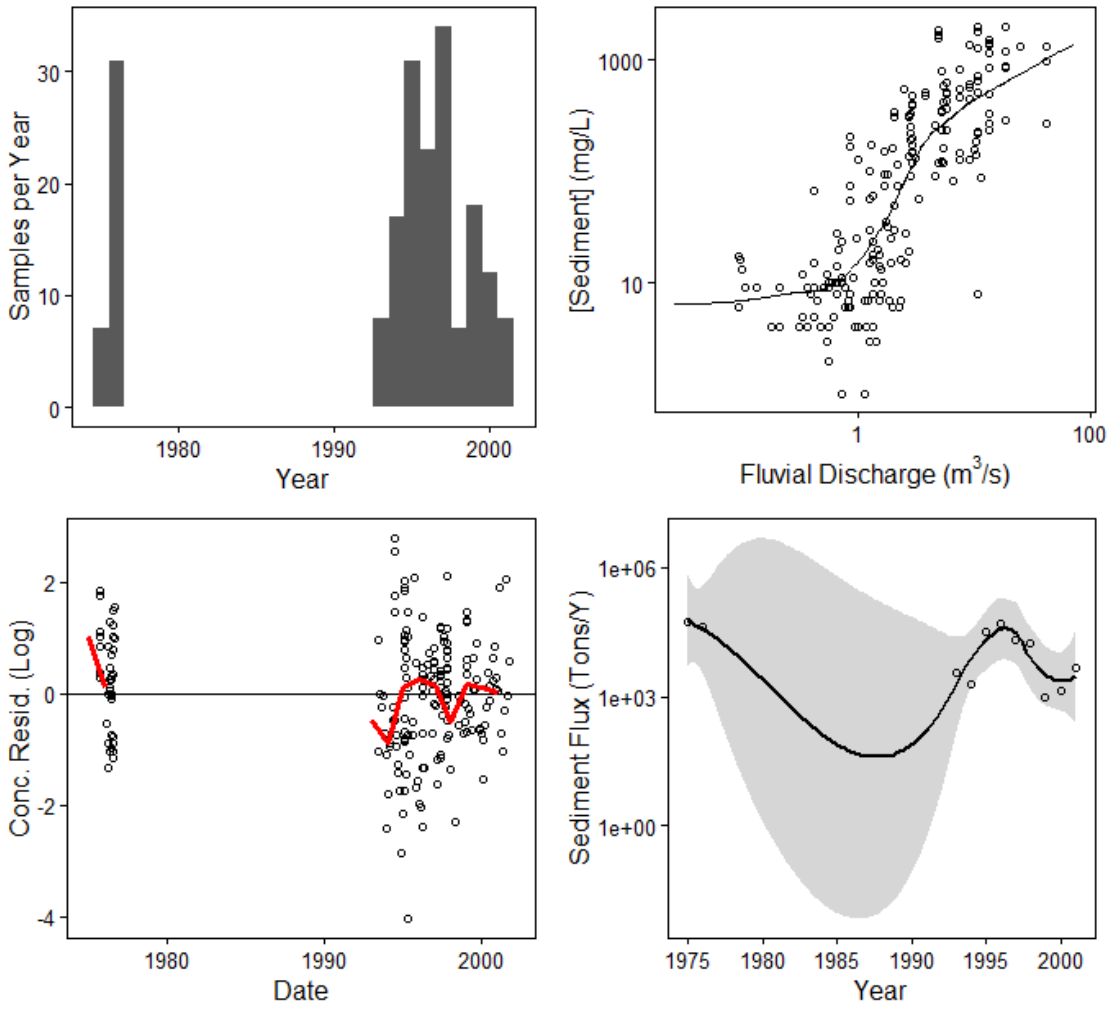


Figure A.2.49-02338000: CHATTAHOOCHEE RIVER NEAR WHITESBURG, GA

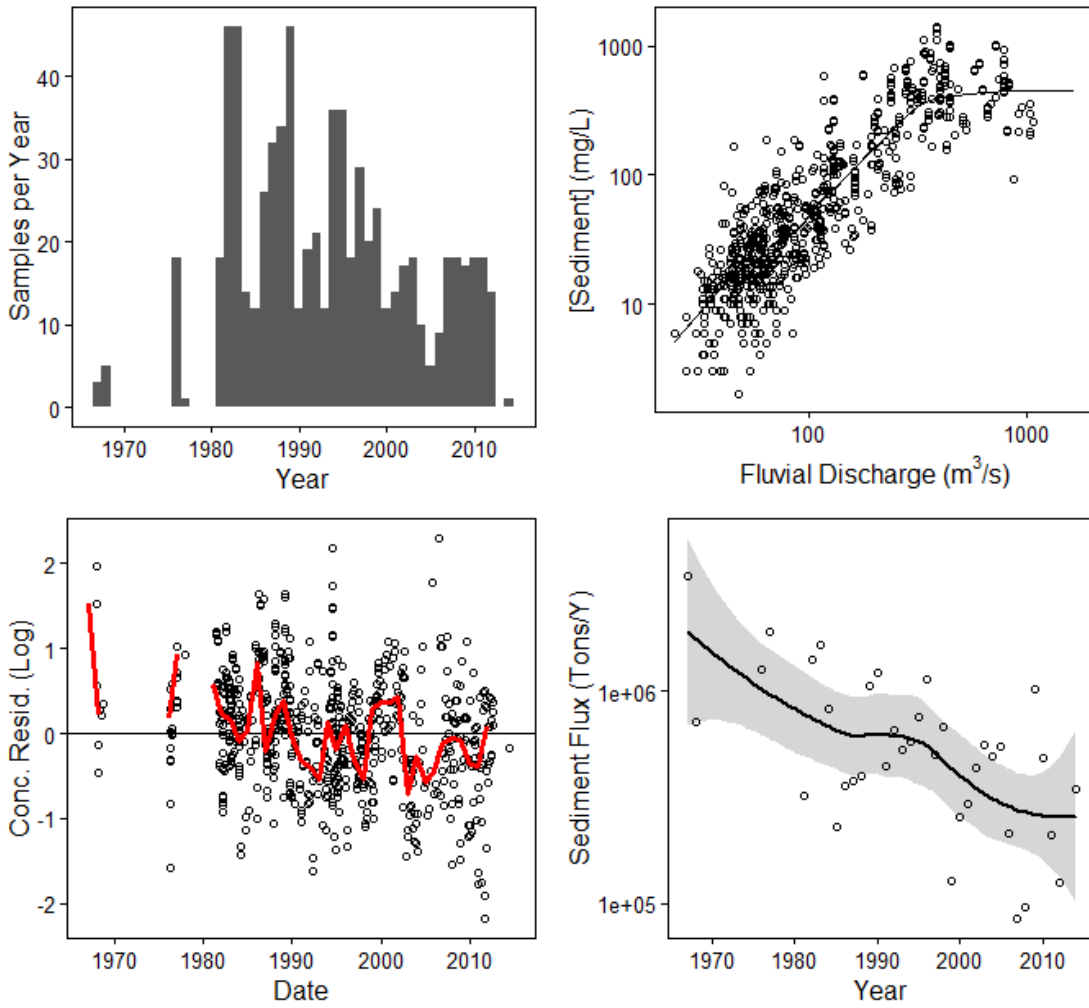


Figure A.2.50-

02338523: HILLABAHATCHEE CREEK AT THAXTON RD, NR FRANKLIN,GA

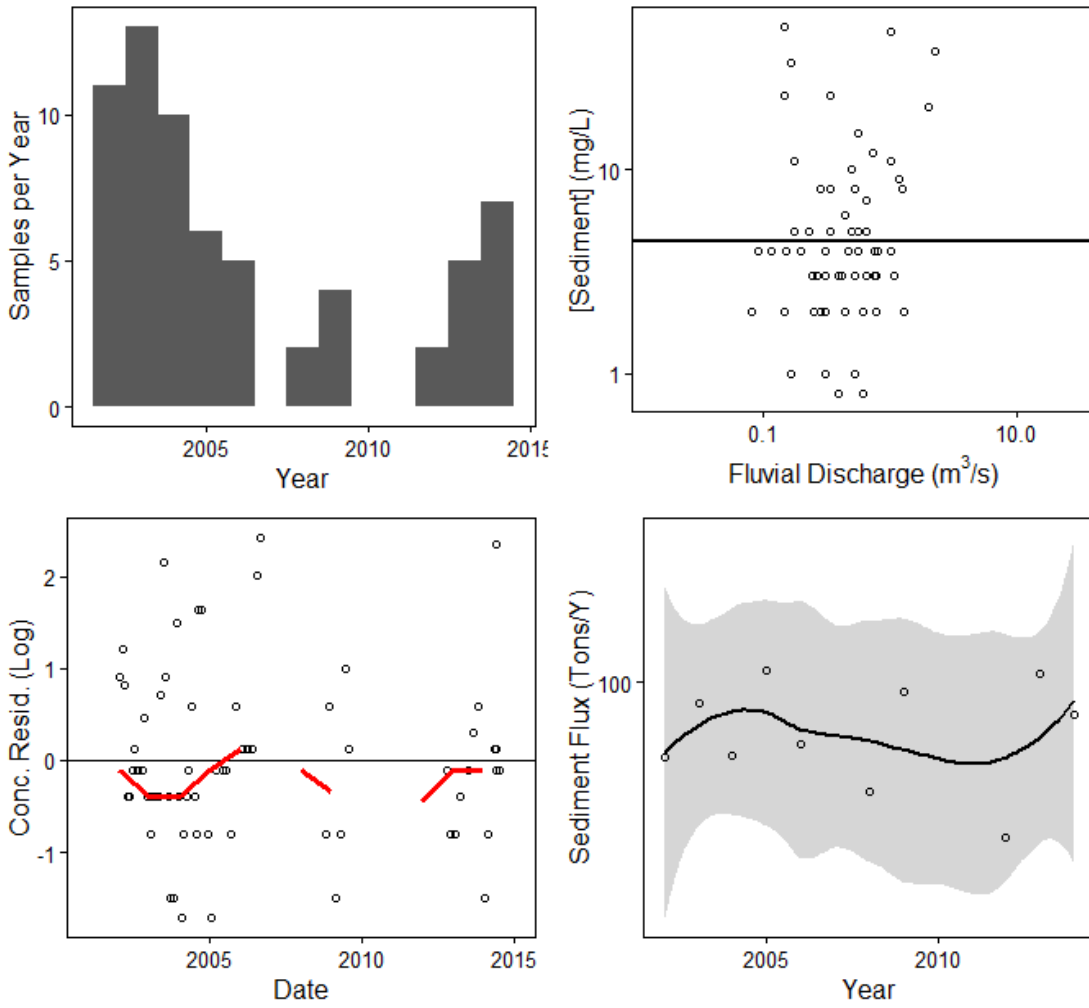


Figure A.2.51-02212600: FALLING CREEK NEAR JULIETTE, GA

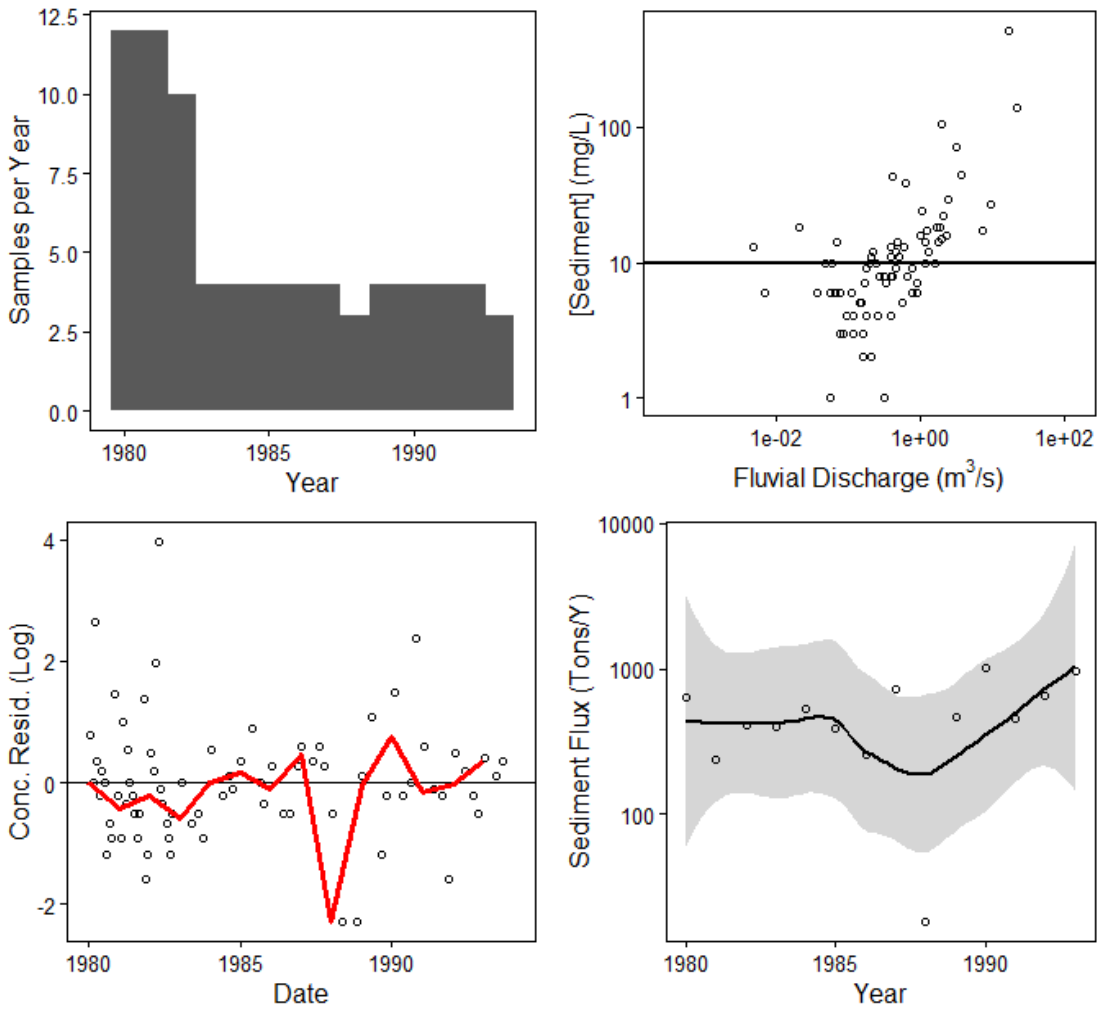
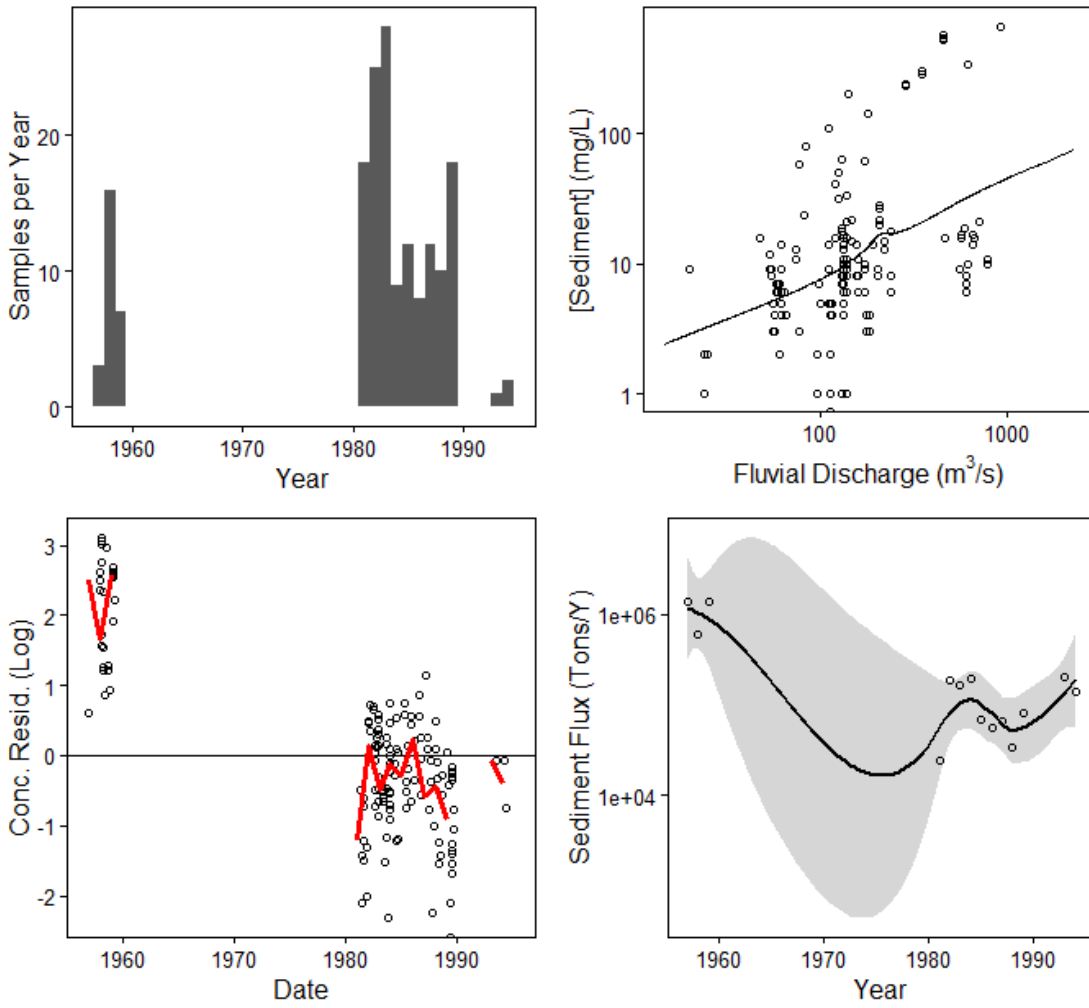


Figure A.2.52-02339500: CHATTAHOOCHEE RIVER AT WEST POINT, GA



APPENDIX B: MARSH CORE SUMMARY TABLES

Table B.1-Core Summary Data from Literature

Reference	CoreID	Lat	Long	n	BD (g/cc)	%OM	Accretion (cm/y)
Chmura_2004	Escuminac3	47.46	-64.89	21	0.27	33	0.20
Chmura_2004	Escuminac1	46.83	-64.92	24	0.22	32	0.33
Chmura_2004	Escuminac2	46.82	-64.91	25	0.29	26	0.29
Chmura_2004	Rustico12	46.48	-63.45	24	0.24	30	0.24
Chmura_2004	Rustico11	46.40	-63.13	24	0.33	26	0.25
Chmura_2004	Rustico10	46.40	-63.13	23	0.28	26	0.37
Chmura_2004	Eastport14	45.13	-66.35	25	0.18	27	0.19
Chmura_2004	Eastport13	45.12	-66.36	12	0.39	20	0.18
Chmura_2004	Eastport15	45.12	-66.36	13	0.38	35	0.15
Chmura_2004	Halifax5	44.70	-63.12	24	0.19	39	0.28
Chmura_2004	Halifax4	44.65	-63.39	24	0.16	60	0.38
Chmura_2004	Halifax6	44.65	-63.39	25	0.28	21	0.33
Chmura_2004	Yarmouth7	43.73	-66.05	24	0.21	33	0.39
Chmura_2004	Yarmouth9	43.71	-66.03	25	0.18	45	0.17
Chmura_2004	Yarmouth8	43.69	-65.78	24	0.38	24	0.28
Portnoy_1997	DD	41.95	-70.06	10	0.56	16	0.16
Portnoy_1997	N.A.	41.88	-70.00	10	0.18	50	0.16
Portnoy_1997	DF	41.87	-70.00	10	0.27	34	0.16
Roman_1997	nauset	41.84	-69.95	50	0.32	28	0.26
Roman_1997	inlet	41.83	-69.95	50	0.22	37	0.42
Roman_1997	ftHill	41.82	-69.96	50	0.33	17	0.40
BrickerUrso_1989	c1	41.80	-71.40	50	0.47	20	0.15
BrickerUrso_1989	c2a	41.77	-71.39	50	0.58	19	0.48
BrickerUrso_1989	c3	41.70	-71.37	49	0.52	17	0.56
BrickerUrso_1989	c4a	41.65	-71.34	49	0.30	37	0.25
BrickerUrso_1989	c5	41.51	-71.37	50	0.47	25	0.32
BrickerUrso_1989	c6	41.36	-71.68	47	0.39	31	0.39
Anisfeld_1999	Branford1	41.28	-72.80	11	0.20	32	0.62
Anisfeld_1999	Branford2	41.28	-72.80	11	0.21	26	0.59
Anisfeld_1999	sluice2	41.28	-72.66	16	0.60	14	0.19
Anisfeld_1999	east2	41.28	-72.65	17	0.29	38	0.29
Anisfeld_1999	east1	41.27	-72.66	14	0.35	19	0.39
Anisfeld_1999	leetes2	41.26	-72.71	16	0.56	18	0.26
Anisfeld_1999	hoadley1	41.26	-72.73	19	0.32	24	0.47
Anisfeld_1999	hoadley2	41.26	-72.73	18	0.28	25	0.40
Anisfeld_1999	sybil3	41.26	-72.80	17	0.41	19	0.20
Anisfeld_1999	hoadley3	41.26	-72.73	13	0.30	24	0.46
Anisfeld_1999	sybil2	41.26	-72.80	16	0.64	9	0.20

Table B.2-Core Summary Data from Literature Continued1

Ref	CoreID	Lat	Long	n	BD (g/cc)	%OM	Accretion (cm/yr)
Anisfeld_1999	leetes1	41.26	-72.71	16	0.56	19	0.31
Anisfeld_1999	sybil1	41.26	-72.80	15	0.15	50	0.18
Armentano_1975	Site2	40.96	-73.14	5	0.23	22	0.63
Armentano_1975	Site3	40.96	-73.14	5	0.25	23	0.47
Orson_1990	WC1A-15	39.86	-75.17	11	0.16	15	1.38
Orson_1990	WC1A-30	39.86	-75.17	11	0.15	16	1.27
Orson_1990	WC1A-45	39.86	-75.17	11	0.12	17	1.10
Craft_1993	BackmarshIrregularly	35.93	-76.38	15	0.14	61	0.24
Craft_1993	StreamsideIrregularly	35.93	-76.38	15	0.15	54	0.36
Craft_1993	BackmarshRegularly	35.78	-75.54	15	1.20	2	0.09
Craft_1993	StreamsideRegularly	35.78	-75.54	15	0.77	4	0.27
Callaway_1997	BILOXI	30.38	-88.77	24	0.29	22	0.56
Hatton_1981	freshwater_inland	29.88	-90.56	10	0.12	57	0.65
Hatton_1981	freshwater_streamside	29.88	-90.56	10	0.11	51	1.06
Hatton_1981	intermediate_inland	29.58	-90.25	10	0.08	72	0.64
Hatton_1981	intermediate_streamside	29.58	-90.25	10	0.16	44	1.35
Nyman_1993	bgoat1	29.40	-90.56	15	0.14	41	1.06
Nyman_1993	bgoat2	29.40	-90.56	11	0.11	45	1.06
Nyman_1993	nmadbay1	29.39	-90.56	15	0.14	43	1.33
Nyman_1993	nmadbay2	29.39	-90.56	15	0.12	44	1.33
Nyman_2006	baymo1	29.37	-91.24	8	0.24	31	0.74
Nyman_2006	baymo2	29.37	-91.24	6	0.27	36	0.74
Nyman_1993	wmadbay	29.36	-90.58	15	0.08	57	0.78
Hatton_1981	brackish_inland	29.35	-90.17	10	0.13	59	0.59
Hatton_1981	brackish_streamside	29.35	-90.17	10	0.27	32	1.40
Nyman_1993	semad1	29.35	-90.55	15	0.13	47	0.67
Nyman_1993	semad2	29.35	-90.55	15	0.11	51	0.67
Nyman_1993	ndeMangu	29.34	-90.57	14	0.16	37	0.94
Nyman_1993	ups1	29.34	-90.59	15	0.20	30	1.22
Nyman_1993	ups2	29.34	-90.59	15	0.19	27	1.22
Nyman_1993	grand	29.33	-90.61	14	0.18	30	1.04
Nyman_2006	mosqu1	29.33	-91.17	10	0.21	34	0.74
Nyman_2006	mosqu2	29.33	-91.17	10	0.20	32	0.74
Nyman_1993	dufrene	29.33	-90.56	8	0.18	33	0.94
Nyman_1993	mdeMangu1	29.33	-90.58	15	0.23	22	1.28
Nyman_1993	mdeMangu2	29.33	-90.58	14	0.26	25	1.28
Nyman_1993	mid1	29.32	-90.59	16	0.24	25	0.75
Nyman_1993	mid2	29.32	-90.59	16	0.23	23	0.75
Nyman_2006	pntha1	29.32	-91.17	8	0.20	31	0.74
Nyman_2006	pntha2	29.32	-91.17	7	0.20	40	0.74

Table B.3-Core Summary Data from Literature Continued2

Ref	CoreID	Lat	Long	n	BD (g/cc)	%OM	Accretion (cm/y)
Nyman_1993	sdeMangu	29.32	-90.58	13	0.27	25	0.56
Nyman_1993	dow1	29.31	-90.59	15	0.24	21	0.98
Nyman_1993	dow2	29.31	-90.59	16	0.25	24	0.98
Nyman_1993	charles1	29.31	-90.54	12	0.26	18	0.98
Nyman_1993	charles2	29.31	-90.54	9	0.28	19	0.98
Nyman_1993	barre1	29.30	-90.60	16	0.31	23	1.78
Nyman_1993	barre2	29.30	-90.60	16	0.30	23	1.78
Nyman_1993	lapeur1	29.30	-90.52	11	0.29	22	0.78
Nyman_1993	lapeur2	29.30	-90.52	11	0.31	19	0.78
Nyman_2006	hammo	29.29	-91.13	8	0.25	30	0.74
Nyman_2006	moyst1	29.26	-91.10	8	0.45	16	0.74
Nyman_2006	moyst2	29.26	-91.10	6	0.43	16	0.74
Nyman_2006	doyst1	29.26	-91.12	5	0.23	28	0.74
Nyman_2006	doyst2	29.26	-91.12	5	0.23	30	0.74
Nyman_2006	uoyst1	29.25	-91.09	5	0.26	27	0.74
Nyman_2006	uoyst2	29.25	-91.09	5	0.27	31	0.74
Nyman_2006	vouvi1	29.24	-91.13	6	0.35	20	0.74
Nyman_2006	vouvi2	29.24	-91.13	4	0.39	18	0.74
Hatton_1981	saline_inland	29.22	-90.10	10	0.30	26	0.75
Callaway_1997	SANBERNARD	28.84	-95.50	22	1.05	5	0.62
Callaway_1997	ARANSAS	28.24	-96.79	17	0.72	11	0.44